1 **Mechanics**

2 **Machine Building and Machine Science**

3 **Information Technology, Computer Science, and Management**

VESTNIK

of
DON STATE
TECHNICAL
UNIVERSITY

Vol. 18, № 4

CONTENT

МЕХАНИКА
MECHANICS

Development and correctness analysis of the mathematical model of transport and suspension sedimentation depending on bottom relief variation [*]

A. I. Sukhinov[1], V. V. Sidoryakina[2][**]

[1] Don State Technical University, Rostov-on-Don, Russian Federation

[2] Taganrog Chekhov Institute, Rostov State University of Economics (RINH) branch, Taganrog, Russian Federation

Построение и исследование корректности математической модели транспорта и осаждения взвесей с учетом изменения рельефа дна[***]

А. И. Сухинов[1], В. В. Сидорякина[2][**]

[1] Донской государственный технический университет, г. Ростов-на-Дону, Российская Федерация

[2] Таганрогский институт имени А. П. Чехова (филиал) РГЭУ (РИНХ), г. Таганрог, Российская Федерация

Introduction. The paper is devoted to the study on the three-dimensional model of transport and suspension sedimentation in the coastal area due to changes in the bottom relief. The model considers the following processes: advective transfer caused by the aquatic medium motion, micro-turbulent diffusion, and gravity sedimentation of suspended particles, as well as the bottom geometry variation caused by the particle settling or bottom sediment rising. The work objective was to conduct an analytical study of the correctness of the initial-boundary value problem corresponding to the constructed model.

Materials and Methods. The change in the bottom relief aids in solution to the initial-boundary value problem for a parabolic equation with the lowest derivatives in a domain whose geometry depends on the desired function of the solution, which in general leads to a nonlinear formulation of the problem. The model is linearized on the time grid due to the "freezing" of the bottom relief within a single step in time and the subsequent recalculation of the bottom surface function on the basis of the changed function of the suspension concentration, as well as a possible change in the velocity vector of the aquatic medium.

Research Results. For the linearized problem, a quadratic functional is constructed, and the uniqueness of the solution to the corresponding initial boundary value problem is proved within the limits of an unspecified time step. On the basis of the quadratic functional transformation, we obtain a prior estimate of the solution norm in the functional space L2 as a function of the integral time estimates of the right side, and the initial condition. Thus, the stability of the solution to the initial

Введение. Настоящая работа посвящена исследованию пространственно-трехмерной модели транспорта и осаждения взвеси в прибрежной зоне с учетом изменения рельефа дна. Модель учитывает следующие процессы: адвективный перенос, обусловленный движением водной среды, микротурбулентную диффузию и гравитационное осаждение частиц взвеси, а также изменение геометрии дна, вызванное осаждением частиц взвеси или подъемом частиц донных отложений.

Целью работы являлось проведение аналитического исследования корректности начально-краевой задачи, соответствующей построенной модели.

Материалы и методы. Изменение рельефа дна приводит к необходимости решать начально-краевую задачу для уравнения параболического типа с младшими производными в области, геометрия которой зависит от искомой функции решения, что приводит, в общем случае, к нелинейной постановке задачи. Выполнена линеаризация модели на временной сетке за счет «замораживания» рельефа дна в пределах одного шага по времени и последующего пересчета функции поверхности дна на основе изменившейся функции концентрации взвешенного вещества, а также возможного изменения вектора скорости движения водной среды.

Результаты исследования. Для линеаризованной задачи построен квадратичный функционал и энергетическим методом доказана единственность решения соответствующей начально-краевой задачи в пределах произвольного шага по времени. На основе преобразования квадратичного функционала получена априорная оценка нормы решения в функциональном пространстве L_2 в зависимости от интегральных оценок по времени правой части, граничных условий и начального условия, и, таким образом, доказана устойчивость решения исходной задачи при из-

problem from the change of the initial and boundary conditions, the right-hand side function, is established.

Discussion and Conclusions. The model can be of value for predicting the spread of contaminants and changes in the bottom topography, both under an anthropogenic impact and due to the natural processes in the coastal area.

менении начального и граничных условий, функции правой части.

Обсуждение и заключения. Модель может представлять ценность при прогнозе распространения загрязнений и изменения рельефа дна, как при антропогенном воздействии, так и в силу естественно протекающих природных процессов в прибрежной зоне.

Introduction. The aquatic habitat protection [1−2] is one of the most important factors that determine the integrated research development of the coastal areas. Damage control over the natural processes, such as pollution, sedimentation, and depletion of water areas, leads to necessity for studying all aspects that affect changes in coastal waters. Maintenance of water bodies in proper condition and timely intervention in its operation mode is directly related to the increase in port capacity and the efficient development of the coastal infrastructure (ensuring an accessway to the berths of ships with a low landing; desilting and aquatic vegetation clearing of the coastal strip; etc.) [3-5]. As a rule, research practice in this field requires the construction of mathematical models that are as close as possible to real processes [6−11].

A continuous mathematical model describing spatial-three-dimensional processes associated with transport and gravitational suspension sedimentation in the aquatic medium with varying bottom relief is considered. This model takes into account micro-turbulent diffusion and advective transfer of suspensions, the effect of gravity on suspension, the presence of the bottom and a free surface, and a bottom contour variation.

The suspension transport model enables to study the hydrophysical processes of aquatic systems, to predict the dynamics of the bottom surface change based on the description of the lifting, transport, sedimentation, changes in the concentration of suspension [12–13]. The uniqueness of the solution to the corresponding initial-boundary value problem is proved, and a prior estimate of the solution norm is obtained depending on the integral estimation of the right-hand side, boundary conditions, and the initial condition.

Materials and Methods. Continuous 3D model of suspension diffusion-convection and the corresponding initial boundary value problem. Consider a continuous mathematical model of sediment spreading in the aqueous media considering diffusion and convection of suspension, gravity action on suspension, presence of the bottom and a free surface. We will use $Oxyz$ Cartesian coordinate system where Ox axis passes along the nonperturbed water surface and is directed toward the sea, and Oz axis is directed vertically downwards. Assume that $h=H+\eta$ is the total water depth, m; H is depth with undisturbed water surface, m; η is elevation of the free surface relative to the geoid (sea level), m (Fig. 1).
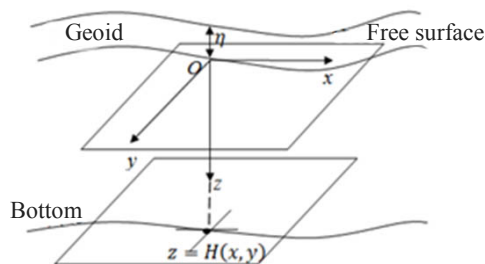
Fig. 1. Introduction of $Oxyz$ coordinate system $Oxyz$

Suppose that in $\overline{G} = \{0 \le x \le L_x, 0 \le y \le L_y, 0 \le z \le H(x,y)\}$ closure region, there are suspensions which have $c = c(x,y,z,t)$ concentration at (x,y,z) point and at t time, mg/l; t is temporary variable, sec. We will also use $L_z \equiv \max\limits_{0 \le x \le L_x, 0 \le y \le L_y} H(x,y)$ notation.

The behavior of the suspended particles will be described by the following system of equations:

$$\begin{cases} \dfrac{\partial c}{\partial t} + \dfrac{\partial(uc)}{\partial x} + \dfrac{\partial(vc)}{\partial y} + \dfrac{\partial\big((w+w_g)c\big)}{\partial z} = \mu_h\left(\dfrac{\partial^2 c}{\partial x^2} + \dfrac{\partial^2 c}{\partial y^2}\right) + \dfrac{\partial}{\partial z}\left(\mu_v \dfrac{\partial c}{\partial z}\right) + F, \\ \dfrac{\partial H}{\partial t} = -\dfrac{\varepsilon}{\rho} w_g c, \end{cases} \tag{1}$$

where *u, v, w* are components of $\vec{U}$ fluid velocity, m/s; w_g is hydraulic size or sedimentation rate, m/s; μ_h, μ_v are coefficients of the horizontal and vertical turbulent diffusion of particles, respectively, m²/s; *F* is power of particle sources; ε is porosity of bottom materials.

Summands on the left side (except for the time derivative) of the first equation of the system (1) describe the advective particle transport due to the inertial motion of the aqueous media, as well as sedimentation under the action of gravity. The summands on the right side describe the suspension diffusion. The vertical diffusion coefficient is chosen different from the horizontal diffusion coefficient due to the fact that the effect of difference between these coefficients is often observed in various media and can be caused by various factors.

As *G* region, we consider $ABCDA_1OC_1D_1$ "parallelepiped" "skewed" to the shore, whose $A_1OC_1D_1$ upper base lies on $(z = 0)$ free surface, and $(z = H(x,y))$ part of the bottom surface is its lower base. Suppose *S* is $\overline{G}$ surface, $\vec{n}$ is the outward normal to the surface of the "skewed parallelepiped". We assume the given $\overrightarrow{U^*}$ as the fluid velocity on $\overline{G}$ side surfaces. Complete with the boundary conditions of first kind for the particle concentration function, this allows determining the suspension flow both towards the coast and along the coast (Fig. 2).
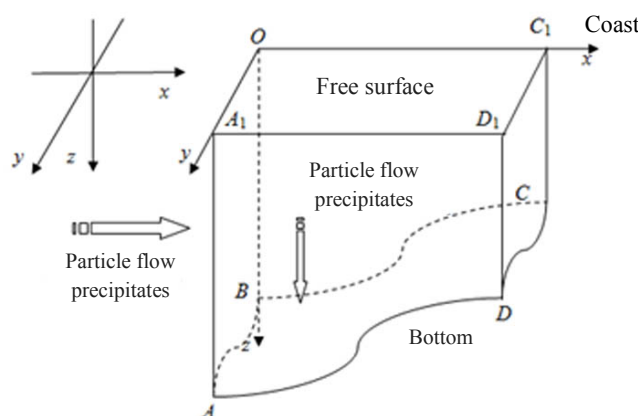
Fig. 2. Solution area for suspension transport

Add the initial and boundary conditions (assuming that the sedimentation is irreversible) to the system (1)
As the initial conditions at $t = 0$ time, we accept

$$c(x,y,z,0) \equiv c_0(x,y,z); \tag{2}$$

$$H(x,y,0) = H_0(x,y). \tag{3}$$

We set boundary conditions on $ABCDA_1OC_1D_1$ faces (we set suspended flows both towards the coast and along the coast):

- on the faces $S_1 \equiv AA_1OB$ $(x = 0,\ 0 \le y \le L_y,\ 0 \le z \le L_z)$, $S_2 \equiv AA_1D_1D$ $(y = L_y,\ 0 \le x \le L_x,\ 0 \le z \le L_z)$ and $S_3 \equiv BOC_1C$ $(y = 0,\ 0 \le x \le L_x,\ 0 \le z \le L_z)$

$$c = c^*, \text{ где } c^* = c^*(x,y,z,t),\ t \in [0,T]; \tag{4}$$

- on the faces $S_4 \equiv DD_1C_1C$ $(x = L_x,\ 0 \le y \le L_y,\ 0 \le z \le L_z)$ and $S_5 \equiv A_1OC_1D_1$ $(z = 0,\ 0 \le x \le L_x,\ 0 \le y \le L_y)$

$$c = 0; \tag{5}$$

- on the surface $S_6 \equiv ABCD$ $(z = H(x,y,t),\ 0 \le x \le L_x,\ 0 \le y \le L_y)$

$$\frac{\partial c}{\partial n} = -\frac{w_g}{\mu_v}c \quad \text{или} \quad \frac{\partial c}{\partial z} = -\frac{w_g}{\mu_v}c \ . \tag{6}$$

The boundary condition (5) occurs with a relatively small slope of the bottom:

$$\max_{S_6}\sqrt{\left(\frac{\partial H}{\partial x}\right)^2 + \left(\frac{\partial H}{\partial y}\right)^2} \ll 1.$$

The following condition of the solution domain nondegeneracy is set up for all (x, y, t) at which the initial boundary value problem is formulated:

$$H(x, y, t) \geq h_0 \equiv const > 0, \qquad 0 \leq t \leq T. \tag{7}$$

When studying combined models of sediment and suspension transport, it is possible to increase the concentration of suspended particles in the bottom layer due to the rising bottom sediment particles if the shear stress exceeds of a certain critical value is exceeded[13–16]. Then, instead of the boundary condition (6), we will consider the boundary condition of the following form

$$\frac{\partial c}{\partial z} = \alpha c, \quad \alpha = const > 0. \tag{8}$$

Linearization of the initial-boundary value problem of transport and suspension sedimentation. To create a linearized model on $0 \leq t \leq T$ time interval, we construct a uniform grid $\omega\tau$ with a step τ, that is, a set of points $\omega_\tau = \{t_n = n\tau, \ n = 0,1,...,N, \ N\tau = T\}$.
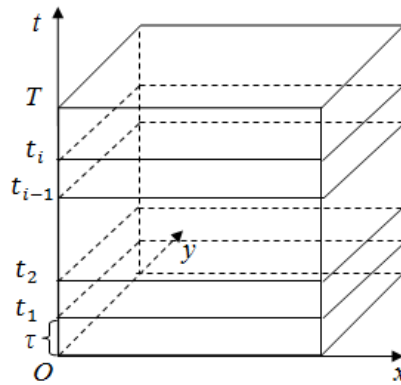
Fig. 3.Construction of time grid

$c^{(n)}(x, y, z, t_{n-1})$ and $H^{(n)}(x, y, t_{n-1})$ functions are determined at each step of ω_τ time grid. If $n = 1$, then functions of the initial condition will suffice to $c^{(1)}(x, y, z, t_0)$, $H^{(1)}(x, y, t_0)$, viz $c^{(1)}(x, y, z, 0) \equiv c_0(x, y, z)$, $H^{(1)}(x, y, t_0) \equiv H_0(x, y)$ respectively. But if $n = 2,..., N$, then $c^{(n)}(x, y, z, t_{n-1}) = c^{(n-1)}(x, y, z, t_{n-1})$ functions are assumed to be known, since the problem (1)−(6) for the previous $t_{n-2} < t \leq t_{n-1}$ time interval is supposed to be solved.

We write the system (1) on $t_{n-1} < t \leq t_n$ interval in the form:

$$\begin{cases} \dfrac{\partial c^{(n)}}{\partial t} + \dfrac{\partial(uc^{(n)})}{\partial x} + \dfrac{\partial(vc^{(n)})}{\partial y} + \dfrac{\partial((w+w_g)c^{(n)})}{\partial z} = \mu_h\left(\dfrac{\partial^2 c^{(n)}}{\partial x^2} + \dfrac{\partial^2 c^{(n)}}{\partial y^2}\right) + \dfrac{\partial}{\partial z}\left(\mu_v\dfrac{\partial c^{(n)}}{\partial z}\right) + F, \\ \dfrac{\partial H^{(n)}}{\partial t} = -\dfrac{\varepsilon}{\rho}w_g c^{(n)} \end{cases} \tag{9}$$

and complete it with the initial conditions:

$$c^{(1)}(x, y, z, t_0) = c_0(x, y, z), c^{(n)}(x, y, z, t_{n-1}) = c^{(n-1)}(x, y, z, t_{n-1}), \quad n = 2,..., N. \tag{10}$$

$$H^{(1)}(x, y, t_0) = H_0(x, y), H^{(n)}(x, y, t_{n-1}) = H^{(n-1)}(x, y, t_{n-1}), \quad n = 2,..., N. \tag{11}$$

The boundary conditions (4)−(6) are assumed to be fulfilled for all $t_{n-1} \leq t \leq t_n$ time intervals.

Mechanics

353

By defining $c^{(n)}(x,y,z,t_{n-1}) = c^{(n-1)}(x,y,z,t_{n-1})$ function on $t_{n-1} < t \le t_n$ time interval, we can find $H^{(n)}(x,y,t_{n-1})$ function. For this end, we integrate both members of the second equation of the system (9) over $t_{n-1} \le t \le t_n$ variable. We will get

$$\int_{t_{n-1}}^{t_n} \frac{\partial H^{(n)}}{\partial t} dt = -\frac{\varepsilon}{\rho} w_g \int_{t_{n-1}}^{t_n} c^{(n)} dt. \tag{12}$$

From the equality (12), it is not difficult to get

$$H^{(n)} = H^{(n-1)} - \frac{\varepsilon}{\rho} w_g \sum_{n=1}^{N} \int_{t_{n-1}}^{t_n} c^{(n)} dt. \tag{13}$$

We introduce $G_{n-1} = \left\{0 < x < L_x, 0 < y < L_y, 0 < z < H^{n-1}(x,y,t_{n-1})\right\}$ domain at each $t_{n-1} \le t \le t_n$ time step.

We have a chain of linear initial-boundary value problems for each time layer, where the system of the type

$$\begin{cases} \dfrac{\partial c^{(n)}}{\partial t} + \dfrac{\partial \left(uc^{(n)}\right)}{\partial x} + \dfrac{\partial \left(vc^{(n)}\right)}{\partial y} + \dfrac{\partial \left((w+w_g)c^{(n)}\right)}{\partial z} = \mu_h\left(\dfrac{\partial^2 c^{(n)}}{\partial x^2} + \dfrac{\partial^2 c^{(n)}}{\partial y^2}\right) + \dfrac{\partial}{\partial z}\left(\mu_v \dfrac{\partial c^{(n)}}{\partial z}\right) + F, \\ (x,y,z) \in G_{n-1}, \quad G_{n-1} = \left\{0 < x < L_x, \ 0 < y < L_y, \ 0 < z < H^{n-1}(x,y,t_{n-1})\right\}, \\ H^{(n)} = H^{(n-1)} - \dfrac{\varepsilon}{\rho} w_g \sum_{n=1}^{N} \int_{t_{n-1}}^{t_n} c^{(n)} dt, \quad n = 1,2,...,N. \end{cases} \tag{14} \tag{15}$$

is considered for $t_{n-1} \le t \le t_n$ interval with the initial conditions:

$$c^{(n)}(x,y,z,t_{n-1}) = c^{(n-1)}(x,y,z,t_{n-1}), \tag{16}$$

$$H^{(n)}(x,y,t_{n-1}) = H^{(n-1)}(x,y,t_{n-1}). \tag{17}$$

Note that at each time step, the boundary surfaces will change (except S_5 face). Considering $t_{n-1} \le t \le t_n$ time interval, we set the boundary conditions on the edges of G_{n-1} domain:

- on $S_{1,n-1}\left(x=0, \ 0 \le y \le L_y, \ 0 \le z \le H^{(n-1)}(0,y,t_{n-1})\right)$, $S_{2,n-1}\left(y=L_y, \ 0 \le x \le L_x, \ 0 \le z \le H^{(n-1)}(x,L_y,t_{n-1})\right)$ and $S_{3,n-1}\left(y=0, \ 0 \le x \le L_x, \ 0 \le z \le H^{(n-1)}(x,0,t_{n-1})\right)$ faces

$$c^{(n)} = c^*, \text{ где } c^* = c^*(x,y,z,t), \ t \in [t_{n-1},t_n]; \tag{18}$$

- on $S_{4,n-1}\left(x=L_x, \ 0 \le y \le L_y, \ 0 \le z \le H^{(n-1)}(L_x,y,t_{n-1})\right)$ и $S_{5,n-1}\left(z=0, \ 0 \le x \le L_x, \ 0 \le y \le L_y\right) \equiv A_1OC_1D_1$ faces

$$c^{(n)} = 0; \tag{19}$$

- on $S_{6,n-1}\left(z=H^{(n-1)}(x,y,t_{n-1}), \ 0 \le x \le L_x, \ 0 \le y \le L_y\right)$ surface

$$\frac{\partial c^{(n)}}{\partial n} = -\frac{w_g}{\mu_v} c^{(n)} \text{ или } \frac{\partial c^{(n)}}{\partial z} = -\frac{w_g}{\mu_v} c^{(n)}. \tag{20}$$

The boundary condition (8) will be replaced by the following

$$\frac{\partial c^{(n)}}{\partial z} = \alpha c^{(n)}, \quad \alpha = const > 0. \tag{21}$$

Thus, it is supposed that the bottom relief within this time step, when calculating the distribution of suspension concentrations, does not change and is taken from the previous time layer. First of all, at this $t_{n-1} \le t \le t_n$ time step, the initial-boundary value problem for the convection-diffusion equation (14) with $H^{(n-1)}$ fixed bottom relief function is solved, and only then the update (recomputation) of $H^{(n)}$ relief function is performed in accordance with the equality (15).

The determination of the conditions of existence, uniqueness and continuous dependence of the solution on the input problem data is carried out on a fixed time layer under these assumptions and subject to the condition (7).

The authors do not plan to study the existence of solutions to the initial-boundary value problems (14) - (20) and (14) - (19), (21) in this paper. Questions of the existence of solutions to the initial-boundary value problems for

parabolic equations with lower derivatives (diffusion-convection equations) are considered, for example, in the monographs [17–18].

Research Results. Investigating uniqueness of the solution to the initial-boundary problem of suspension transport.

Consider the initial boundary value problem (14) - (20) formulated for the arbitrary $t_{n-1} < t \leq t_n$ time layer.

Multiply the left and right member of equation (14) by $c^{(n)}$ function and get:

$$\frac{\partial c^{(n)}}{\partial t} + \frac{\partial \left(u c^{(n)} \right)}{\partial x} + \frac{\partial \left(v c^{(n)} \right)}{\partial y} + \frac{\partial \left(\left(w + w_g \right) c^{(n)} \right)}{\partial z} = \mu_h c^{(n)} \left(\frac{\partial^2 c^{(n)}}{\partial x^2} + \frac{\partial^2 c^{(n)}}{\partial y^2} \right) + c^{(n)} \frac{\partial}{\partial z} \left(\mu_v \frac{\partial c^{(n)}}{\partial z} \right) + c^{(n)} F . \tag{22}$$

The left member of the equality (22) can be transformed as follows:

$$c^{(n)} \frac{\partial c^{(n)}}{\partial t} + c^{(n)} \left(\frac{\partial \left(u c^{(n)} \right)}{\partial x} + \frac{\partial \left(v c^{(n)} \right)}{\partial y} + \frac{\partial \left(\left(w + w_g \right) c^{(n)} \right)}{\partial z} \right) = \frac{1}{2} \frac{\partial \left(c^{(n)} \right)^2}{\partial t} + c^{(n)} div \left(c^{(n)} \vec{U} \right) =$$

$$= \frac{1}{2} \frac{\partial \left(c^{(n)} \right)^2}{\partial t} + \frac{1}{2} div \left(\left(c^{(n)} \right)^2 \vec{U} \right) \quad , \tag{23}$$

where $\vec{U} = \left\| u, v, w + w_g \right\|^T$.

With regard to (23), the equation (22) will be written as

$$\frac{1}{2} \frac{\partial \left(c^{(n)} \right)^2}{\partial t} + \frac{1}{2} div \left(\left(c^{(n)} \right)^2 \vec{U} \right) = \mu_h c^{(n)} \left(\frac{\partial^2 c^{(n)}}{\partial x^2} + \frac{\partial^2 c^{(n)}}{\partial y^2} \right) + c^{(n)} \frac{\partial}{\partial z} \left(\mu_v \frac{\partial c^{(n)}}{\partial z} \right) + c^{(n)} F . \tag{24}$$

Then we integrate both members of the equation (24) over $t_{n-1} \leq t \leq t_n$ interval, and, after that, over the spatial variables in G_{n-1} domain. In the first term, the order of integration is changed due to the Fubini theorem [19]. We obtain

$$\iiint_{G_{n-1}} \frac{1}{2} \left(\int_{t_{n-1}}^{t_n} \frac{\partial \left(c^{(n)} \right)^2}{\partial t} dt \right) dG_{n-1} + \int_{t_{n-1}}^{t_n} \frac{1}{2} \left(\iiint_{G_{n-1}} div \left(\left(c^{(n)} \right)^2 \vec{U} \right) dG_{n-1} \right) dt =$$

$$= \int_{t_{n-1}}^{t_n} \left(\iiint_{G_{n-1}} c^{(n)} \mu_h \left(\frac{\partial^2 c^{(n)}}{\partial x^2} + \frac{\partial^2 c^{(n)}}{\partial y^2} \right) dG_{n-1} \right) dt + \int_{t_{n-1}}^{t_n} \left(\iiint_{G_{n-1}} c^{(n)} \frac{\partial}{\partial z} \left(\mu_v \frac{\partial c^{(n)}}{\partial z} \right) dG_{n-1} \right) dt + \tag{25}$$

$$\int_{t_{n-1}}^{t_n} \left(\iiint_{G_{n-1}} c^{(n)} F dG_{n-1} \right) dt.$$

The first term on the left side of the equation (25) is obviously equal to

$$\iiint_{G_{n-1}} \frac{1}{2} \left(\int_{t_{n-1}}^{t_n} \frac{\partial \left(c^{(n)} \right)^2}{\partial t} dt \right) dG_{n-1} = \iiint_{G_{n-1}} \frac{1}{2} \left(\left(c^{(n)} \right)^2 \left(x, y, z, t_n \right) - \left(c^{(n)} \right)^2 \left(x, y, z, t_{n-1} \right) \right) dG_{n-1} . \tag{26}$$

Next, we turn to the transformation of the second term of the left-hand side of the equality (25). Considering the Gauss-Ostrogradsky formula and the boundary conditions (18) - (20), it can be written as [20]:

$$\int_{t_{n-1}}^{t_n} \left(\frac{1}{2} \iiint_{G_{n-1}} div \left(\left(c^{(n)} \right)^2 \vec{U} \right) dG_{n-1} \right) dt = \frac{1}{2} \int_{t_{n-1}}^{t_n} \left(\iint_{S_{1,n-1}} \left(c^* \right)^2 \left(\overrightarrow{U^*}, \vec{n} \right) dydz \right) dt + \frac{1}{2} \int_{t_{n-1}}^{t_n} \left(\iint_{S_{6,n-1}} c^2 w_g dxdy \right) dt +$$

$$+ \int_{t_{n-1}}^{t_n} \left(\iint_{S_{3,n-1}} \left(c^* \right)^2 \left(\overrightarrow{U^*}, \vec{n} \right) dxdz \right) dt + \frac{1}{2} \int_{t_{n-1}}^{t_n} \left(\iint_{S_{2,n-1}} \left(c^* \right)^2 \left(\overrightarrow{U^*}, \vec{n} \right) dxdz \right) dt = -\frac{1}{2} \int_{t_{n-1}}^{t_n} \left(\iint_{S_{1,n-1}} \left(c^* \right)^2 udydz \right) dt - \tag{27}$$

$$- \frac{1}{2} \int_{t_{n-1}}^{t_n} \left(\iint_{S_{3,n-1}} \left(c^* \right)^2 vdxdz \right) dt + \frac{1}{2} \int_{t_{n-1}}^{t_n} \left(\iint_{S_{2,n-1}} \left(c^* \right)^2 vdxdz \right) dt + \frac{1}{2} \int_{t_{n-1}}^{t_n} \left(\iint_{S_{6,n-1}} \left(c^{(n)} \right)^2 w_g dxdy \right) dt.$$

where $\overrightarrow{U^*}$ is the known velocity of the aquatic medium on the faces where the boundary conditions of the first kind are specified; in fact, these are all side faces, except for $S_{4,n-1}$ and $S_{5,n-1}$ top cover on which the suspension concentration is zero, and therefore the flows through them are zero.

Let us turn to the transformation of the right side of the equation (25). The following equality occurs

Mechanics

$$\iiint_{G_{n-1}} \left[c^{(n)} \left(\mu_h \frac{\partial}{\partial x} \left(\frac{\partial c^{(n)}}{\partial x} \right) + \mu_h \frac{\partial}{\partial y} \left(\frac{\partial c^{(n)}}{\partial y} \right) + \frac{\partial}{\partial z} \left(\mu_v \frac{\partial c^{(n)}}{\partial z} \right) \right) \right] dG_{n-1} =$$

$$= \iiint_{G_{n-1}} \left[\mu_h \frac{\partial}{\partial x} \left(c^{(n)} \frac{\partial c^{(n)}}{\partial x} \right) + \mu_h \frac{\partial}{\partial y} \left(c^{(n)} \frac{\partial c^{(n)}}{\partial y} \right) + \frac{\partial}{\partial z} \left(c^{(n)} \mu_v \frac{\partial c^{(n)}}{\partial z} \right) \right] dG_{n-1} - \tag{28}$$

$$- \iiint_{G_{n-1}} \left[\mu_h \left(\frac{\partial c^{(n)}}{\partial x} \right)^2 + \mu_h \left(\frac{\partial c^{(n)}}{\partial y} \right)^2 + \mu_v \left(\frac{\partial c^{(n)}}{\partial z} \right)^2 \right] dG_{n-1}.$$

Suppose $\vec{Q} = \{Q_x, Q_y, Q_z\} = \left\{ \mu_h c^{(n)} \frac{\partial c^{(n)}}{\partial x}, \mu_h c^{(n)} \frac{\partial c^{(n)}}{\partial y}, c^{(n)} \mu_v \frac{\partial c^{(n)}}{\partial z} \right\}$. Then, in virtue of the Gauss-Ostrogradsky

theorem, we have:

$$\iiint_{G_{n-1}} \left[\mu_h \frac{\partial}{\partial x} \left(c^{(n)} \frac{\partial c^{(n)}}{\partial x} \right) + \mu_h \frac{\partial}{\partial y} \left(c^{(n)} \frac{\partial c^{(n)}}{\partial y} \right) + \frac{\partial}{\partial z} \left(c^{(n)} \mu_v \frac{\partial c^{(n)}}{\partial z} \right) \right] dG_{n-1} = \iiint_{G_{n-1}} div\vec{Q} dG =$$

$$= \iint_{S_{2,n-1}} Q_y dxdz + \iint_{S_{4,n-1}} Q_x dydz + \iint_{S_{3,n-1}} Q_y dxdz + \iint_{S_{1,n-1}} Q_x dydz + \iint_{S_{6,n-1}} Q_z dxdy + \iint_{S_{5,n-1}} Q_z dxdy = \tag{29}$$

$$= \iint_{S_{2,n-1}} Q_y dxdz + \iint_{S_{3,n-1}} Q_y dxdz + \iint_{S_{1,n-1}} Q_x dydz + \iint_{S_{6,n-1}} Q_z dxdy.$$

Transforming each term from the right-hand side of (29) subject to the conditions on the boundary (18) - (20), we obtain

$$\iiint_{G_{n-1}} \left[\mu_h \frac{\partial}{\partial x} \left(c^{(n)} \frac{\partial c^{(n)}}{\partial x} \right) + \mu_h \frac{\partial}{\partial y} \left(c^{(n)} \frac{\partial c^{(n)}}{\partial y} \right) + \frac{\partial}{\partial z} \left(c^{(n)} \mu_v \frac{\partial c^{(n)}}{\partial z} \right) \right] dG_{n-1} =$$

$$= \iint_{S_{2,n-1}} c^* \mu_h \frac{\partial c^*}{\partial y} dxdz + \iint_{S_{3,n-1}} c^* \mu_h \frac{\partial c^*}{\partial y} dxdz + \iint_{S_{1,n-1}} c^* \mu_h \frac{\partial c^*}{\partial x} dydz - \iint_{S_{6,n-1}} w_g \left(c^{(n)} \right)^2 dxdy. \tag{30}$$

In virtue of (26), (28), (29) and (30), the equality (25) takes on form

$$\frac{1}{2} \iiint_{G_{n-1}} \left(c^{(n)} \right)^2 (x,y,z,t_n) dG_{n-1} - \int_{t_{n-1}}^{t_n} \left(\iint_{S_{1,n-1}} \left(\frac{1}{2} \left(c^* \right)^2 u + c^* \mu_h \frac{\partial c^*}{\partial x} \right) dydz \right) dt -$$

$$- \int_{t_{n-1}}^{t_n} \left(\iint_{S_{3,n-1}} \left(\frac{1}{2} \left(c^* \right)^2 v + c^* \mu_h \frac{\partial c^*}{\partial y} \right) dxdz \right) dt + \int_{t_{n-1}}^{t_n} \left(\iint_{S_{2,n-1}} \left(\frac{1}{2} \left(c^* \right)^2 v - c^* \mu_h \frac{\partial c^*}{\partial y} \right) dxdz \right) dt +$$

$$+ \frac{3}{2} \int_{t_{n-1}}^{t_n} \left(\iint_{S_{6,n-1}} w_g \left(c^{(n)} \right)^2 dxdy \right) dt + \int_{t_{n-1}}^{t_n} \left[\iiint_{G_{n-1}} \left(\left(\frac{\partial c^{(n)}}{\partial x} \right)^2 + \mu_h \left(\frac{\partial c^{(n)}}{\partial y} \right)^2 + \mu_v \left(\frac{\partial c^{(n)}}{\partial z} \right)^2 \right) dG_{n-1} \right] dt = \tag{31}$$

$$= \frac{1}{2} \iiint_{G_{n-1}} \left(c^{(n)} \right)^2 (x,y,z,t_{n-1}) dG_{n-1} + \int_{t_{n-1}}^{t_n} \left(\iiint_{G_{n-1}} c^{(n)} F dG_{n-1} \right) dt.$$

The identity (31) will be fundamental under studying the uniqueness and obtaining a prior estimate of the solution norm of the initial boundary value problem (14) - (20). In case of replacing the boundary condition (20) with the boundary condition (21), the quadratic functional (31) changes as follows:

$$\frac{1}{2} \iiint_{G_{n-1}} \left(c^{(n)} \right)^2 (x,y,z,t_n) dG_{n-1} - \int_{t_{n-1}}^{t_n} \left(\iint_{S_{1,n-1}} \left(\frac{1}{2} \left(c^* \right)^2 u + c^* \mu_h \frac{\partial c^*}{\partial x} \right) dydz \right) dt -$$

$$- \int_{t_{n-1}}^{t_n} \left(\iint_{S_{3,n-1}} \left(\frac{1}{2} \left(c^* \right)^2 v + c^* \mu_h \frac{\partial c^*}{\partial y} \right) dxdz \right) dt + \int_{t_{n-1}}^{t_n} \left(\iint_{S_{2,n-1}} \left(\frac{1}{2} \left(c^* \right)^2 v - c^* \mu_h \frac{\partial c^*}{\partial y} \right) dxdz \right) dt +$$

$$+ \int_{t_{n-1}}^{t_n} \left(\iint_{S_{6,n-1}} \left(\frac{1}{2} w_g - \alpha \mu_v \right) \left(c^{(n)} \right)^2 dxdy \right) dt + \int_{t_{n-1}}^{t_n} \left[\iiint_{G_{n-1}} \left(\left(\frac{\partial c^{(n)}}{\partial x} \right)^2 + \mu_h \left(\frac{\partial c^{(n)}}{\partial y} \right)^2 + \mu_v \left(\frac{\partial c^{(n)}}{\partial z} \right)^2 \right) dG_{n-1} \right] dt = \tag{32}$$

$$= \frac{1}{2} \iiint_{G_{n-1}} \left(c^{(n)} \right)^2 (x,y,z,t_{n-1}) dG_{n-1} + \int_{t_{n-1}}^{t_n} \left(\iiint_{G_{n-1}} c^{(n)} F dG_{n-1} \right) dt.$$

Suppose that the equation (14) with the same conditions (16) - (20) satisfy two different solutions to $c_1 = c_1(x,y,z,t)$, $c_2 = c_2(x,y,z,t)$ problem. For their $\tilde{c} = c_1 - c_2$ difference, the following initial-boundary problem is valid:

Sukhinov A. I.and the others. Development and correctness analysis of the mathematical model of transport and suspension sedimentation

Сухинов А. И. и др. Построение и исследование корректности математической модели транспорта и осаждения взвесей

$$\frac{\partial \tilde{c}}{\partial t} + \frac{\partial \left(u\tilde{c}\right)}{\partial x} + \frac{\partial \left(v\tilde{c}\right)}{\partial y} + \frac{\partial \left(\left(w + w_g\right)\tilde{c}\right)}{\partial z} = \mu_h \left(\frac{\partial^2 \tilde{c}}{\partial x^2} + \frac{\partial^2 \tilde{c}}{\partial y^2}\right) + \frac{\partial}{\partial z}\left(\mu_v \frac{\partial \tilde{c}}{\partial z}\right),$$ (33)

$$\tilde{c}\left(x, y, z, 0\right) = 0, \quad \left(x, y, z\right) \in \overline{G}_{n-1},$$ (34)

- on $S_{1,n-1}$, $S_{2,n-1}$, $S_{3,n-1}$, $S_{4,n-1}$, $S_{5,n-1}$ faces

$$\tilde{c} = c^* - c^* = 0 ;$$ (35)

- on $S_{6,n-1}$ surface

$$\frac{\partial \tilde{c}}{\partial z} = -\frac{w_g}{\mu_v}\left(c_1 - c_2\right) = -\frac{w_g}{\mu_v}\tilde{c} .$$ (36)

For $\tilde{c}$ function, the equality (33) will take the form considering the equalities (34)−(36)

$$\frac{1}{2}\iiint\limits_{G_{n-1}} \tilde{c}^2\left(x, y, z, t_n\right)dG_{n-1} + \frac{3}{2}\int\limits_{t_{n-1}}^{t_n}\left(\iint\limits_{S_{6,n-1}} w_g \tilde{c}^2 dxdy\right)dt +$$
$$+ \int\limits_{t_{n-1}}^{t_n}\left[\iiint\limits_{G_{n-1}}\left[\mu_h\left(\frac{\partial \tilde{c}}{\partial x}\right)^2 + \mu_h\left(\frac{\partial \tilde{c}}{\partial y}\right)^2 + \mu_v\left(\frac{\partial \tilde{c}}{\partial z}\right)^2\right]dG_{n-1}\right]dt = 0.$$ (37)

Since $w_g > 0$ and other known values under the sign of integrals are positive $\mu h> 0$, $\mu v> 0$, then the equality (36) is satisfied only under the condition

$$\tilde{c}\left(x, y, z, t\right) \equiv 0, \quad \left(x, y, z\right) \in G_{n-1}, \quad t_{n-1} < t \le t_n,$$ (38)

which completes the proof of the uniqueness of the initial-boundary value problem (14) - (20) solution.

In case of replacing the boundary condition (20) by the relation (21), instead of the expression (37), we obtain the following equality

$$\frac{1}{2}\iiint\limits_{G_{n-1}} \tilde{c}^2\left(x, y, z, t_n\right)dG_{n-1} + \int\limits_{t_{n-1}}^{t_n}\left(\iint\limits_{S_{6,n-1}}\left(\frac{1}{2}w_g - \alpha\mu_v\right)\tilde{c}^2 dxdy\right)dt +$$
$$+ \int\limits_{t_{n-1}}^{t_n}\left[\iiint\limits_{G_{n-1}}\left[\mu_h\left(\frac{\partial \tilde{c}}{\partial x}\right)^2 + \mu_h\left(\frac{\partial \tilde{c}}{\partial y}\right)^2 + \mu_v\left(\frac{\partial \tilde{c}}{\partial z}\right)^2\right]dG_{n-1}\right]dt = 0.$$ (39)

We require the fulfillment of the inequality

$$\frac{1}{2}w_g - \alpha\mu_v \ge 0, \quad \left(x, y, z\right) \in S_{6,n-1}, \quad t_{n-1} < t \le t_n$$

or

$$\alpha \le \frac{w_g}{2\mu_v}, \quad \left(x, y, z\right) \in S_{6,n-1}, \quad t_{n-1} < t \le t_n,$$ (40)

then all the terms in the equation (39) are nonnegative, and zero equality is possible if and only if $\tilde{c}\left(x, y, z, t\right) \equiv 0, \quad \left(x, y, z\right) \in G_{n-1}, \quad t_{n-1} < t \le t_n$, that means the solution uniqueness and in this case.

Reasoning is similarly repeated for all layers of ω_τ time grid. The modification of the boundary conditions associated with the continuous change in the bottom relief depending on the time variable requires additional study and is going beyond the scope of this article.

Theorem. Suppose we are given a system of equations

$$\begin{cases} \dfrac{\partial c^{(n)}}{\partial t} + \dfrac{\partial \left(uc^{(n)}\right)}{\partial x} + \dfrac{\partial \left(vc^{(n)}\right)}{\partial y} + \dfrac{\partial \left(\left(w + w_g\right)c^{(n)}\right)}{\partial z} = \mu_h\left(\dfrac{\partial^2 c^{(n)}}{\partial x^2} + \dfrac{\partial^2 c^{(n)}}{\partial y^2}\right) + \dfrac{\partial}{\partial z}\left(\mu_v \dfrac{\partial c^{(n)}}{\partial z}\right) + F, \\ \left(x, y, z\right) \in G_{n-1} , \quad G_{n-1} = \left\{0 < x < L_x, 0 < y < L_y, 0 < z < H^{n-1}\left(x, y, t_{n-1}\right)\right\}, \\ H^{(n)} = H^{(n-1)} - \dfrac{\varepsilon}{\rho}w_g \sum\limits_{n=1}^{N}\int\limits_{t_{n-1}}^{t_n} c^{(n)}dt, \quad n = 1, 2, ..., N \end{cases}$$

in $\Omega_{n-1} = G_{n-1} \times \left(t_{n-1} < t < t_n\right)$, $G_{n-1} = \left(0 < x < L_x, 0 < y < L_y, 0 < z < H^{(n-1)}\left(x, y, t_{n-1}\right)\right)$,   simply connected domain with a sufficiently smooth boundary defined by the smoothness of $z = H^{(n-1)}\left(x, y\right)$, $0 \le x \le L_x$, $0 \le y \le L_y$ function with the

initial and boundary conditions (16) - (20). Let the functions of $c^{(n)}(x,y,z,t_{n-1})$ solution, the velocity vector of $\|u,v,w+w_g\|^T$ aquatic medium, $c^{(n-1)}(x,y,z,t_{n-1})$ initial condition, $F(x,y,z,t)$, right member of $c^*(x,y,z,t)$ boundary condition, $\mu_v = \mu_v(z), (x,y,z) \in G_{n-1}$ coefficient of $\mu_v = \mu_v(z), (x,y,z) \in G_{n-1}$ vertical turbulent exchange satisfy the following smoothness conditions:

$$c^{(n)}(x,y,z,t_{n-1}) \in C^2(\Omega_{n-1}) \cap C(\overline{\Omega}_{n-1}), \qquad grad\, c^{(n)} \in C(\overline{\Omega}_{n-1}), \qquad \|u,v,w+w_g\|^T \in C^1(\Omega_{n-1}) \cap C(\overline{\Omega}_{n-1}),$$

$$c^{(n-1)}(x,y,z,t_{n-1}) \in C(\overline{G}_{n-1}) \quad, \qquad F(x,y,z,t) \in C(\Omega_{n-1}) \quad, \qquad \mu_v(x,y,z) \in C^1(G_{n-1}) \cap C(\overline{G}_{n-1}) \quad,$$

$$c^*(x,y,z,t) \in C(S_{n-1}) \times [t_{n-1} \le t \le t_n], \qquad\qquad S_{n-1} = \overline{G}_{n-1} \setminus G_{n-1} \qquad\qquad\qquad,$$

$$\frac{\partial c^*}{\partial n} \in C\Big(\big(0 \le x \le L_x, \quad 0 \le y \le L_y, \quad z = H^{(n-1)}(x,y) \big) \times [t_{n-1} \le t \le t_n] \Big) \quad, \quad \text{as} \quad \text{well} \quad \text{as} \quad c^*(x,y,z,0) = c_0(x,y,z),$$

$$(x,y,z) \in S_{n-1} \setminus \big(0 < x < L_x, 0 < y < L_y, \quad z = H^{(n-1)}(x,y) \big), \qquad\qquad \frac{\partial c_0}{\partial z} = -\frac{\mu_v}{w_g} c^*,$$

$$\big(0 < x < L_x, 0 < y < L_y, \quad z = H^{(n-1)}(x,y) \big), \qquad \text{conditions of consistency of the boundary and initial conditions, then the}$$

solution to this problem exists and is unique.

Comment. In case of replacing the boundary condition (20) with the boundary condition (21), the inequality (40) should be added as a sufficient condition for the previous theorem.

Studying the continuous dependence of the solutions to the initial-boundary value problem of suspension transport on the initial, boundary conditions and the right-hand side function. The next stage is connected with the study of the continuous solution dependence on the functions of the right-hand side, boundary and initial conditions for the system (14)–(15).

Suppose that

$$c^* \ge c_0^* \equiv const > 0,$$
$$0 \le x \le L_x, \quad 0 \le y \le L_y, \quad 0 < z < H^{(n)}(x,y,t_{n-1}), \quad t_{n-1} \le t \le t_n. \tag{41}$$

For convenience, we introduce the notations: union of all parts of the lateral cylindrical surface (boundaries of G_{n-1} region) is denoted as $S_{c,n-1}$, and the lower base of region – as $G_{n-1} - S_{b,n-1}$. In virtue of the smoothness conditions listed under the above theorem, extrema of functions on the bounded closed sets are reached:

$$M_{1,n-1} \equiv \max_{\Omega_{n-1}} \big\{ |c^{(n)}| \big\}, \quad M_{2,n-1} \equiv \max_{S_{n-1}} \bigg\{ \bigg| \frac{\partial c^{(n)}}{\partial x} \bigg|, \bigg| \frac{\partial c^{(n)}}{\partial y} \bigg| \bigg\},$$
$$M_{3,n-1} \equiv \max_{S_{c,n-1}} \big\{ \mu_h \big\}, \quad M_{4,n-1} \equiv \max_{S_{c,n-1} \times [t_{n-1} \le t \le t_n]} \big\{ |u|, |v| \big\}, \quad M_{5,n-1} \equiv \min_{\overline{G}_{n-1}} \big\{ \mu_h, \mu_v \big\}. \tag{42}$$

We will focus on the equation (31) if the boundary condition (20) is used, and on the equality (32) in case of the boundary condition (21). Evoking Friedrichs inequality, we have a chain of inequalities:

$$\iiint_{G_{n-1}} \bigg(\mu_h \bigg(\frac{\partial c^{(n)}}{\partial x} \bigg)^2 + \mu_h \bigg(\frac{\partial c^{(n)}}{\partial y} \bigg)^2 + \mu_v \bigg(\frac{\partial c^{(n)}}{\partial z} \bigg)^2 \bigg) dG_{n-1} \ge$$

$$\ge \min_{G_{n-1}} \big\{ \mu_h, \mu_v \big\} \iiint_{G_{n-1}} \bigg(\bigg(\frac{\partial c^{(n)}}{\partial x} \bigg)^2 + \bigg(\frac{\partial c^{(n)}}{\partial y} \bigg)^2 + \bigg(\frac{\partial c^{(n)}}{\partial z} \bigg)^2 \bigg) dG_{n-1} \ge \tag{43}$$

$$\ge M_{5,n-1} \bigg(\pi^2 \bigg(\frac{1}{L_x^2} + \frac{1}{L_y^2} + \frac{1}{\big(H^{(n-1)}\big)^2} \bigg) \bigg) \iiint_{G_{n-1}} \big(c^{(n)} \big)^2 dG_{n-1}.$$

We turn to the equation (26) from which, in virtue of (42) and (43), we obtain the inequality:

$$\iiint\limits_{G_{n-1}}\left(c^{(n)}\right)^2 dG_{n-1} + 2M_{5,n-1}\left(\pi^2\left(\frac{1}{L_x^2}+\frac{1}{L_y^2}+\frac{1}{\left(H^{(n-1)}\right)^2}\right)\right)\int\limits_{t_{n-1}}^{t_n}\left(\iiint\limits_{G_{n-1}}\left(c^{(n)}\right)^2 dG_{n-1}\right)dt +$$

$$+3\int\limits_{t_{n-1}}^{t_n}\left(\iint\limits_{S_{b,n-1}} w_g\left(c^{(n)}\right)^2 dxdy\right)dt \leq \iiint\limits_{G_{n-1}} c_0^2 dG_{n-1} + M_{4,n-1}\int\limits_{t_{n-1}}^{t_n}\left(\iint\limits_{S_{c,n-1}}\left(c^*\right)^2 dS_{n-1}\right)dt + \tag{44}$$

$$+2M_{2,n-1}M_{3,n-1}\int\limits_{t_{n-1}}^{t_n}\left(\iint\limits_{S_{c,n-1}}\left|c^*\right|dS_{n-1}\right)dt + 2M_{1,n-1}\int\limits_{t_{n-1}}^{t_n}\left(\iiint\limits_{G_{n-1}}|F|dG_{n-1}\right)dt.$$

From inequality (44), there are two inequalities

$$\iiint\limits_{G_{n-1}}\left(c^{(n)}\right)^2 dG_{n-1} \leq \iiint\limits_{G_{n-1}} c_0^2 dG_{n-1} + M_{4,n-1}\int\limits_{t_{n-1}}^{t_n}\left(\iint\limits_{S_{c,n-1}}\left(c^*\right)^2 dS_{n-1}\right)dt +$$

$$+2M_{2,n-1}M_{3,n-1}\int\limits_{t_{n-1}}^{t_n}\left(\iint\limits_{S_{c,n-1}}\left|c^*\right|dS_{n-1}\right)dt + 2M_1\int\limits_{t_{n-1}}^{t_n}\left(\iiint\limits_{G_{n-1}}|F|dG_{n-1}\right)dt. \tag{45}$$

and

$$\iiint\limits_{G_{n-1}}\left(c^{(n)}\right)^2 dG_{n-1} \leq M_{6,n-1}\left(\iiint\limits_{G_{n-1}} c_0^2 dG_{n-1} + \right.$$

$$\left. + M_{4,n-1}\int\limits_{t_{n-1}}^{t_n}\left(\iint\limits_{S_{c,n-1}}\left(c^*\right)^2 dS_{n-1}\right)dt + 2M_{2,n-1}M_{3,n-1}\int\limits_{t_{n-1}}^{t_n}\left(\iint\limits_{S_{c,n-1}}\left|c^*\right|dS_{n-1}\right)dt + 2M_{1,n-1}\int\limits_{t_{n-1}}^{t_n}\left(\iiint\limits_{G_{n-1}}|F|dG_{n-1}\right)dt\right). \tag{46}$$

where $M_{6,n-1}=\dfrac{1}{2M_{5,n-1}}\left(\pi^2\left(\dfrac{1}{L_x^2}+\dfrac{1}{L_y^2}+\dfrac{1}{\left(H^{(n-1)}\right)^2}\right)\right)^{-1}.$

The inequalities obtained imply the continuous dependence (stability) of the solution to the problem (14) - (20) on the functions of the initial condition, the boundary conditions and the right-hand side, in L_2 norm for any instant of $0 < T < +\infty$ time, and also in L_2 time-integral norm.

Obviously, if the inequality (45) and the theorem condition are satisfied, the initial-boundary problem (14) - (19), (20) will also have a solution that depends continuously on the functions of the initial condition, the boundary conditions and the right-hand side in the corresponding norms.

Discussion and Conclusions. Novelty of the proposed non-stationary spatial-three-dimensional mathematical model of suspension transport lies in the fact that, alongside with considering the processes of advective transfer, micro-turbulent diffusion and gravity sedimentation of suspended particles, the model describes the change in bottom geometry caused by the particle settling or bottom sediment rising.

The linearization of the corresponding initial-boundary problem on the time grid is carried out, and the conditions for the uniqueness of the solution to the initial-boundary problem and continuous dependence on the input data – on the functions of the initial condition, boundary conditions, and the right-hand side in L_2 Hilbert space norm in L_2 time integral norm for two variants of boundary conditions are obtained for the arbitrary $t_{n-1} \leq t \leq t_n$ time step.

References

1. Leontyev, I.O., et al. Pribrezhnaya dinamika: volny, techeniya, potoki nanosov. [Coastal dynamics: waves, flows, deposits drifts.] I.O. Leontyev, ed. Moscow: GEOS, 2001, 272 p. (in Russian).

2. Matishov, G.G., et al. Prirodnye katastrofy v Azovo-Chernomorskom basseyne v nachale XXI veka. [Natural disasters in the Azov-Black Sea basin at the beginning of XXI century.] Rostov-on-Don: SRC RAS Publ. House, 2017, 160 p. (in Russian).

3. Petrov, P.G. Dvizhenie sypuchey sredy v pridonnom sloe zhidkosti. [Motion of a bed load.] Journal of Applied Mechanics and Technical Physics, 1991, vol. 32, iss. 5, pp. 72–76 (in Russian).

4. Barnard, P.L., Jaffe, B.E. and Schoellhamer, D.H. A multi-discipline approach for understanding sediment transport and geomorphic evolution in an estuarine-coastal system—San Francisco Bay. Marine Geology, 2013, vol. 345, pp. 1–2. DOI:10.1016/j.margeo.2013.09.010. DOI: https://doi.org/10.1016/j.margeo.2013.09.010

5. Xiaoying, L., Shi, Q., Yuan, H., Yuehong, C., Pengfei, D. Predictive modeling in sediment transportation across multiple spatial scales in the Jialing River Basin of China. International Journal of Sediment Research, 2015, vol. 30, iss. 3, pp. 250–255.

Mechanics

6. Lusher, A.L., McHugh, M., Thompson, R.C. Occurrence of microplastics in gastrointestinal tract of pelagic and demersal fish from the English channel. Marine Pollution Bulletin, 2013, vol. 67, pp. 94-99.

7. Marchuk, G.I., et al. Matematicheskie modeli v geofizicheskoy gidrodinamike i chislennye metody ikh realizatsii. [Mathematical models in geophysical hydrodynamics and numerical methods for their implementation.] Leningrad: Gidrometeoizdat, 1987, 296 p. (in Russian).

8. Belikov, V.V., Borisova, N.M., Gladkov, G.L. Matematicheskaya model' transporta nanosov dlya rascheta zanosimosti dnouglubitel'nykh prorezey i ruslovykh kar'erov. [Mathematical model of sediment transport for calculating the sediment accumulation in dredge cuts and channel pits.] Journal of University of Water Communications, 2010, vol. 2, pp. 105–113 (in Russian).

9. Sanne, L.N. Modelling of sand dunes in steady and tidal flow. Denmark: Technical University of Copenhagen, 2003, 185 p.

10. Ballent, A., Pando, S., Purser, A., Juliano, M., Thomsen, L. Modelled transport of benthic marine microplastic pollution in the Nazaré Canyon. Biogeosciences, 2013, vol. 10, pp. 7957-7970. https://doi.org/10.5194/bg-10-7957-2013, 2013. https://doi.org/10.5194/bg-10-7957-2013

11. Miles, J. Wave shape effects on sediment transport. J. Coastal Res., 2013, vol. 2, iss. 65, pp. 1803–1808. DOI::10.2112/SI65-305.1 DOI: https://doi.org/10.2112/SI65-305.1

12. Popkov, V.I. Strukturnye osobennosti i genezis dislokatsiy dna Azovskogo morya. [Structural features and genesis of dislocations of the Sea of Azov bottom.] Geology, Geography and Global Energy, 2008, no. 1, pp. 77–90 (in Russian).

13. Sidoryakina, V.V., Sukhinov, A.I. Issledovanie korrektnosti i chislennaya realizatsiya linearizovannoy dvumernoy zadachi transporta nanosov. [Well-posedness analysis and numerical implementation of a linearized two-dimensional bottom sediment transport problem.] Computational Mathematics and Mathematical Physics, 2017, vol. 57, no. 6, pp. 985–1002 DOI: https://doi.org/10.7868/S0044466917060138 (in Russian). DOI: https://doi.org/10.7868/S0044466917060138

14. Sukhinov, A.I., Sidoryakina, V.V. O skhodimosti resheniya linearizovannoy posledovatel'nosti zadach k resheniyu nelineynoy zadachi transporta nanosov. [Convergence of linearized sequence tasks to the nonlinear sediment transport task solution.] Mathematical Models and Computer Simulations, 2017, vol. 29, no. 11, pp. 19–39 (in Russian). http://mi.mathnet.ru/mm3905

15. Sukhinov, A.I., Sidoryakina, V.V., Sukhinov, A.A. Dostatochnye usloviya skhodimosti polozhitel'nykh resheniy linearizovannoy dvumernoy zadachi transporta nanosov. [Sufficient conditions for convergence of positive solutions to linearized two-dimensional sediment transport problem.] Vestnik of DSTU, 2017, vol. 17, no. 1, pp. 5–17 (in Russian). DOI: https://doi.org/10.23947/1992-5980-2017-17-1-5-17

16. Sukhinov, A.A., Sukhinov, A.I. 3D Model of Diffusion-Advection-Aggregation Suspensions in Water Basins and Its Parallel Realization. Parallel Computational Fluid Dynamics, Mutidisciplinary Applications, Proceedings of Parallel CFD 2004 Conference, Las Palmas de Gran Canaria, Spain, ELSEVIER, Amsterdam-Berlin-London-New York-Tokyo, 2005, pp. 223-230. DOI: 10.1016/B978-044452024-1/50029-4. DOI: https://doi.org/10.1016/B978-044452024-1/50029-4

17. Protter, M.H., Weinberger, H.F. Maximum Principles in Differential Equation. Springer-Verlag New York, Inc. 1984, 276 p. DOI 10.1007/978-1-4612-5282-5. DOI https://doi.org/10.1007/978-1-4612-5282-5

18. Ladyzhenskaya, O.A., et al. Lineynye i kvazilineynye uravneniya parabolicheskogo tipa. [Linear and quasilinear parabolic equations.] Moscow: Nauka, 1967, 736 p. (in Russian).

19. Vladimirov, V.S., et al. Uravneniya matematicheskoy fiziki. [Equations of mathematical physics.] Moscow: Nauka, 1981, 512 p. (in Russian).

20. Tikhonova, A.N., et al. Uravneniya matematicheskoy fiziki. [Equations of mathematical physics.] Moscow: Nauka, 1977, 735 p. (in Russian).

Authors:

Sukhinov, Alexander I.,
Head of the Mathematics and Computer Sciences
Department, Don State Technical University (1, Gagarin
sq., Rostov-on-Don, 344000, RF), Dr.Sci. (Phys.-Math.),
professor,
ORCID: http://orcid.org/0000-0002-5825-1523
Scopus Author ID: 8573972700,
WoS Researcher ID: I-1091-2016
sukhinov@gmail.com

Sidoryakina,Valentina V.,
Head of the Mathematics Department, Taganrog Chekhov
Institute, Rostov State University of Economics (RINH)
branch, (48, Initsiativnaya St., Taganrog, 347936, RF),
Cand.Sci. (Phys.-Math.), associate professor,
ORCID: https://orcid.org/0000-0001-7744-015X
cvv9@mail.ru
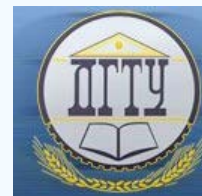
Mechanics

МЕХАНИКА
MECHANICS

Numerical simulation of the transverse flow over spans of girder bridges [*]

Yu. A. Gosteev[1], A. D. Obukhovskiy[2], S. D. Salenko[3][**]
[1,2,3] Novosibirsk State Technical University, Novosibirsk, Russian Federation

Численное моделирование поперечного обтекания пролетных строений балочных мостов[***]

Ю. А. Гостеев[1], А. Д. Обуховский[2], С. Д. Саленко[3][**]
[1,2,3] Новосибирский государственный технический университет, г. Новосибирск, Российская Федерация

Introduction. The technique of numerical modeling of the transverse flow over span structures of bridges on the basis of the two-dimensional URANS (Unsteady Reynolds-averaged Navier-Stokes) approach used in the modern methods and software packages for computational fluid dynamics is verified. The work objective was debugging and experimental substantiation of this technique with the use of the database on the aerodynamic characteristics of the cross-sections of span structures of girder bridges of standard shapes pre-developed by the authors.

Materials and Methods. A numerical simulation of the transverse flow of low-turbulent (smooth) and turbulent air flows around the bridge structures in a range of practically interesting attack angles is carried out. SST $k - \omega$ turbulence model was used as the closing one. The technique was preliminarily tested on the check problem for the flow of the rectangular cross-section beams. Calculations were carried out using the licensed ANSYS software.

Research Results. The calculated dependences on the attack angle of the aerodynamic coefficients of forces (drag and lift) and the moment of the cross sections of the girder bridges of standard shapes are obtained. These data refer to the span structures at the construction phase (without deck and parapets, without parapets) and operation phase, under the conditions of model smooth and turbulent incoming flow. The latter allows us to outline the boundaries for more weighted estimates of the aerodynamic characteristics of the girder bridges in a real wind current. The best agreement with the experimental data was obtained from the drag of the cross-section. The magnitude of the lifting force is more sensitive to the presence and extent of the separation regions, so its numerical determination is less accurate. The reproduction of the angle-of-attack effect on the aerodynamic moment of the cross-section is the most challeng-

Введение. Верифицирована методика численного моделирования поперечного обтекания пролетных строений мостов на основе нестационарного решения Рейнольдса для уравнений Навье — Стокса (URANS, Unsteady Reynolds-averaged Navier — Stokes). Данный двумерный подход используется в современных методах и пакетах прикладных программ вычислительной гидроаэродинамики. Цели работы — отладка и экспериментальное обоснование указанной методики. Для реализации поставленной цели использована ранее разработанная авторами база данных по аэродинамическим характеристикам поперечных сечений пролетных строений балочных мостов типовых форм.

Материалы и методы. Проведено численное моделирование поперечного обтекания мостовых строений низкотурбулентными (гладкими) и турбулентными воздушными потоками в диапазоне практически интересных углов атаки. В итоге использовалась модель турбулентности SST $k - \omega$. Методика предварительно отработана на тестовой задаче обтекания балок прямоугольного поперечного сечения. Расчеты проводились с помощью лицензионного программного комплекса ANSYS.

Результаты исследования. Показано, каким образом угол атаки определяет силы (подъемную и лобового сопротивления) и момент поперечных сечений балочных мостов типовых форм. Полученные расчетные зависимости относятся к пролетным строениям на стадиях монтажа (без плиты перекрытия и ограждений, без ограждений) и эксплуатации в условиях модельных набегающих потоков — гладкого и турбулентного. Это позволяет очертить границы для более взвешенных оценок аэродинамических характеристик балочных мостов в реальном ветровом потоке.

Лобовое сопротивление сечению демонстрирует наилучшее согласование с опытными данными. Величина подъемной силы более чувствительна к наличию и протяженности отрывных зон, поэтому ее расчетное определение менее точно. Наиболее проблемным для большинства конфигураций является воспроизведение

ing for the majority of configurations.

Discussion and Conclusions. Comparison of the calculated and experimental data indicates the applicability of the URANS approach to the operational prediction of the aerodynamic characteristics of the single-beam span structures. In the case of multi-beam span structures, where the aerodynamic interference between separate girders plays an important role, the URANS approach must apparently give way to more accurate eddy-resolving methods. The results obtained can be used in the aerodynamic analysis of structures and in practice of the relevant design organizations in the field of transport construction.

влияния угла атаки на аэродинамический момент сечения.

Обсуждение и заключения. Сравнение расчетных и опытных данных свидетельствует о применимости URANS-подхода к оперативному предсказанию аэродинамических характеристик однобалочных пролетных строений. Если же речь идет о многобалочных пролетных строениях, существенную роль играет аэродинамическая интерференция между отдельными балками. В этом случае вместо URANS-подхода следует применять более точные вихреразрешающие методы. Полученные результаты могут быть использованы в исследованиях аэродинамики сооружений и в практике проектных организаций в сфере транспортного строительства.

Introduction. It is known that wind flow around engineering structures is, as a rule, instable turbulent in nature; different-scale eddy structures are observed in the flow [1, 2]. Nearby bluff bodies (to which, in particular, bridge spans belong), unsteady detached flow regions occur [3]. Accordingly, adequate modeling of the turbulence effects is now an important requirement for the simulation experiment techniques.

Large Eddy Simulation, LES, and Detached Eddy Simulation, DES, are used to evaluate the aerodynamics of structures. However, the use of these methods is complicated by their high resource intensity, the reasons for which are as follows:

— tridimensionality of the task;

— strict requirements to the computational grid density in the near-wall region and in the "focus" region [4];

— restrictions on the time integration step;

— relatively large time window length for gathering nonstationary statistics in steady state.

At the same time, it is known [5] that for cylindrical prisms that are close in shape to beam bridge spans, the two-dimensional approach reproduces the basic flow properties (primary unstable mode in the body wake is essentially two-dimensional). Thus, a POD analysis (Proper Orthogonal Decomposition) of the flow near the prism with $B / H = 5$ (H is depth of section) relative section depth was performed in [6]. As a result, it was established that the 1st and 2nd disturbance modes are two-dimensional (constant over the span) and correspond to the vorticity transfer along the surface. Three-dimensional modes change along the span at a reference length that is no less than B section depth.

For the operational prediction of aerodynamic characteristics (ADC) of bridge structures and wind-tunnel test tracking, the authors used nonstationary 2D modeling based on URANS approach, Unsteady Reynolds-averaged Navier-Stokes. Its applicability to the definition of ADC of the bluff bodies (stationary and oscillating) was studied in a number of works by foreign authors (see, for example, [7]).

Materials and Methods. When setting up computer-based experiments, the recommendations given in [8–10] were considered. The calculations were carried out in the ANSYS Fluent program.

The technique was preliminary tested on the check problem of flow around beams with rectangular cross-section. As a result, k — ω shear stress transport (SST) model was chosen to describe the flow turbulence, and the grid parameters and the numerical algorithm were selected.

Mechanics

The extension of the rectangular computational domain is (30 ... 40) H lengthwise, and (14 ... 20) H – transversely. The front face of the streamlined body was spaced apart from the input boundary at (8 ... 12) H.

We used low-Reynolds-number grids ($y^+ \leq 4$ ... 5 dimensionless distance of the first node to the wall) that enabled to calculate the boundary layer separation and reattachment. Considering the complexity of the streamlined body contours, multiblock grids were constructed. The internal female block consisted of quadrilateral elements whose density increased closer to the body surface. A layer with a structured orthogonal quadrilateral grid was generated immediately at the wall. The wake region was covered with a grid of square cells sizing of no more than $H/15$ ... $H/10$. The cell size increased to $H/4$ ... $H/3$ to the outer boundaries. The cross-sectional perimeter contained about 10^2 ... 10^3 cells depending on its shape. The total number of cells ranged from 40–50 thousand (for sections of simple shapes) to 250–300 thousand (for complex ones). An example of the computational grid near a beam of trapezoidal section with overlapping and fencing is shown in Fig. 1.
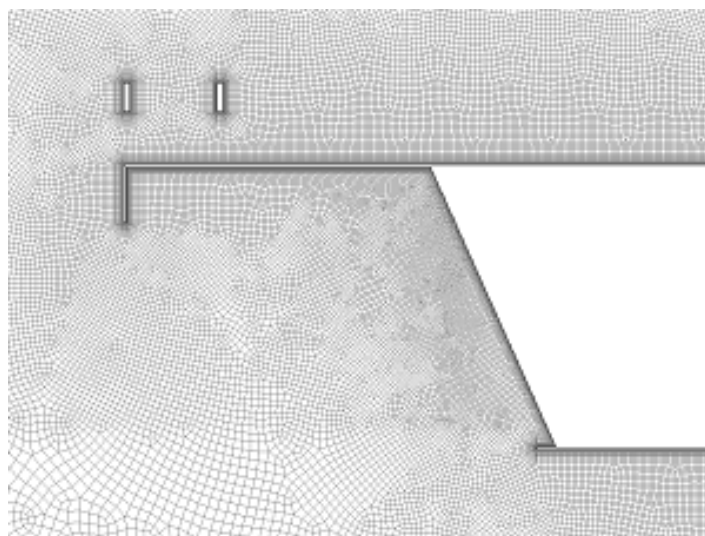
Fig. 1. Example of computational grid (fragment)

When solving the Navier – Stokes equations, the velocity – pressure relationship was implemented using the SIMPLE algorithm. The convection and viscous terms of the equations of flow and the transport of turbulent parameters were approximated by schemes of second-order accuracy.

The numerical integration was carried out by an implicit time scheme of the second-order accuracy. Δt integration step was (0.02… 0.04) H/V (V is incident flow velocity), i.e., under the vortex shedding with dimensionless frequency $f\,H/V = 0.1$, it was approximately 250–300 times less than $1/f$ period, and this provided an acceptable resolution of the non-stationary flow parameters. The established vortex trail was usually formed by H/V moment (60 ... 120). Thus, the total number of integration steps averaged 6000 ÷ 10,000. To collect nonstationary statistics, a time interval of at least 5 periods was used.

An example of a qualitative comparison of the computational and experimental flow patterns near the span is shown in Fig. 2.

a)

b)
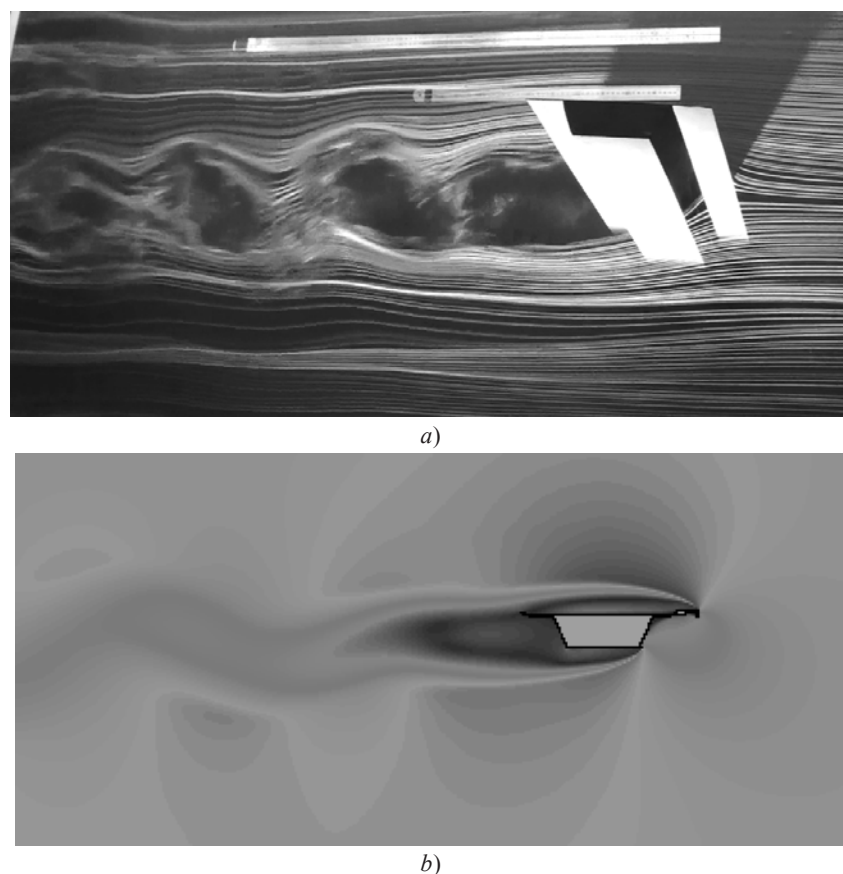
Fig. 2. Example of flow pattern over bridge span: experiment (*a*), calculation (*b*)

Research Results. Detailed information on ADC typical cross sections can be found in [11]. Figures 3–14 present a comparison of the computational and experimental data on the coefficients of averaged aerodynamic forces (drag, lift) and the moment for some specific sections.
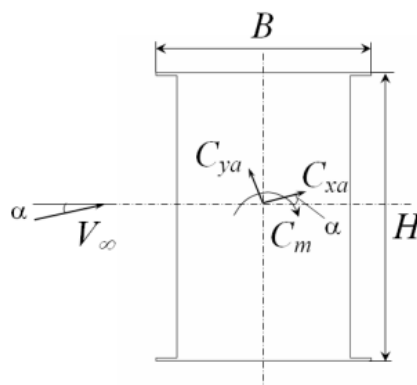
Fig. 3. Coefficients of averaged aerodynamic forces. Here: $\bar{C}_{xa}$ is drag; $\bar{C}_{ya}$ is lifting force; $\bar{C}_m$ is moment; B and H are longitudinal and transverse section dimensions (excluding fencing); α is angle of attack

The incident smooth flow is characterized by the intensity of 0.5%, the turbulent one – of 8%. The computation data is represented by solid lines.

Mechanics
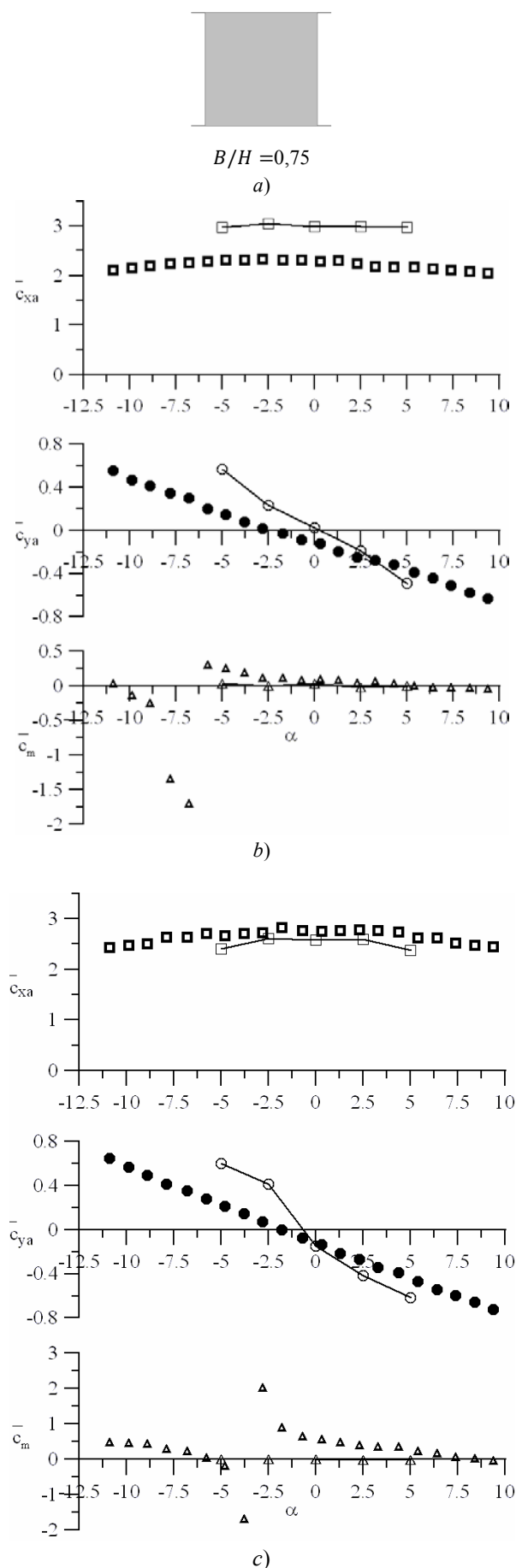
Fig. 4. Narrow single square girder (B/H 0.75 ratio): cross-section shape (*a*); smooth flow (*b*); turbulent flow (*c*)

Gosteev Yu. A. and the others. Numerical simulation of the transverse flow over spans of girder bridges

Гостеев Ю. А. и др. Численное моделирование поперечного обтекания пролетных строений балочных мостов
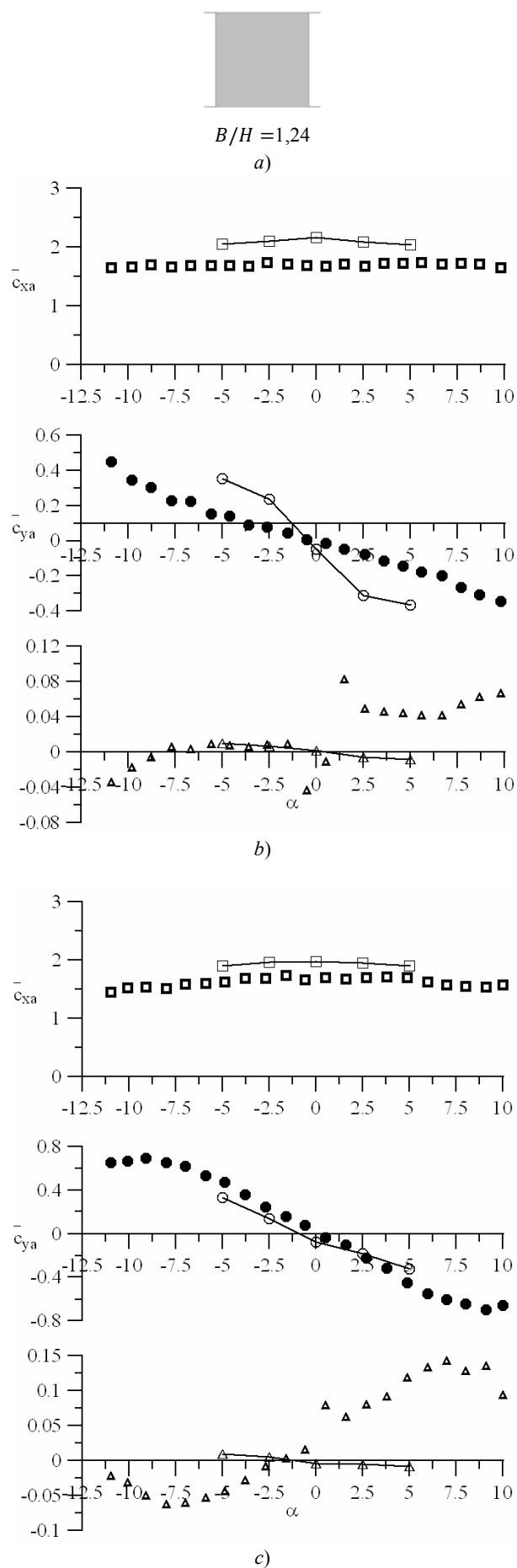
Fig. 5. Narrow single square girder (B/H 1.24 ratio): cross-section shape (*a*); smooth flow (*b*); turbulent flow (*c*)

Vestnik of Don State Technical University. 2018. Vol. 18, no. 4, pp. 362–378. ISSN 1992-5980 eISSN 1992-6006

Вестник Донского государственного технического университета. 2018. Т. 18, № 4. С. 362–378. ISSN 1992-5980 eISSN 1992-6006
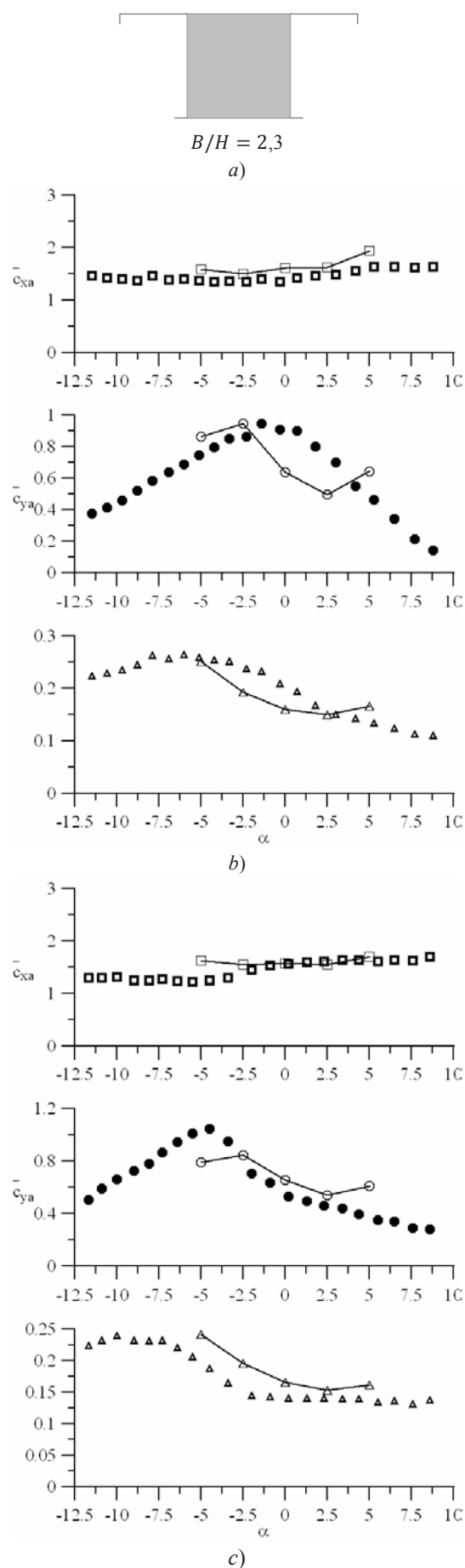
Fig. 6. Narrow single girder with overlapping (B/H 2.3 ratio): cross-section shape (*a*); smooth flow (*b*); turbulent flow (*c*)

Gosteev Yu. A. and the others. Numerical simulation of the transverse flow over spans of girder bridges

Гостеев Ю. А. и др. Численное моделирование поперечного обтекания пролетных строений балочных мостов

$B/H = 2,3$

a)

b)

c)
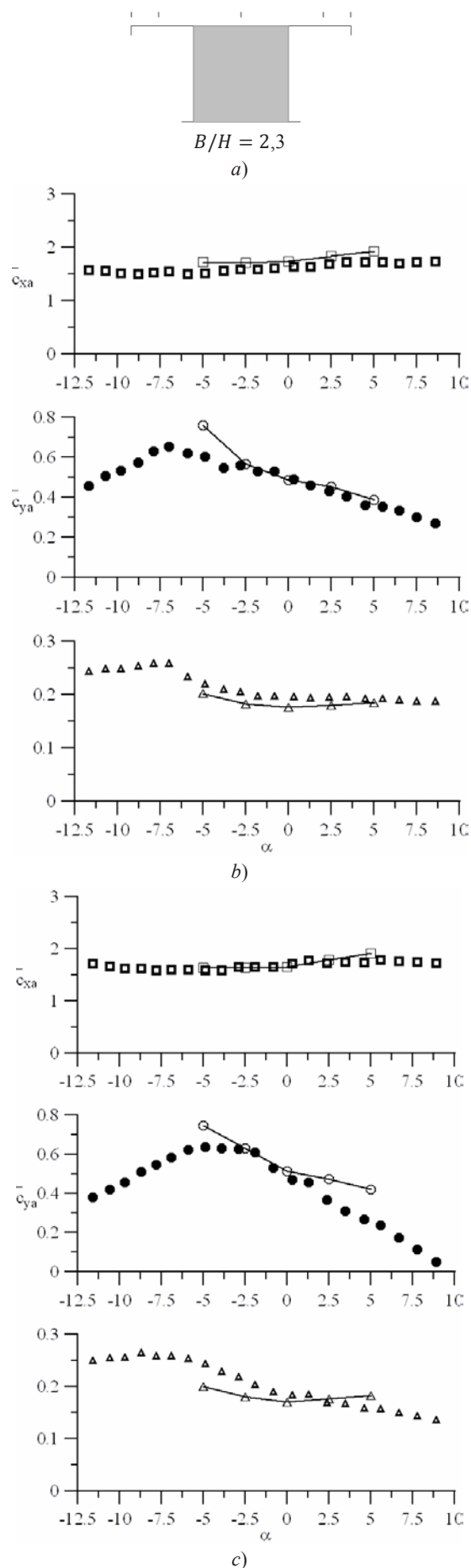
Fig. 7. Narrow single girder with overlapping and fencing (B/H 2.3 ratio): cross-section shape (*a*); smooth flow (*b*); turbulent flow (*c*)

Vestnik of Don State Technical University. 2018. Vol. 18, no. 4, pp. 362–378.   ISSN 1992-5980 eISSN 1992-6006

Вестник Донского государственного технического университета. 2018. Т. 18, № 4. С. 362–378.   ISSN 1992-5980 eISSN 1992-6006

$B/H = 1{,}85$

a)

b)

c)
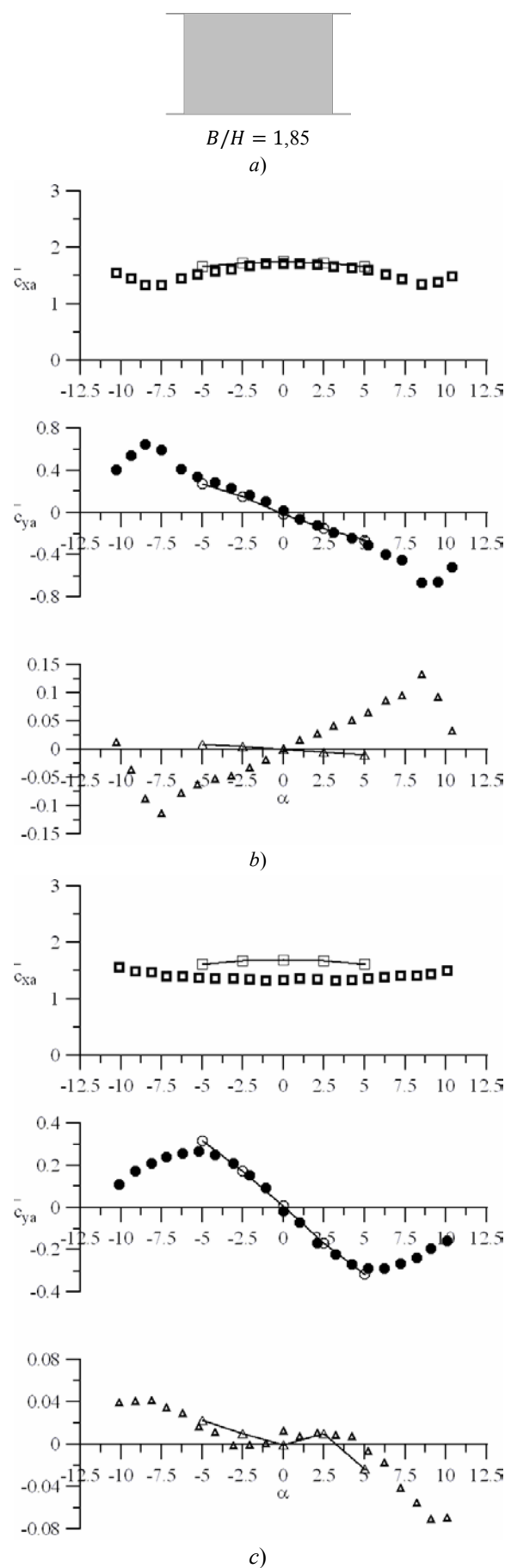
Fig. 8. Wide single square girder (B/H 1.85 ratio): cross-section shape (*a*); smooth flow (*b*); turbulent flow (*c*)

Gosteev Yu. A. and the others. Numerical simulation of the transverse flow over spans of girder bridges

Гостеев Ю. А. и др. Численное моделирование поперечного обтекания пролетных строений балочных мостов
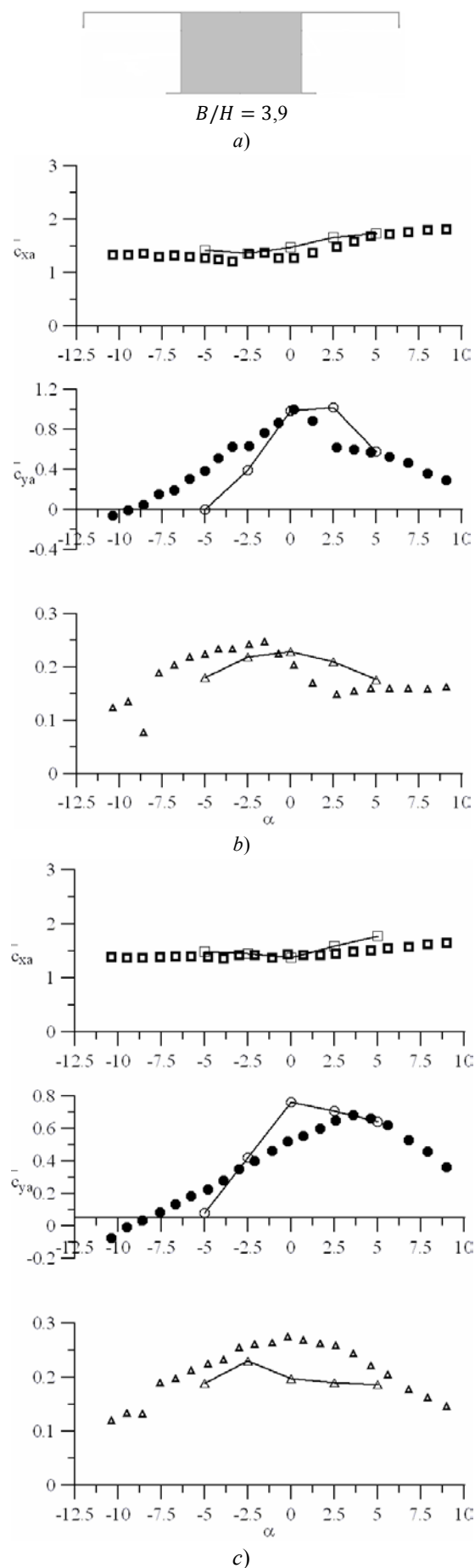
Fig. 9. Wide single girder with overlapping (B/H 3.9 ratio): cross-section shape (*a*); smooth flow (*b*); turbulent flow (*c*)

$B/H = 3{,}09$

a)

b)

c)
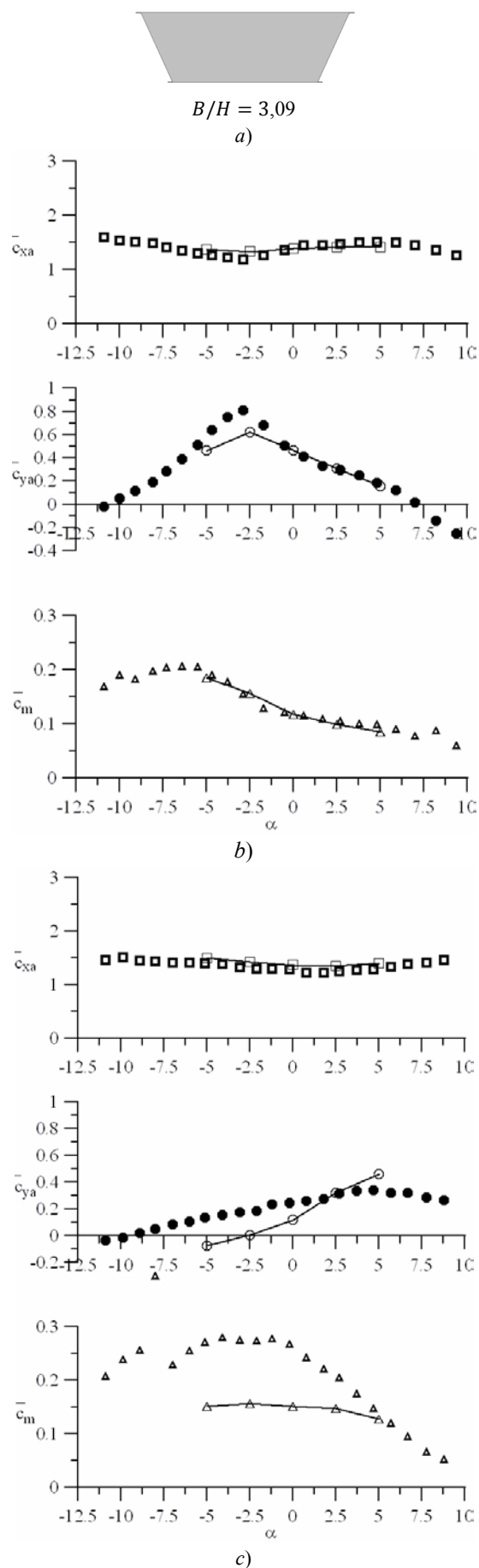
Fig. 10. Trapezoidal girder (B/H 3.09 ratio): cross-section shape (*a*); smooth flow (*b*); turbulent flow (*c*)

$B/H = 5{,}1$

a)

b)

c)
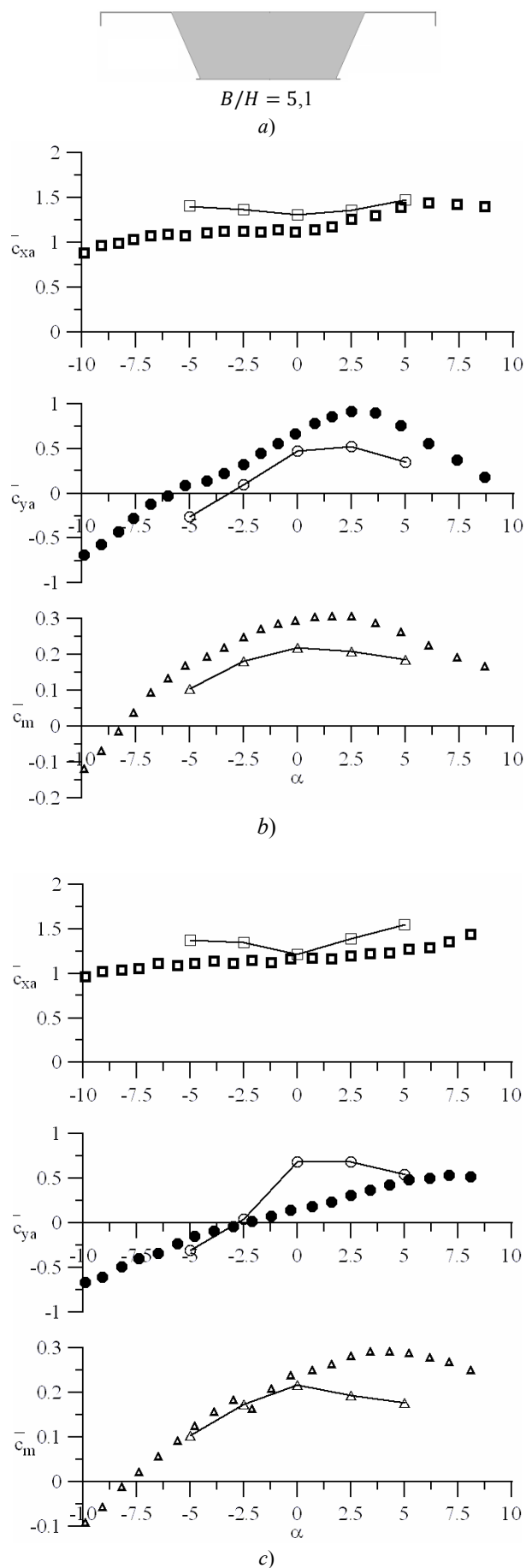
Fig. 11. Trapezoidal girder with overlapping (B/H 5.1 ratio): cross-section shape (*a*); smooth flow (*b*); turbulent flow (*c*)

Mechanics

Vestnik of Don State Technical University. 2018. Vol. 18, no. 4, pp. 362–378.   ISSN 1992-5980 eISSN 1992-6006

Вестник Донского государственного технического университета. 2018. Т. 18, № 4. С. 362–378.   ISSN 1992-5980 eISSN 1992-6006

$B/H = 2{,}75$

a)

b)

c)
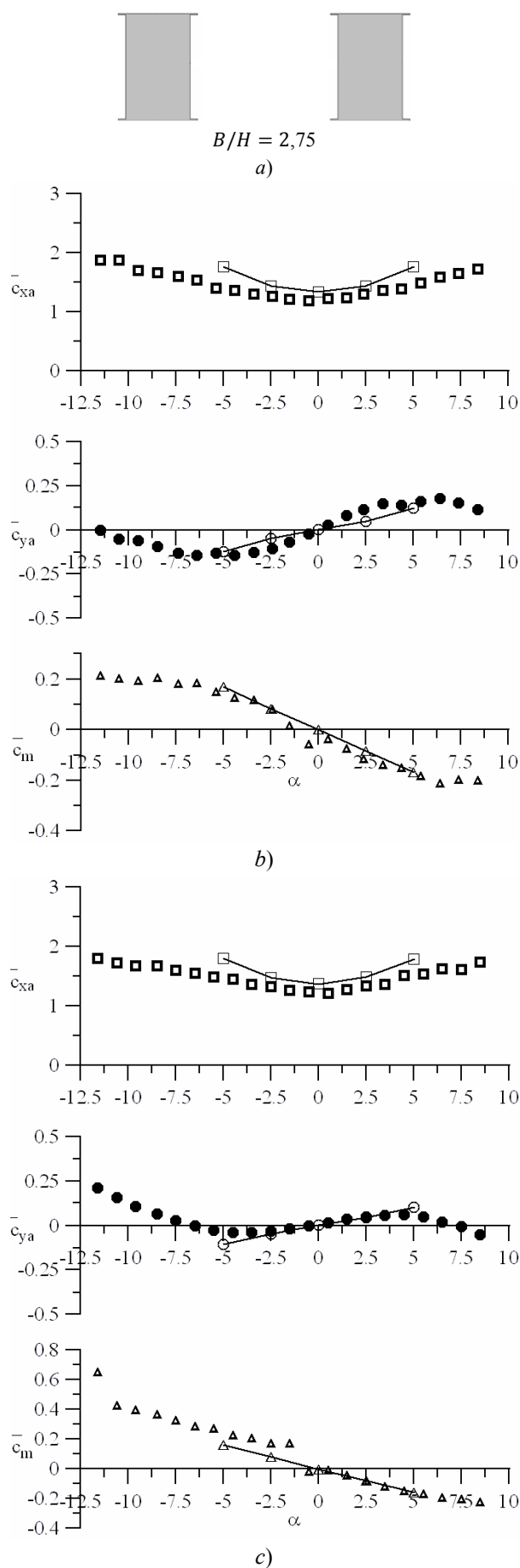
Fig. 12. Double-girder structure (B/H 2.75 ratio): cross-section shape (*a*); smooth flow (*b*); turbulent flow (*c*)

$B/H = 3,85$

a)

b)

c)
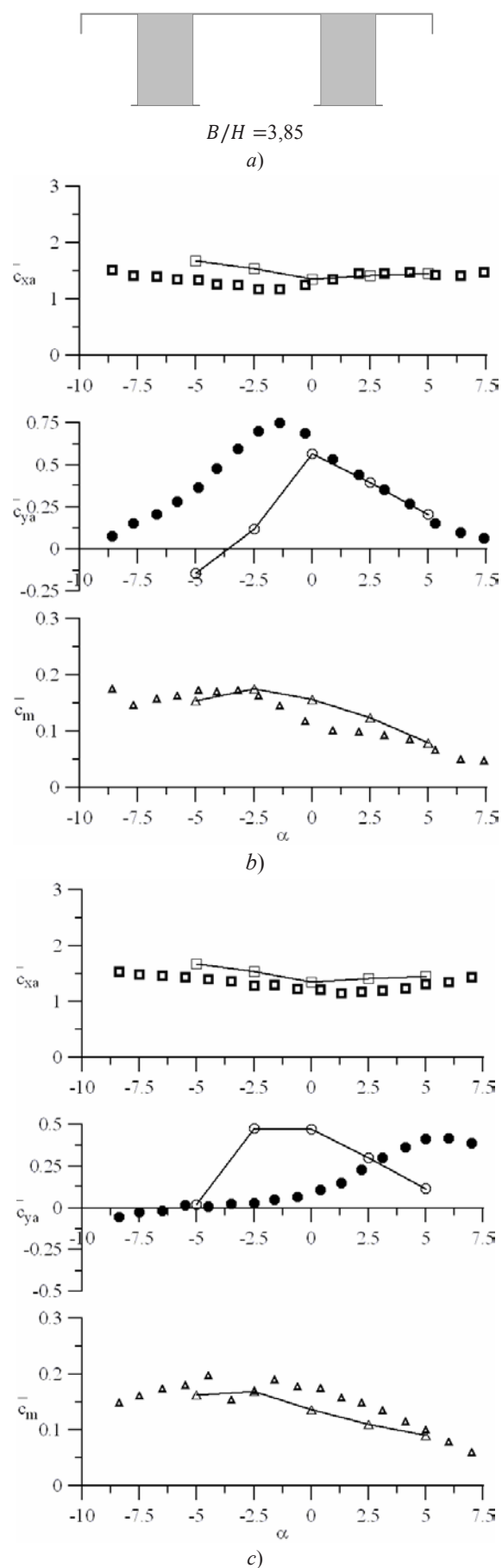
Fig. 13. Double-girder overlapping structure (B/H 3.85): cross-section shape (*a*); smooth flow (*b*); turbulent flow (*c*)

Mechanics

Vestnik of Don State Technical University. 2018. Vol. 18, no. 4, pp. 362–378.   ISSN 1992-5980 eISSN 1992-6006

Вестник Донского государственного технического университета. 2018. Т. 18, № 4. С. 362–378.   ISSN 1992-5980 eISSN 1992-6006

$B/H = 9$

a)

b)

c)
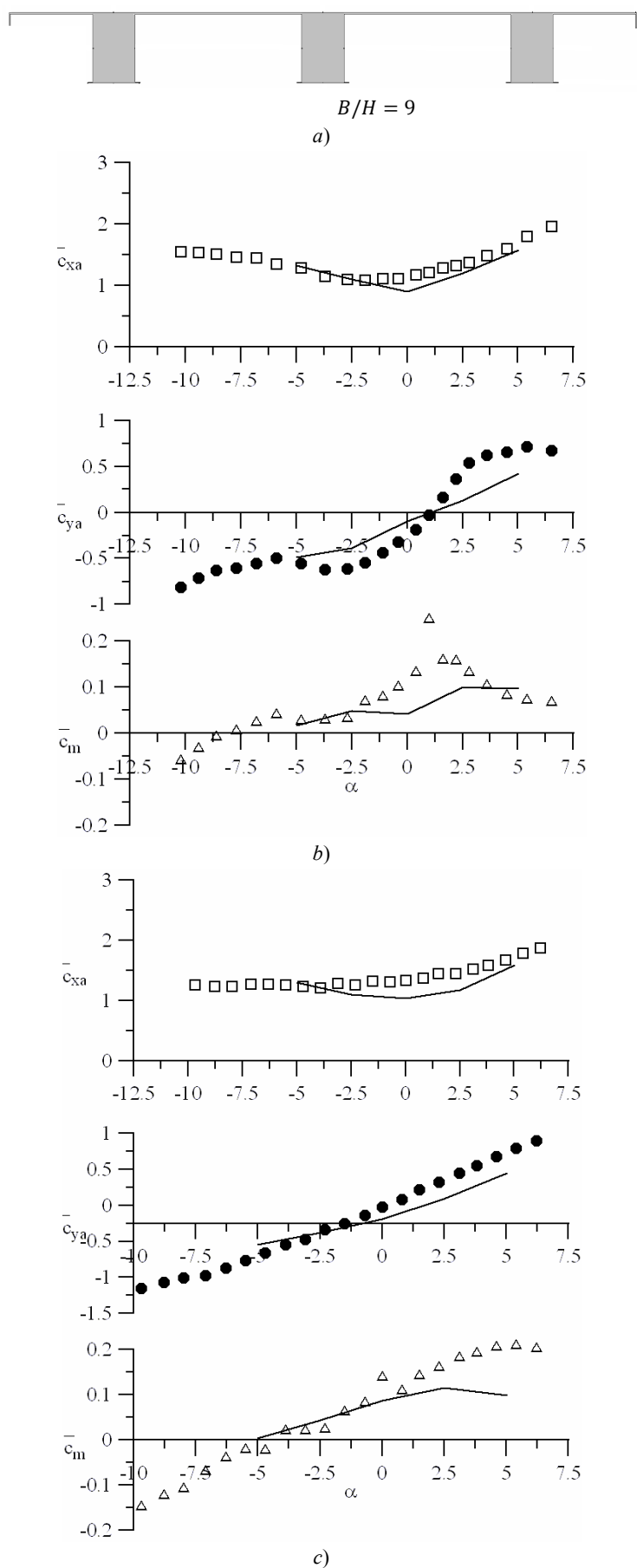
Fig. 14. Multi-girder structure with overlapping (B/H 9): cross-sectional shape (*a*); smooth flow (*б*); turbulent flow (*в*)

Discussion and Conclusions. The analytical results show that, with some exceptions, with an increase in the relative width of the B / H cross section of a single-beam structure, the accuracy of the calculated prediction of its ADC rises. As a rule, the best agreement is indicated for the frontal resistance of the section. For most configurations, the computation data is slightly higher than the drag coefficient obtained experimentally. It should be clarified that for the considered bluff bodies, the major contribution to the cross-section drag is made by the form (pressure) drag, which is mainly determined by the difference in pressure forces on the upstream and leeward sides of the cross section. The accepted theoretical approach coarsens the dynamics of the vortex structures in the zone behind the body, which leads to an underestimated pressure recovery in this area.

The lift magnitude is more sensitive to the presence, extent and type (open/closed) of the detached flow regions. This applies especially to the span structure equipped with a slab; in this case, it is possible to re-attach the flow to the upper side of the slab with the formation of a closed separation zone (approximately at $B/H \geq 5$). Therefore, in comparison with frontal resistance, the calculated determination of lift force is less accurate, especially for superstructures with a floor slab.

The reproduction of the angle-of-attack effect on the aerodynamic moment of the cross section is a challenge for most configurations.

If the aerodynamic interference [12] occurs under the cross-flow around multi-girder spans between beams, the accuracy of the ADC prediction falls with an increase in the number of beams (relative overall section width). In this case, it is advisable to use more accurate DES and LES eddy-resolving methods instead of the URANS approach.

References

1. Simiu, E., Scanlan, R. Vozdeystvie vetra na zdaniya i sooruzheniya. [Wind effects on buildings and structures.] Moscow: Stroyizdat, 1984, 360 p. (in Russian).

2. Paidoussis, M.-P., Price, S.-J., de Langre, E. Fluid-structure interactions: cross-flow-induced instabilities. New York: Cambridge University Press, 2011, 402 p.

3. Kavrakov, I., Morgenthal, G. A synergistic study of a CFD and semi-analytical models for aeroelastic analysis of bridges in turbulent wind conditions. Journal of Fluids and Structures, 2018, vol. 82, pp. 59–85.

4. Spalart, P.-R. Young person's guide to detached-eddy simulation grids. NASA CR-2001-211032; Boeing Commercial Airplanes. Available at: https://ntrs.nasa.gov/archive/nasa/casi.ntrs.nasa.gov/20010080473.pdf (accessed: 05.09.18).

5. Monkewitz, P.A., Nguyen, L.N. Absolute instability in the near-wake of two-dimensional bluff bodies. Journal of Fluids and Structures, 1987, vol. 1, iss. 2, pp. 165–184.

6. Bruno, L., Coste, N., Fransos, D. Analysis of the separated flow around a 5:1 rectangular cylinder through computational simulation. Fifth European & African Conference on Wind Engineering: Proc. Florence, 2009. Available at: http://www.iawe.org/Proceedings/5EACWE/115.pdf (accessed: 05.09.18).

7. Brusiani, F., et al. On the evaluation of bridge deck flutter derivatives using RANS turbulence models. Journal of Wind Engineering and Industrial Aerodynamics, 2013, vol. 119, pp. 39–47.

8. Franke, J., et al. Recommendations on the use of CFD in wind engineering. ResearchGate. Available at: https://www.researchgate.net/publication/257762096_Recommendations_on_the_use_of_CFD_in_predicting_pedestrian_wind_environment (accessed: 05.09.18).

9. Belostotskiy, A.M., Dubinskiy, S.I., Afanasyeva, I.N. Chislennoe modelirovanie zadach stroitel'noy aerodinamiki. Razrabotka metodik i issledovaniya real'nykh ob"ektov. [Numerical simulation of problems of construction aerodynamics. Development of techniques and study of real-life objects.] International Journal of Computational Civil and Structural Engineering, 2010, vol. 6, no. 1/2, pp. 67–69 (in Russian).

10. Guvernyuk, S.V., et al. Vychislitel'naya aerodinamika stroitel'nykh sooruzheniy. Zadachi i metody. [Computational aerodynamics of building constructions. Problem and methods.] Vestnik MGSU, 2011, vol. 2, no. 2, pp. 113–119 (in Russian).

11. ODM 218.2.040—2014. Otraslevoy dorozhnyy metodicheskiy dokument. Metodicheskie rekomendatsii po otsenke aerodinamicheskikh kharakteristik secheniy proletnykh stroeniy mostov. [ODM 218.2.040—2014. Industry road guidance document. Guidelines for the evaluation of aerodynamic characteristics of the cross sections of bridge spans.] Novosibirsk State Technical University; Federal Road Agency (Rosavtodor). Moscow: Izd-vo FGUP «Informavtodor», 2014, 87 p. (in Russian).

12. Salenko, S.D., Gosteev, Yu.A., Obukhovskiy, A.D. Aerodinamicheskie issledovaniya tipovykh mnogobalochnykh konstruktsiy. [Aerodynamic studies of typical multi-beam structures.]Thermophysics and Aeromechanics, 2013, vol. 20, no. 4, pp. 451–460 (in Russian).

Mechanics

Authors:

Gosteev, Yury A.,
associate professor of the Aerohydrodynamics Department,
Novosibirsk State Technical University (20, K. Marks Pr.,
Novosibirsk, 630073, RF), Cand.Sci. (Phys.-Math.), associate
professor,
ORCID:http://orcid.org/0000-0002-4979-3174
gosteev@corp.nstu.ru

Obukhovskiy, Alexander D.,
associate professor of Aerohydrodynamics Department, No-
vosibirsk State Technical University (20, K. Marks Pr., Novo-
sibirsk, 630073, RF), Cand. Sci. (Eng.), associate professor,
ORCID:http://orcid.org/0000-0002-8842-0178,
obuxovskij@corp.nstu.ru

Salenko, Sergey D.,
head of the Aerohydrodynamics Department, Novosibirsk
State Technical University (20, K. Marks Pr., Novosibirsk,
630073, RF), Dr.Sci. (Eng.), professor,
ORCID:http://orcid.org/0000-0003-8885-1885
salenkosd@yandex.ru

МАШИНОСТРОЕНИЕ И МАШИНОВЕДЕНИЕ

MACHINE BUILDING AND MACHINE SCIENCE
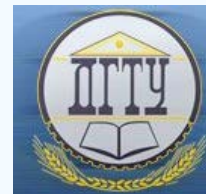
Effect of recuperative volume parameters on dynamic characteristics of pneumatic drive under braking[*]

A. N. Sirotenko[1], S. A. Partko[2], Wael Salloum[3][**]

[1,2] Don State Technical University, Rostov-on-Don, Russian Federation.
[3] University of Aleppo. Aleppo, Syria

Влияние параметров рекуперативного объема на динамические характеристики пневмопривода при торможении[***]

А. Н. Сиротенко[1], С. А. Партко[2], Ваел Саллум[3][**]

[1,2] Донской государственный технический университет, г. Ростов-на-Дону, Российская Федерация.
[3] Алеппо университет, г. Алеппо, Сирия

Introduction. Methods of energy saving in pneumatic drive are considered. The method of braking by creating back pressure in the exhaust cavity of the pneumatic actuator is of interest. Under braking, the compressed air energy is stored in the recuperative volume. It is possible to control the braking dynamics through setting the initial parameters of the recuperative volume. The work objective is to create a mathematical model describing the dynamic processes taking place in the pneumatic drive under braking by backpressure, with a constant mass enclosed in the cavities of the air motor, and considering variation of the initial parameters of the braking volume.

Materials and Methods. A mathematical model is proposed that describes the speed change of the output link, pressures and temperatures in the cavities of the pneumatic drive depending on the initial parameters of the recuperative volume. The solution to the mathematical model is carried out by the numerical integration method.

Research Results. The dependences of the output link velocity, pressures and temperatures in the pneumatic drive cavities on the initial parameters of the recuperative volume are obtained. Adequacy of the built mathematical model is confirmed by Fisher's criterion.

Discussions and Conclusions. The results obtained can be used to solve the problems of energy saving in pneumatic drives under the organization of backpressure braking. The use of recuperative volume increases the technological flexibility of the drive during its readjustment and extends the possibilities of energy saving.

Введение. Рассмотрены способы энергосбережения в пневматическом приводе. Интерес представляет способ торможения созданием противодавления в выхлопной полости пневмопривода. При этом энергия сжатого воздуха накапливается в рекуперативном объеме. Задавая начальные параметры рекуперативного объема, возможно управлять динамикой торможения. Цель работы — создание математической модели, описывающей динамические процессы, происходящие в пневматическом приводе при торможении противодавлением, с постоянной массой, заключенного в полостях пневмодвигателя воздуха, и с учетом изменения начальных параметров тормозного объема.

Материалы и методы. Предложена математическая модель, описывающая изменение скорости движения выходного звена, давлений и температур в полостях пневмопривода в зависимости от начальных параметров рекуперативного объема. Решение математической модели осуществлялось методом численного интегрирования.

Результаты исследования. Получены зависимости скорости выходного звена, давлений и температур в полостях пневмопривода от начальных параметров рекуперативного объема. Адекватность полученной математической модели подтверждена по критерию Фишера.

Обсуждения и заключения. Полученные результаты могут быть полезны для решения задач энергосбережения в пневмоприводах при организации торможения противодавлением. Применение рекуперативного объема повышает технологическую гибкость привода при его переналадке и расширяет возможности энергосбережения.

Keywords: pneumatic drive, recuperation, energy saving, backpressure, braking, recuperative volume

Ключевые слова: пневматический привод, рекуперация, энергосбережение, противодавление, торможение, рекуперативный объем.

Introduction. Pneumatic drives are widely used for automation and mechanization of secondary processes. Energy consumption of the pneumatic equipment may be more than 20% of the total consumption of the enterprise. Therefore, the issues of energy saving in pneumatic drives are urgent problems [1-3]. Such features as compressibility of the working environment and inertia of the output links impede shockless braking, complicate the control and drive design [1, 3, and 4]. It is possible to control the law of pneumatic actuator braking both by affecting a regulator device [1, 2, 5, and 6] and by selecting the most useful technique of braking [7–9].

These above features enable to use compressed air as a brake damper and to accumulate braking energy, which is effectively implemented under braking the pneumatic actuator through back pressure [7]. While changing the switch coordinate for braking, pressure in the brake and injection cavities, connecting additional volume to the exhaust cavity, it is possible not only to provide shockless braking, but also to recuperate the energy of compressed air under braking [2, 7, and 10].

By setting the initial parameters of the regenerative volume, it is possible to affect the braking and energy-speed parameters of the pneumatic drive. However, this issue is not adequately investigated.

Research objective is to create a mathematical model describing the dynamic processes occurring in the pneumatic drive under braking by backpressure, with a constant mass enclosed in the cavities of the air motor, and considering variation of the initial parameters of the braking volume.

Problem Statement. It is required to describe mathematically the dependence of the dynamic characteristics of a pneumatic drive under backpressure braking on the initial parameters of the regenerative volume.

Mathematical Dependences. Consider the backpressure braking by complete overlapping of the pump and exhaust lines. The disadvantage of this method is that when you change the working movement and the external load on the output link, you have to re-set the braking actuation coordinate. An alternative is the connection of a regenerative volume to the brake cavity of the pneumatic motor upon braking. It is possible to affect the final pressure in the brake volume and the braking path of the output link of a pneumatic drive by setting its initial parameters before braking [8].

The following assumptions were made for a mathematical description of the gas-dynamic processes occurring in the cavities of the pneumatic drive [10, 12]: pressure in the lines is assumed constant; thermodynamic processes occurring in the cavities of the pneumatic actuator are considered adiabatic; the working medium in the cavities of the pneumatic drive compressed under braking is taken as an ideal gas.

The backpressure braking is based on the principle of creating a resistance force to the movement of the output link of an air motor. This is achieved by partial or complete overlapping of the pump and exhaust channels. Complete overlap is more efficient because there is no release of pneumatic air from the brake cavity. The dynamics of the pneumatic drive before braking is determined by a known system of equations that considers the subcritical and over-critical discharge regimes [10].

The pneumatic drive parameters are shown in Fig. 1. The working medium parameters are identified as follows: $V_м$, $p_м$, $T_м$ are volume, pressure, and temperature of the air compressed in the channel, respectively; V_n, p_n, T_n, are volume, pressure, and temperature of the air compressed in the head end of the air motor; $V_ш$, $p_ш$, $T_ш$ are volume, pressure, and temperature of the air compressed in the rod or head end of the air engine; $V_{рек}$, $p_{рек}$, $T_{рек}$ are volume, pressure, and temperature of the air compressed in the regenerative volume; V_{am}, p_{am}, T_{am} are volume, pressure, and temperature of the free air. The air motor geometrics have the following identifiers: F_n, $F_ш$ are head and rod useful areas of the air motor; $f_н$, $f_в$ are passage areas of the pump and exhaust lines respectively; x, x_{0n}, $x_{0ш}$ are the coordinates of the current displacement, constant head and rod "passive" volumes, respectively; s is maximum driving stroke; P is workload.

Fig. 1. Pneumatic drive parameters under braking by backpressure in recuperative volume

Under braking, there is a constant amount of the compressed air in the cavities of the pneumatic engine. We consider that heat exchange with the environment is insignificant, therefore, we regard the thermodynamic process to be adiabatic, with the adiabatic index $k = 1.4$ [10]. For braking, the control valve spool will switch to the neutral position and overlap the pump and exhaust lines ($f_н=0, f_в=0$). The switching time of the valve spool is not taken into account, the discharge and exhaust channels are overlapped simultaneously. The connection of the recuperative volume with the rod end of the air motor is considered instantaneous.

Considering the data of the assumptions of the cavity, the working medium pressure in the head end of the air motor will be presented in the following form:

$$p_n=(v_{nm}/v_n)^k \cdot p_{nm}, \qquad (1.1)$$

where p_n, p_{nm} are current and initial pressure at the time of switching to braking in the head end of the air motor; v_n, v_{nm} are current and initial specific volumes of the head end of the air motor; k is adiabatic index.

Reduce equation (1.1) dividing it by the area of the air motor piston:

$$p_n=((x_{0n}+x_m)/(x_{0n}+x))^k \cdot p_{nm}, \qquad (1.2)$$

where x_{0n}, x_m, x are coordinates: original, brake actuation, and current position of air motor piston, respectively.

At the moment of shifting the distributor on braking, the regenerative and braking volumes are combined; in this case the compressed air parameters will be determined by the following system (1.3):

$$(1.3) \begin{cases} p_{шт} \cdot v_{шт}^k = p \cdot v_1^k & (1.3.1) \\[2mm] p_{рек} \cdot v_{рек}^k = p \cdot v_2^k & (1.3.2) \end{cases}$$

where $v_{шт}$, $v_{рек}$ are specific volumes of the air compressed at the start of braking in the rod end and in the regenerative air volume; v_1, v_2 are "conditional" specific air volumes in the rod end and in the recuperative air volume; $p_{шт}$, $p_{рек}$, p are pressures of the air compressed at the start of braking in the rod end, recuperative volume, and in the "combined" volume, respectively.

We express v_1, v_2 specific volumes in the system of equations (1.3):

$$(1.4) \begin{cases} p_{шт} \cdot v_{шт}^k = p \cdot v_1^k \Rightarrow p_{шт} \cdot \left(\dfrac{V_{шт}}{m_{шт}}\right)^k = p \cdot \left(\dfrac{V_1}{m_{шт}}\right)^k \Rightarrow \\[6mm] \Rightarrow V_{шт} \cdot \left(p_{шт}\right)^{\frac{1}{k}} = V_1 \cdot \left(p\right)^{\frac{1}{k}} & (1.4.1) \\[6mm] p_{рек} \cdot v_{рек}^k = p \cdot v_2^k \Rightarrow p_{рек} \cdot \left(\dfrac{V_{рек}}{m_{рек}}\right)^k = p \cdot \left(\dfrac{V_2}{m_{рек}}\right)^k \Rightarrow \\[6mm] \Rightarrow V_{рек} \cdot \left(p_{рек}\right)^{\frac{1}{k}} = V_2 \cdot \left(p\right)^{\frac{1}{k}} & (1.4.2) \end{cases}$$

where $V_{шт}$, $V_{рек}$, are rod and recuperative volumes, respectively, at the time of the start of braking; V_1, V_2 are rod and recuperative volumes connected to the "combined" volume; $m_{шт}$, $m_{рек}$ are air mass compressed in the rod and recuperative volume at the time of the start of braking; p is pressure in the "combined" volume.

To determine pressure in the "combined" volume, we sum up the equations (1.4.1) and (1.4.2):

$$p = \left(\frac{V_{шт} \cdot \left(p_{шт}\right)^{\frac{1}{k}} + V_{рек} \cdot \left(p_{рек}\right)^{\frac{1}{k}}}{V_1 + V_2} \right)^k , \qquad (1.5)$$

Using the Clapeyron equation, we can find temperature of the working medium in the "combined" volume:

$$p \cdot v = R \cdot T \Rightarrow T = \frac{p \cdot v}{R} = \frac{p}{R} \cdot \left(\frac{V_{шт} + V_{рек}}{\dfrac{V_{шт}}{v_{шт}} + \dfrac{V_{рек}}{v_{рек}}} \right) , \qquad (1.6)$$

where T is temperature of the air compressed under braking in the "combined" air volume; R is absolute gas constant.

The final dependence of the air temperature in the brake chamber of the pneumatic actuator on the initial parameters of the regenerative volume will be obtained through determining the values of specific volumes in the equation (1.6) and reducing it to the area of the rod end of the pneumatic motor:

$$T = p \cdot ((s + x_{0ш} + h_{рек} - x) \frac{T_{шт} \cdot T_{рек}}{(s + x_{0ш} - x) \cdot T_{рек} \cdot p_{шт} + h_{рек} \cdot T_{шт} \cdot p_{рек}})) \qquad (1.7)$$

where $h_{рек}$ is reduced to the rod area of the air motor, recuperative volume; T, $T_{шт}$, $T_{рек}$ are absolute temperatures in the "combined", rod and recuperative volumes, respectively.

$$
\left\{
\begin{aligned}
& m \frac{d^2 x}{dt^2} = p_n \cdot F_n - P - p_ш \cdot F_ш && (1.8.1) \\
& p_n = \left(\frac{x_{0n} + x_m}{x_{0n} + x} \right)^k \cdot p_{nm} && (1.8.2) \\
& p = \left(\frac{(s + x_{02} - x)(p_{шт})^{\frac{1}{k}} + h_{рек} \left((p_{рек})^{\frac{1}{k}} \right)}{(s + x_{02} + h_{рек} - x)} \right)^k && (1.8.3) \\
& T_n = \left(\frac{p_{nm}}{p_n} \right)^{\frac{k-1}{k}} \cdot T_{nm} && (1.8.4) \\
& T = p \cdot ((s + x_{0ш} + h_{рек} - x) \frac{T_ш \cdot T_{рек}}{(s + x_{0ш} - x)T_{рек} \cdot p_ш + h_{рек} \cdot T_ш \cdot p_{рек}})) && (1.8.5)
\end{aligned}
\right. \qquad (1.8)
$$

The air motor piston movement is described by the equation (1.8.1). The general system of equations for the braking process of a pneumatic device will have the form (1.8).

Here: m is mass of the working body reduced to the air motor rod; $T_н$ is absolute air temperature in the pump line; T_{nm} is initial value of the air temperature in the head end of the air motor at the time of shifting to braking.

The equations (1.8.2) and (1.8.3) describe the pressure variation, and the equations (1.8.4) and (1.8.5) describe the temperature change in the piston and brake chambers of the air motor, respectively.

The simultaneous solution of the system of equations describing the braking dynamics of the pneumatic actuator (1.8) and its acceleration by Runge-Kutta numerical quadrature method [14] enables to study the dependence of the dynamic characteristics of the pneumatic actuator on the initial parameters of the regenerative volume. The bench assessment of the characteristic coincidence of theoretical and practical dependences showed satisfactory convergence [13], which allowed us to test the adequacy of the obtained mathematical model upon the Fisher's variance ratio. For this purpose, a two-factor experiment was conducted. The initial pressure and the value of the regenerative volume were chosen as independent factors. The factors changed according to three levels of variation, which allowed the use of nine combinations of the factors with three-time replication of each experiment.

The mathematical model is adequate to the practical results obtained through the experimental verification, since the calculated value of the Fisher's criterion is 2.67, which is less than the tabulated one (2.7) [15].

The results obtained have enabled to proceed to a computational experiment, which will allow us to determine rational combinations of the initial parameters of the regenerative volume for the given law of pneumatic actuator braking and for maintaining high-speed parameters.

Conclusions:

1. A mathematical model that adequately describes the dynamic processes taking place in the pneumatic drive chambers under backpressure braking with accumulation of the compressed air energy into the recuperative volume is developed.

2. Mathematical dependences of the pneumatic drive parameters on the initial parameters of the regenerative volume under backpressure braking are obtained.

References

1. Blagojevic, Vladislav A. and Jankovic, Predrag Lj. Advantages of restoring energy in the execution part of pneumatic system with semi-rotary actuator. Thermal Science, 2016, vol. 20, Suppl. 5, pp. S1599-S1609. DOI : https://doi.org/10.2298/TSCI16S5599B

2. Krytikov, Gennadyj, Strizhak, Marjana, Strizhak, Vsevolod. The synthesis of structure and parameters of energy efficient pneumatic actuator. Eastern-European Journal of Enterprise Technologies, 2017, vol. 1, no. 7 (85), pp. 38-44. DOI: https://doi.org/10.15587/1729-4061.2017.92833

3. Mohd Yusop, M. Y. Energy Saving for Pneumatic Actuation using Dynamic Model Prediction [Text]: Submitted for the degree of PhD. School of Engineering. Cardiff University. Wally, UK, 2006, 212 p.

4. Blagojevic, Vladislav A., Šešlija, Dragan and Stojiljkovic, Miodrag. Cost effectiveness of restoring energy in execution part of pneumatic system. Journal of Scientific & Industrial Research, February 2011, vol. 70, pp. 170-176. DOI: http://nopr.niscair.res.in/handle/123456789/10968

5. Dyachenko, A.G., Savostina, T.P., Kolpakov, M.V. Razrabotka konstruktsii podayushchego ustroystva dlya tsilindricheskikh detaley. [Design of feeder for cylindrical parts.] Innovatsionnye materialy i tekhnologii: sb. statey po itogam mezhdunar. nauch.-prakt. konf. [Innovative materials and technologies: Proc. Int. Sci.-Prac. Conf.] Sterlitamak, 2018, pp.11−13 (in Russian).

6. Dolgov, G.A. Sistema upravleniya pozitsionnym pnevmoprivodom zapornoy armatury. [Control system for positional actuator valves.] Young Researcher of the Don, 2017, no. 3 (6), pp. 21−28 (in Russian).

7. Filipov, I.B. Tormoznye ustroystva pnevmoprivodov. [Brake devices of pneumatic actuators.] Moscow: Mashinostroenie, 1987, 143 p. (in Russian).

8. The Anh Dao, Sidorenko, V.S., Dymochkin, D.D. Issledovanie tochnosti pozitsionirovaniya avtomatizirovannogo pnevmoprivoda s vneshnim tormoznym ustroystvom. [Study on positioning accuracy of automated pneumatic drive with an outer brake.] Vestnik of DSTU, 2015, vol. 15, no. 4 (83), pp. 46−53 (in Russian). DOI : https://doi.org/10.12737/16077

9. Grishchenko, V.I., Kilina, M.S., Chernavskiy, V.A. Dinamika protsessa pozitsionirovaniya privodov s gidroamortizatorom. [Positioning dynamics of drive gears with hydroabsorber.] Vestnik of DSTU, 2012, vol. 12, no. 4 (65), pp. 16−21 (in Russian).

10. Gerts, E.V. Dinamika pnevmaticheskikh sistem mashin. [Dynamics of pneumatic systems of machines.] Moscow: Mashinostroenie, 1985, 265 p. (in Russian).

11. Sirotenko A.N., Dyachenko, A.G., Partko S.A. Rekuperatsiya energii v pnevmoprivode fasovochno-napolnitel'nogo oborudovaniya. [Energy recovery in pneumatic drive of packing and filling equipment.] Sostoyanie i

perspektivy razvitiya sel'skokhozyaystvennogo mashinostroeniya: sb. statey 6-y mezhdunar. nauch.-prakt. konf. v ramkakh 16-y mezhdu-nar. agroprom. vystavki «Interagromash-2013». [State and prospects for development of agricultural engineering: Proc. 6th Int. Sci.-Pract. Conf. in framework of 16th Int. Agroindustrial Exhibition "Interagromash-2013".] Rostov-on-Don, 2013, pp. 69–71 (in Russian).

12. Sirotenko A.N., Partko S.A. Matematicheskaya model' dinamicheskikh protsessov pnevmoprivoda, pri tormozhenii protivodavleniem, s rekuperatsiey energii v dopolnitel'nyy ob"em. [Mathematical model of dynamic processes of pneumatic drive during braking by reverse pressure with recovery of energy into additional volume.] Science Review, 2017, no. 21, pp. 67–74 (in Russian).

13. Sirotenko A.N., Partko S.A. Decrease in Power Inputs in Pneumodrive Weighing-and-Packing Machine. International Journal of Applied Engineering Research, 2017, vol. 12, no. 14, pp. 4599-4603.

14. Sirotenko A.N., Partko S.A. Raschet dinamicheskikh parametrov pnevmogidravlicheskogo privoda s rekuperatsiey energii: svidetel'stvo 2018613130 Ros. Federatsiya. [Calculation of dynamic parameters of pneumatic-hydraulic drive with energy recovery.] RF Certificate no. 2018613130, 2018 (in Russian).

15. Sirotenko A.N., Partko S.A., Saed Bakir Ala. Zavisimost' energoskorostnykh kharakteristik pnevmoprivoda ot nachal'nykh parametrov dopolnitel'nogo ob"ema, pri tormozhenii protivodavleniem. [Dependence of energy-speed characteristics of pneumatic drive on initial parameters of additional volume under counterpressure braking.] Vestnik of DSTU, 2017, vol. 17, no. 4 (91), pp. 69–76 (in Russian). DOI : https://doi.org/10.23947/1992-5980-2017-17-4-69-76

Authors:

Sirotenko, Andrey N.,
associate professor of the Machine Design Principles
Department, Don State Technical University (1, Gagarin
sq., Rostov-on-Don, 344000, RF), Cand.Sci. (Eng.),
associate professor,
ORCID: http://orcid.org/0000-0001-9956-1032
andsirotenko@yandex.ru

Partko, Svetlana A.,
associate professor of the Machine Design Principles
Department, Don State Technical University
(1, Gagarin sq., Rostov-on-Don, 344000, RF), Cand.Sci.
(Eng.), associate professor,
ORCID: http://orcid.org/0000-0002-8568-0716
parlana@spark-mail.ru

Wael Salloum,
professor of the Agricultural Engineering Department,
Aleppo University (Aleppo, Syria), Dr.Sci. (Eng.),
professor,
ORCID: http://orcid.org/0000-0003-0032-2918
w_salloum@yahoo.com

МАШИНОСТРОЕНИЕ И МАШИНОВЕДЕНИЕ
MACHINE BUILDING AND MACHINE SCIENCE
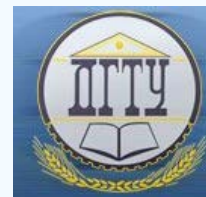
Linear-logical decision-making algorithm for signal processing[*]

V. S. Plaksienko[1][**]

[1] Institute for Radiotechnical Systems and Control, Southern Federal University, Taganrog, Russian Federation

Линейно-логический алгоритм принятия решения при обработке сигналов[***]

В. С. Плаксиенко[1][**]

[1]Институт радиотехнических систем и управления Южного федерального университета, г. Таганрог, Российская Федерация

Introduction. Heuristic synthesis is used to improve the efficiency of reception and processing of discrete signals under aprior information pressure. The analysis of the decision-making algorithm for the linear-logical processing of discrete signals in case of the incomplete aprior data on their parameters is presented. The work objective is to develop and analyze the efficiency of the linear-logical algorithms.

Materials and Methods. New mathematical algorithms for the signal reception and processing, effective under conditions of a priori uncertainty, are proposed. They are based on the consideration of the structure of emissions and process exceedance in the signal processing channels.

Research Results. Linear-logical algorithms for processing discrete signals are developed. They are based on the consideration of one, two and more detailed characteristics of emissions or exceedance of random processes.

Discussion and Conclusion. The results obtained can be useful in the synthesis of algorithms and devices for the signal reception and processing. Algorithms and devices are implemented both in an analog form and in the form of algorithms for computers. The simulation programs for the signal processing under conditions of the considerable uncertainty of aprior information on the signals and the channels of their distribution are developed.

Keywords: decision rules, heuristic synthesis, reception and processing of discrete signals, probability distribution densities, emissions and exceedance of random processes.

Введение. Для повышения эффективности приема и обработки дискретных сигналов в условиях дефицита априорных сведений применяют эвристический синтез. Представлен анализ алгоритма принятия решения при линейно-логической обработке дискретных сигналов в случае, если априорные данные об их параметрах неполны. Цель работы — построение и анализ эффективности линейно-логических алгоритмов.

Материалы и методы. Предложены эффективные в условиях априорной неопределенности математические алгоритмы приема и обработки сигналов. Они основаны на учете структуры выбросов и превышений процессов в каналах обработки.

Результаты исследования. Созданы линейно-логические алгоритмы обработки дискретных сигналов. Они основаны на учете одной, двух и более детальных характеристик выбросов или превышений случайных процессов.

Обсуждение и заключения. Полученные результаты могут быть полезны в процессе синтеза алгоритмов и устройств приема и обработки сигналов. Алгоритмы и устройства реализуемы как в аналоговом виде, так и в виде алгоритмов для ЭВМ. Созданы программы моделирования при обработке сигналов в условиях значительной априорной неопределенности информации о сигналах и о каналах их распространения.

Ключевые слова: решающие правила, эвристический синтез, прием и обработка дискретных сигналов, плотности распределения вероятностей, выбросы и превышения случайных процессов.

Introduction. Heuristic engineering synthesis of nonparametric decision rules is used to optimize signal processing under conditions of considerable a priori uncertainty. This procedure is based on the analysis of

---

the emission parameters of random processes at the output of the demodulator of the receiver of discrete signals [1–7]. The emission theory is of considerable use in the engineering practice. However, the analysis of regularities and detailed characteristics of emissions is a complex analytical task even at a constant or slowly varying threshold. In the course of the analytical approach, relations are obtained that lead to nonconvergent series, which explains the absence of physically meaningful results.

At present and in the near future, the use of discrete multiposition signals is promising. They include discrete address systems, multiple telegraphy systems (frequency telegraphy, multiposition frequency telegraphy), and systems with D and E codes in which elementary parcels of T_c duration at one or different frequencies are transmitted serial/parallel in time [5, 8–10].

When receiving binary signals at the resolver input, two random processes occur, and the decision procedure is reduced to the problem of statistical hypothesis testing. It is necessary to determine which random process (of the compared ones) has more energy on the observation interval. In this case, the decision-making procedure can be reduced to comparing the difference signal value at the receiver output with a constant zero threshold. Hence, it is necessary to compare at least two random processes (at the best case, a random process from the output of the receiver of discrete signals at a slowly varying threshold is analyzed).

Statistical testing of hypotheses is reduced to the analysis of the mutual exceedance of two or more processes. The analytical presentation of this problem is cumbersome, and it does not provide engineering solutions [1, 11–15]. Heuristic synthesis and computer-based statistical modeling enable to obtain significant engineering applications.

When receiving multiposition signals, the following can be simplified:
- their spectra $S(f)$;
- amplitude-frequency characteristics (AFC) of the filters of $K(f)$ receivers (Fig. 1).
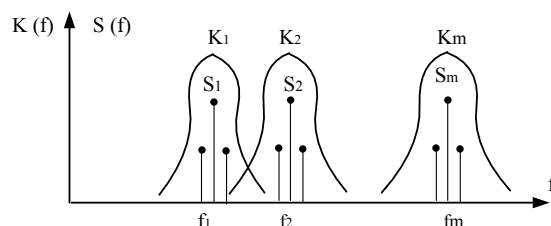
Fig. 1. Frequency response of filters

A linear receiver of multiposition signals should have:
- common intermediate frequency amplifier (IFA),
- general decision making circuit (DMC).

Sets of separation filters (see Fig. 1) and amplitude detectors (AD) are also required. The analysis of such receivers shows [1] the following: the greater the number of m signal locations, the lower their immunity. Requirements for the frequency response of filters (see Fig. 1) are quite rigid. AFC should not be overlapped to ensure frequency orthogonality. In this case, the noise at the filter outputs will be independent. There should be no overlapping regions between the AFC filters tuned to f_i, frequencies (see Fig. 1). The AFC form should have a flat area in the neighborhood of the resonant frequency, so that the signal spectra are not distorted.

Some existing contradictions should be observed. Thus, narrowband filters limit the operating speed. In case of signal depression and the Doppler effect, the degradation of quality and even failure of communication may occur. Broadband filters lead to the interpenetration of the signals of the neighboring frequency channels, i.e. the orthogonality is violated, and, accordingly, the reception quality decreases.

The procedures at the filter outputs of the adjacent channels in the signal detection and processing systems are characterized by the statistical relationships that increase with extending the mutual overlapping of the signal spectra or AFC filters. A detailed examination of the frequency-sharing procedure shows that we can speak of pairwise dependent workflows in the frequency co-channels when processing multiposition signals in the case of the overlapping AFC filters. This is of particular importance when used to optimize the reception of multiposition signals of nonlinear or linear logic procedures [1, 11–14].

Research Objective. Under conditions of considerable prior uncertainty, the signal frequency is known with limited accuracy, and the range of variation of the elementary symbol durations can change up to a thousand times. Additional requirement is real-time operation. For simplicity, we will restrict ourselves to the case of processing binary signals.

2

Decision algorithm synthesis. In papers [1, 11–13], some features of processing discrete signals under conditions of a considerable prior uncertainty of the information about a symbol duration are considered. The problem can be solved through the linear procedures by parallelism of the decision algorithm. The problem becomes more involved through increasing the required accuracy and expanding the variation range of the elementary symbol duration.

Under such conditions, the use of the adaptive procedures requires significant amount of time to adapt; either it is almost unrealizable due to high prior uncertainty. Let us analyze the possibilities of the heuristic synthesis of the algorithm based on the statistical properties of the mutual exceedance of two or more random processes [1, 11–12].

Consider a broadband reception with integration or filtering after the detector, when $\Delta f_\text{п} T \gg 1$ ($\Delta f_\text{п}$ is fп is the receiver bandwidth, T is the duration of the elementary symbol). In this case, the counts of the process at the resolver output can be considered near-normally distributed. The expectation and dispersion of this process are determined by the relations [4]:

$$\Delta M[x] = M[x_1] — M[x_2], \qquad D[x] = D[x_1] + D[x_2].$$

The probability of erroneous reception is calculated from the formula [1–3, 12]:

$$P = \frac{1}{2}[1 - \Phi(\alpha)].$$

Here $\Phi(\alpha) = \sqrt{\frac{2}{\pi}} \int_0^\alpha \exp(-\frac{x^2}{2})dx$ is Kramp function; $\alpha = \frac{\Delta M}{\sqrt{D}} = \frac{h}{\sqrt{2 + 2\Delta f T / h^2}}$ is ratio of the constant component to

the effective value of the variable; $h^2 = \frac{a^2}{2v^2}$ is ratio of the signal element energy to the noise spectral density, where a

is the signal normalized amplitude, and v^2 is the noise spectral density.

When processing discrete signals under these conditions, only non-parametric decision algorithms can be used. The statistical characteristics of emissions of random processes are interesting themselves: $t_\text{П}$ duration of the emissions (exceedance), $T_\text{И}$ duration of the intervals between emissions, ξ_m values of emission maxima, etc. [3]. The optimization decision algorithms can be based on one of the detailed characteristics, for example: the crossing threshold number during the observation period, the duration of the threshold crossing intervals, etc. It is necessary to determine the informative features of such detailed characteristics of the mutual exceedance of random processes. Technically realizable engineering metering data will optimize the algorithm for receiving and processing signals under the specified conditions.

In the context of energy, the greatest accuracy under the conditions of considerable prior uncertainty will be ensured by the consideration of $S_\text{П}$ areas of mutual exceedance (within the energy limit). However, to implement it in real time algorithmically and a fortiori technically is difficult.

The concept of emissions is a special case of the concept of mutual exceedance for two or more processes, including random ones. When processing binary signals, the problem of analyzing the emissions of the difference process with respect to the zero threshold is set. It is adequate to the task of analyzing the mutual exceedance of two envelope processes in the signal processing channels [3, 11].

To optimize the decision-making problem in real time, it is advisable to simultaneously consider two or more detailed characteristics of emissions, for example, the duration and exceedance value. The product of the duration by the level (amplitude) of the exceedance is an evaluation of the exceedance area (considering the shape factor of the exceedance) [11].

We use two detailed characteristics.

1. q relative level of excess:

$q = X_i(t) / X_j(t)$, where $X_i(t)$ and $X_j(t)$ are the analyzed processes.

2. Θ relative duration of excess:

$\Theta = t_\text{П} / \tau_\text{К}$, where $\tau_\text{К}$ is the correlation interval of the processes at the output of the linear part of the receiver determined by its passband.

To consider these characteristics in combination is not so hard technically.

Joint consideration of these characteristics is relatively not difficult. Совместный учет указанных характеристик технически сравнительно не труден

At the same time, its reliability is close to the indicators obtained allowing for $S_\text{П}$ areas of exceedance. Considering the meaning of the term "excess", q should be greater than 1, therefore in a binary situation, when forming two-parameter distributions, q is determined by the relation [11]:

$$q = \begin{cases} \dfrac{x_1(t)}{x_2(t)}; & x_1(t) \geq x_2(t); \\ \dfrac{x_2(t)}{x_1(t)}; & x_2(t) \geq x_1(t). \end{cases} \tag{1}$$

This approach allows us to analyze the multiparameter distributions of mutual excesses of two or more random processes.

To improve the quality of decision-making, it is necessary to reduce the total number of mutual exceedance of processes. This follows from the analysis results of the two-dimensional laws of the mutual exceedance distribution of the signal-noise mixture envelope and noise envelope [11]. It is necessary to transform the processes in such a way that, without disturbing the likelihood ratio, to obtain the two-dimensional distribution forms, easily distinguished by the resolver [12].

Both problems are solved using a modified combined addition algorithm [1, 11, 14]:

$$X_{1\Pi}(t) = [X_1(t) - K\,X_{2\Pi}(t)]\,1[X_1(t) - K\,X_2(t)],$$

$$X_{2\Pi}(t) = [X_2(t) - K\,X_{1\Pi}(t)]\,1[X_2(t) - K\,X_1(t)], \tag{2}$$

where K is a coefficient taking values from 0 to 1; 1 $[Z(t)]$ is a single step function, with 1 $[Z(t)] = 1$ for $Z(t) > 0$ and 1 $[Z(t)] = 0$ for $Z(t) < 0$.

The spectra of the $X_{1\Pi}(t)$ and $X_{2\Pi}(t)$ processes formed after processing by the algorithm (2) are extended. They should be limited to the width of the spectra of the initial information processes $X_1(t)$ and $X_2(t)$.

The value of K determines the implemented modifications of the algorithm and devices of the combined addition. We are talking about the algorithm of mutual transformation, the method of combined addition, the cross-blocking system [1, 11].

When $K = 1$, only the fact of the process exceedance is taken into account of all the detailed characteristics of the exceedance. The auto-selection algorithm is implemented when the diversity technique is used [4], and the mutual conversion – under decision making [11].

When $K = 0.414$, both the fact that one process is exceeded by another, and the level of q excess are considered [4]. The combined addition is implemented in the diversity reception. When $1 > K > 0$, not only the fact of excess, but also q level of excess is taken into account. The modified method of combined addition is implemented under making decision.

Linear-logical procedures implemented as a result of heuristic synthesis enable statistically to transform the original random processes. When $K = 1$ in (2), auto-selection of processes is realized in time. Temporally continuous processes (Fig. 2, *a*) turn into sequences of pulses with $X_1^{(1)}(t)$ and $X_2^{(1)}(t)$ random amplitudes (Fig. 2, *b* and 2, *c*).

a)

b)

c)

d)
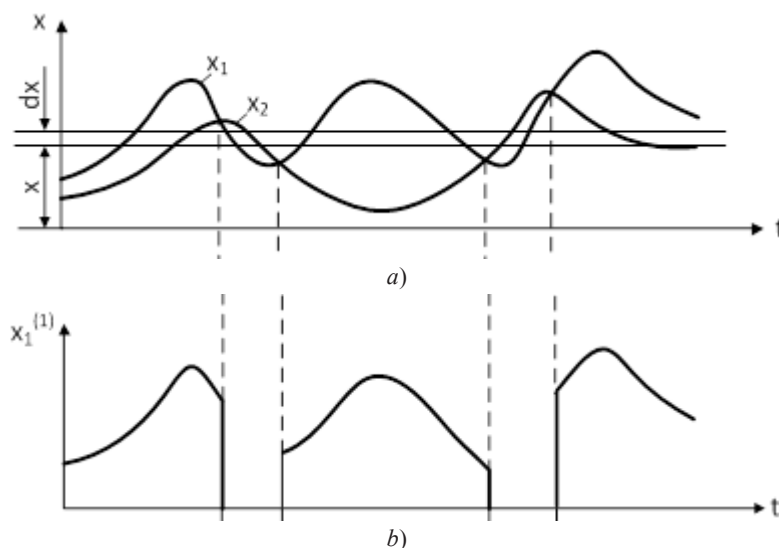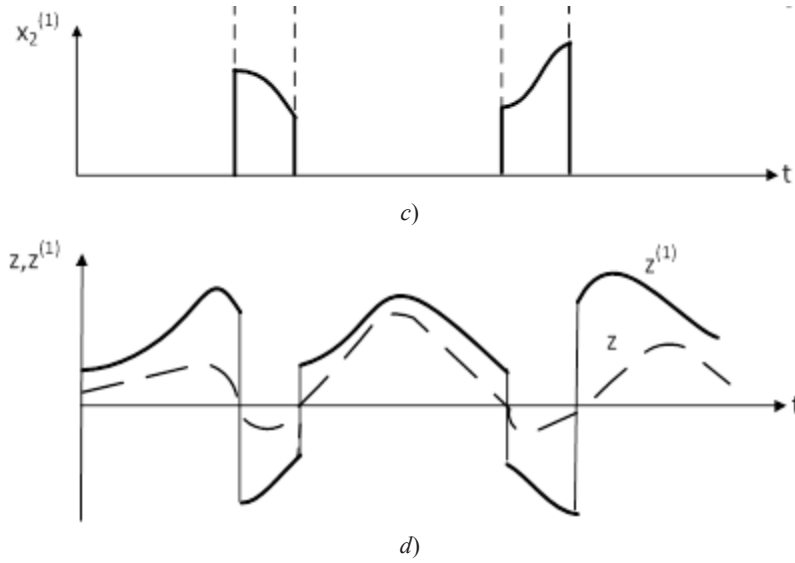
Fig. 2. Combined addition at *K*=1

In Fig. 2, *d*, the difference processes are presented: $Z = X_1 - X_2$ without processing and $Z^{(1)} = x_1^{(1)} - x_2^{(1)}$ after processing according to rule (2).

Density of probability distribution of $X_1^{(1)}(t)$ and $X_2^{(1)}(t)$ processes:

$$W_1^{(1)}(x) = A_1\delta(x) + W_1(x)F_2(x) \tag{3}$$

$$W_2^{(1)}(x) = A_2\delta(x) + W_2(x)F_1(x). \tag{4}$$

A_1 and A_2 coefficients are determined from the normalization condition:

$$A_1 = 1 - \int_0^\infty W_1(x)F_2(x)dx, \tag{5}$$

$$A_2 = 1 - \int_0^\infty W_2(x)F_1(x)dx, \tag{6}$$

where $F_1(x)$ and $F_2(x)$ are cumulative distribution functions.

From the consideration of Fig. 2, *a* - 2, *c*, it follows that $X_1^{(1)}(t)$ and $X_2^{(1)}(t)$ processes are equal to zero for some time. Therefore, their $W_1^{(1)}(x)$ and $W_2^{(1)}(x)$ probability distribution densities will contain $\delta(x)$ delta functions (Fig. 3).

a)   *b)*
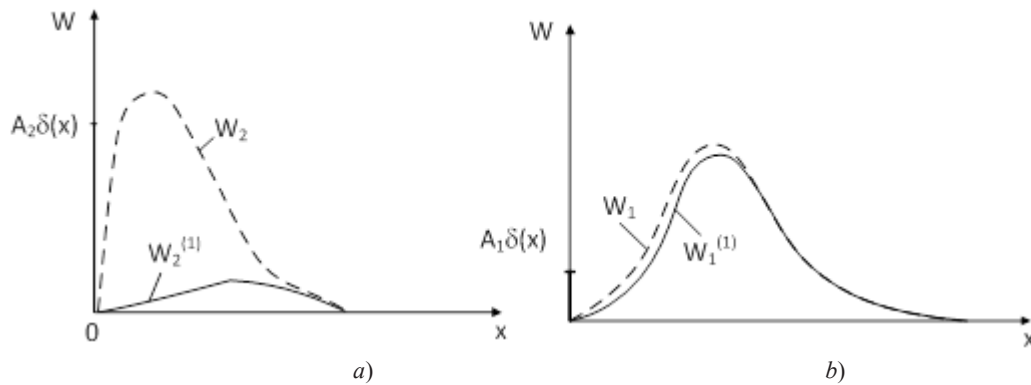
Fig. 3. Density of probability distribution of processes

Fig. 4 shows the probability distribution density of difference processes $W(z)$ without processing according to rule (2) (Fig. 4, *a*) and $W_1^{(1)}(Z)$ after processing (Fig. 4, *b*). Here, Δ is the erasing zone of the resolver.
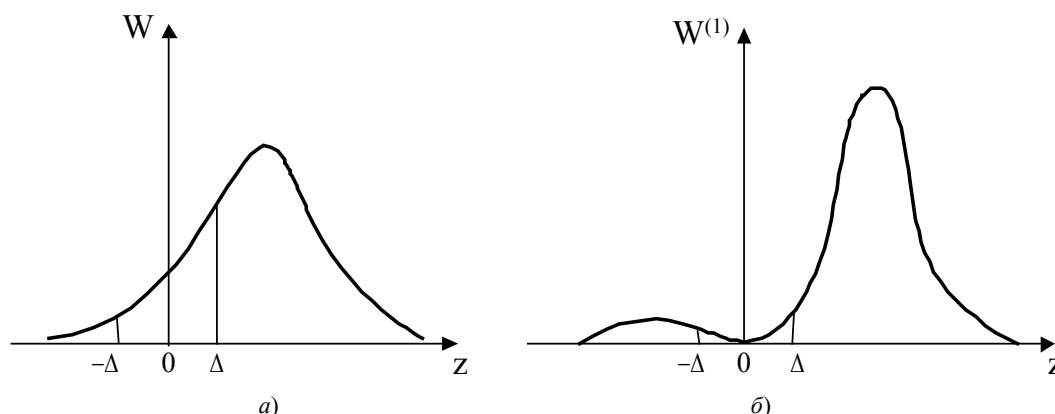
Fig. 4. Density of probability distribution of $Z(t)$, $Z^{(1)}(t)$ processes

In accordance with Fig. 2, *b* and 2, *c*, the processes after treatment according to rule (2) are impulsive. Their spectra will be broader than the spectra of the source processes. Thus, processing according to rule (2) does not lead to an increase in the quality of reception, but only improves the threshold properties [11–12, 16].

Their spectra will be broader than those of the source processes. Thus, processing according to rule (2) will not lead to an increase in the reception quality, but it will only improve the threshold properties [11–12, 16].

A full treatment procedure includes two operations:

- linear-logical operation according to rule (2) (it is pertinently non-linear, since there appear components in the spectrum that were not at the input);

- filtering.

Filtering considers the second parameter of Θ exceedance – relative duration. The expanded spectra of processes remain within the boundaries specified under the formation of $X_1(t)$ and $X_2(t)$ source processes (see Fig. 2, *a*).

Processing according to rule (2) can repeat depending on the variation range of the duration of the expected signals and reception conditions [12]. In this case, the values of *K* parameter are different, they are always less than 1, and increase in the subsequent processing cycles.

Problems of the automatic frequency control are solved more efficiently when using devices that implement linear-logical processing [14, 17–18]. Locking and retention bands are extended by low-end techniques. Certain parameter stability of the automatic frequency control under the additive interference is provided.

Research Results. The results of studying the algorithm (2) in case when signals are dependent are beyond the scope of this paper. However, the data already obtained have shown the algorithm efficiency up to the values of the cross-correlation coefficients of $\rho = 0.5–0.6$ processes. This is in good agreement with the results of solving the tasks of the diverted reception [2–4]. Algorithms of the modified combined addition of signals are effective both under the diversity technique, and in decision-making problems. Yet, the consideration of their implementation features is beyond the scope of the paper.

Thus, the optimization of the decision-making procedure for processing discrete signals under conditions of considerable prior uncertainty can be performed on the basis of non-parametric algorithms with the heuristic consideration of the detailed characteristics of mutual exceedance of random processes. More detailed characteristics complicate the algorithm. Still, it is this algorithm that provides greater invariance in terms of noise immunity under varying the duration of the expected signals. The synthesized algorithms can be implemented in the form of additional processing procedures on a computer, and technically – in the form of analog devices [14, 19].

References

1. Fink, L.M. Teoriya peredachi diskretnykh soobshcheniy. [Theory of transmission of discrete messages.] Moscow: Sovetskoe radio, 1970, 728 p. (in Russian).

2. Yarlykov, M.S., Chernyakov, M.V., eds. Svyaz' s podvizhnymi ob"ektami na SVCh. [Communication with mobile objects on the microwave.] Moscow: Svyaz', 1979, 520 p. (in Russian).

3. Fomin, Ya.A. Teoriya vybrosov sluchaynykh protsessov. [Theory of random process emissions.] Moscow: Svyaz', 1980, 216 p. (in Russian).

4. Parsons, J.-D. The Mobile Radio Propagation Channel. Hoboken: Wiley & Sons, 2000, 433 p.

5. Ipatov, V.P. Shirokopolosnye sistemy i kodovoe razdelenie signalov. Printsipy i prilozheniya. [Broadband systems and code division of signals. Principles and Applications.] Moscow: Tekhnosfera, 2007, 488 p. (in Russian).

6. Andronov, I.S., Fink, L.M. Peredacha diskretnykh soobshcheniy po parallel'nym kanalam. [Sending discrete messages through parallel channels.]. Moscow: Sovetskoe radio, 1971, 408 p. (in Russian).

7. Stratonovich, R.L. Printsipy adaptivnogo priema. [Principles of adaptive reception.] Moscow: Nauka, 1973, 144 p. (in Russian).

8. Tikhonov, V.I. Optimal'nyy priem signalov. [Optimum signal detection.] Moscow: Radio i svyaz', 1983, 320 p. (in Russian).

9. Filippov, L.I. Osnovy teorii radiopriema diskretnykh signalov. [Fundamentals of radioreception of discrete signals.] Moscow: Nauka, 1974, 192 p. (in Russian).

10. Sikarev, A.A., Falko, A.I. Optimal'nyy priem diskretnykh soobshcheniy. [Optimum discrete signal detection.] Moscow: Svyaz', 1978, 288 p. (in Russian).

11. Plaksienko, V.S. Urovnevaya statisticheskaya obrabotka diskretnykh signalov. [Level statistical processing of discrete signals.] Moscow: Uchebnaya literatura, 2006, 274 p. (in Russian).

12. Plaksienko, V.S., Plaksienko, N.E. Issledovanie dvumernykh raspredeleniy, vzaimnykh prevysheniy sluchaynykh protsessov. [Study on two-dimensional distributions, mutual excesses of random processes.] Izvestiya TRTU, 2000, no. 1, pp. 29–33 (in Russian).

13. Plaksienko, V.S., Plaksienko, D.V. Kombinirovannoe slozhenie signalov. [Signal combining.] Radioengineering, 2001, iss. 54, no. 7, pp. 70–72 (in Russian).

14. Plaksienko, V.S., et al. Ustroystvo fazovoy avtopodstroyki chastoty : a. s. 1290519 SSSR, A1 MKI N03L7/00. [Phase-locked loop.] USSR Authorship Certificate, no. 1290519, 1987 (in Russian).

15. Klovskiy, D.D. Peredacha diskretnykh soobshcheniy po radiokanalam. [Discrete radiomessaging.] Moscow: Radio i svyaz', 1982, 304 p. (in Russian).

16. Plaksienko, V.S. Optimizatsiya nekogerentnykh algoritmov prinyatiya resheniya. [Optimization of non-coherent decision-making algorithms.] Electronic devices and information technologies, 1994, iss. 6, pp. 18–20 (in Russian).

17. Shakhgildyan, V.V., Lokhvitskiy, M.S. Metody adaptivnogo priema signalov. [Adaptive reception methods.] Moscow: Svyaz', 1974, 160 p. (in Russian).

18. Shakhgildyan, V.V., Lyakhovkin, A.A. Sistemy fazovoy avtopodstroyki chastoty. [Phase Locking Systems.] Moscow: Svyaz', 1972, 448 p. (in Russian).

19. Plaksienko, V.S., Plaksienko, N.E., Sidenkov, A.S. Osobennosti lineyno-logicheskoy obrabotki signalov. [Features of linear-logical signal processing.] Prospero, 2014, no. 1, pp. 108–113 (in Russian).

Author:

Plaksienko, Vladimir D.,
professor of the Embedded and Radio Receiving Systems
Department, Institute for Radiotechnical Systems and
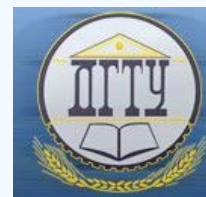Control, Southern Federal University
(1, Engels St., Taganrog, 347922, RF), Dr.Sci. (Eng.),
professor,
ORCID: http://orcid.org/0000-0002-1730-628X
vsp46@mail.ru

МАШИНОСТРОЕНИЕ И МАШИНОВЕДЕНИЕ
MACHINE BUILDING AND MACHINE SCIENCE

Reliability of parts and unrestorable components in the machine design[*]

Yu. P. Manshin[1], E. Yu. Manshina[2][**]

[1,2] Don State Technical University, Rostov-on-Don, Russian Federation

Надежность деталей и неремонтируемых узлов при проектировании машин[***]

Ю. П. Маньшин[1], Е. Ю. Маньшина[2][**]

[1, 2] Донской государственный технический университет, г. Ростов-на-Дону, Российская Федерация

Введение. В статье рассматриваются вопросы нормирования показателей надежности на ранних стадиях проектирования машин. Такой подход обеспечивает соблюдение заданного уровня надежности при разработке деталей, критичных с точки зрения стабильной эксплуатации. Цель работы — исследовать проблемы проектирования в указанной сфере. Анализ методов нормирования надежности позволяет утверждать, что их недостаточно для проектирования. Кроме того, отмечены противоречия, связанные с использованием в проектировании экспоненциального закона надежности.

Материалы и методы. На стадии технического задания определены численные значения наработки и безотказности машины. Затем значения вероятностей безотказной работы или отказов системы и ее элементов представлены степенными выражениями. В них степени являются параметрами ранжирования показателей безотказности элементов системы.

Результаты исследования. Синтезирован альтернативный подход к нормированию, который позволяет выполнить полный структурный анализ проекта. Таким образом, могут быть оценены показатели надежности всей системы или деталей, безотказность которых определяет надежность машин. Детали и другие элементы, отказы которых не внезапны, рассматриваются без применения экспоненциального закона. При этом сохраняется свойственная ему простота математических операций.

Обсуждение и заключения. Для проектирования с заданным уровнем надежности недостаточно числового значения вероятности безотказной работы (ВБР) машины в целом, принимаемого на стадии технического задания. Необходимы требуемые ВБР и наработки элементов системы, которые являются источниками отказов, развивающихся по разным законам. Полученные результаты могут быть использованы как при проектировании новых механических систем с заданным уровнем надежности, так и при модернизации машин.

Introduction. The issues on standardization of reliability indices in the early stages of machine design are considered. This approach maintains the target level of reliability when developing parts that are critical in view of stable operation. The work objective is to study design problems in this area. The analysis of the reliability regulation methods suggests that they are insufficient to design. Besides, there are some contradictions associated with the use of the exponential failure law in design.

Materials and Methods. At the stage of the task order, the numerical values of the operation time and reliability of the machine are determined. Then the values of the reliability probabilities or failures of the system and its elements are shown by exponential expressions. In them, degrees are the ranking parameters of the system reliability indices.

Research Results. The alternative approach to normalization is synthesized; it enables to complete a full structural analysis. Thus, the reliability indices of the entire system or parts, whose operational safety determines the machine reliability, can be assessed. Parts and other components, whose failures are not sudden, are considered without using the exponential law. This preserves the inherent simplicity of mathematical operations.

Discussion and Conclusions. The numerical value of the reliability probability (RP) of the machine as a whole, taken at the stage of the task order, is insufficient for the reliability target design. The specified RP and running time of the system elements, which are sources of failures developing according to different laws, are required. The results obtained can be used both in designing new mechanical systems with the reliability target, and in the modernization of machines.

Ключевые слова: надежность, вероятность, безотказность, наработка, машина, техническая система, элемент.

Keywords: reliability, probability, failure-free performance, running time, machine, technical system, element.

Introduction. The conditions for launching mechanical products into manufacture and the unified system for design documentation (ESKD) [1–2] require considering the following engineering systems (ES) reliability parameters under the machine designing:
- durability - calendar time (T_k));
- reliability - probability of failure-free operation $P(t)$ ...);
- lifelength $t = T$ hours (probability of failure-free operation should be guaranteed for this period).

The given factors characterize the machine as a whole and are coordinated at the stage of the technical specifications (TS). The developer should affect the failsafety, which is the key feature of the reliability of nonrecoverable ES and forms the durability of the restorable ES during the workover intervals.

t lifelength is the argument of $P(t)$ reliability function. By any law of reliability, $P(t)$ monotonously decreases with increasing t. In virtue of this, to achieve the required reliability probability (RP), the lifelength must be efficiently minimized and selected according to the ES behavior [3].

Parts and nonrepairable products, being worn out, determine the time between failures (TBF). Ideally, the TBF of the elements should be the same or at least be a multiple of the selected ES lifelength. In this case, T_k calendar time and the required T lifelength are related as follows:

$$T = T_k \cdot 365 \cdot K_{zod} \cdot 24 \cdot K_{cym} \cdot \Pi B \, , \, ч, \tag{1}$$

wher T_k is calendar life in years; K_{zod} is the coefficient of ES possible use p.a.; K_{cym} is the coefficient of ES use per day; ΠB is duty factor, which is the average ratio of on-time (acceleration time and steady-state motion time) to the ES work-cycle time.

High RP is possible while reducing the required lifelength. If it needs to be significantly increased, failsafety will have to be maintained as follows:
- to perform maintenance more often;
- to budget disadvantage costs for ensuring the quality of products when designing key elements [4, 5].

The project RP can be selected from existing industry standards, from competitive conditions, and on other grounds, including the conventional reliability categories adopted for the engineering products (Table 1).

Table 1

Reliability categories of engineering products

Reliability category	0	1	2	3	4	5
RP acceptable value $P(t)$	≤ 0.9	≥ 0.9	≥ 0.99	≥ 0.999	≥ 0.9999	1

When considering the reliability categories, the following groups of the ES characteristics are taken into account [3, 6, 7].

1. According to the structural type of products. Technological complexes, machines, units, mechanisms and hierarchy (levels) of their assembly units and parts are considered. Under the sequential component interaction in most machines, the RP grows with the transition to the lower levels of the reliability structure diagram. Then the RP of the details under the structural analysis may approach the indices of 3-5 reliability categories.

2. According to the ES types. The projected level of RP directly depends on the level of the manufacturer's responsibility before the ES consumer. Undoubtedly, the highest level of RP is planned, for example, for aircraft, chemical machinery, medical equipment, military equipment, etc.

3. According to types of failure effects. The projected level of RP directly depends on the potential damage level in case of a machine failure (economic, environmental, reputational, etc.).

It is generally accepted [5, 6, 8–13] that the ES failures are presented as sudden. In this case, the RP is described by the exponential law

$$P(t) = e^{-\lambda t} \, . \tag{2}$$

Here, λ failure rate in the period of normal operation after run-in is associated with $\check{T}$ mean time between system failures

$$\lambda = 1 / \check{T} \tag{3}$$

with failsafety parameters

$$\lambda = (-\ln P(T)) / T \ . \tag{4}$$

From here, the ES mean time between failures (MTBF) can be calculated

$$\breve{T} = -T / (\ln P(T)) \ . \tag{5}$$

This algorithm for forming the ES reliability parameters has both protagonists and opponents [7, 10, 14]. Do all failures occur suddenly? How correct are the ES reliability parameters (3) - (5) arising from the exponential law?

How correct are the ES reliability parameters (3) - (5) arising from the exponential law? These questions arise when determining the failure rate (4) and the corresponding ES RP (3) regardless of the estimation technique:

- according to specified T lifelength and $P(T)$ RP;
- on $\breve{T}$ MTBF;
- according to $\breve{T}$ test results.

In the literature, structural analysis of the ES reliability of the ES, which transform the input effect (IE) into output parameters (OP), is usually referred to as a bottom-up network analysis from the RP components to the RP systems. Herewith, the following schematic structures are considered: sequential (Fig. 1, a), parallel (Fig. 1, b), and combined (Fig. 1, c).
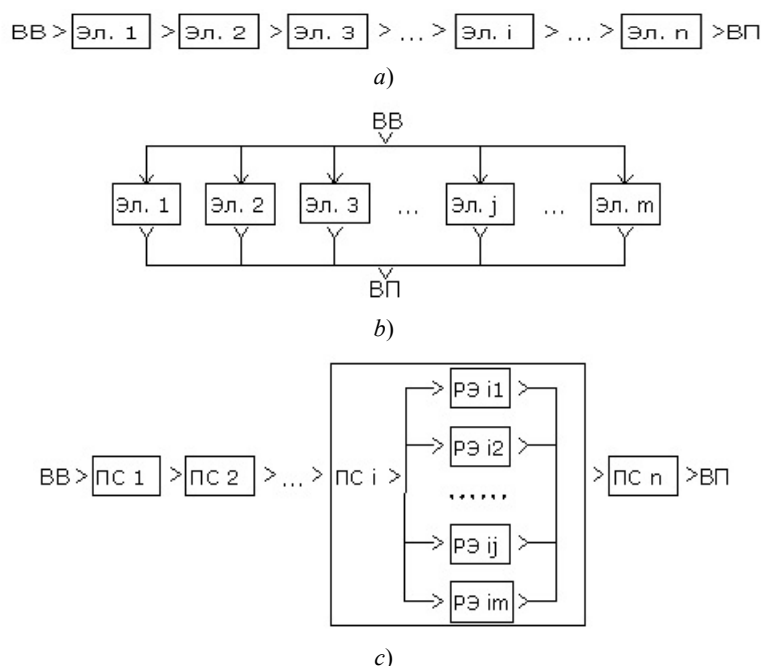
Fig. 1. Schematic structures of ES reliability under various types of component
interaction (ВВ=IE; ВП=OP)

Under the sequential interaction of the ES components (see Fig. 1, a) whose failures are independent, the exponential law (2) represents a convenient mathematical model. If $P(t)$ system RP and components - $P_i(t)$ subsystems are in the ratio

$$P(t) = \prod_{i=1}^{n} P_i(t), \tag{6}$$

then the failure rates of λ system and λ_i subsystems are in the ratio

$$\lambda = \sum_{i=1}^{n} \lambda_i \tag{7}$$

and they are ranked depending on the accepted principle of intensity distribution over the components.

A hierarchical schematic structure developed from the nested levels of subsystems and components [3, 6, 8–12] enables, selectively or throughout the structure, to perform a top-down analysis [3, 9] (from ES RP to RP of components). The required values of the RP of components along with the required lifelength are the initial data for designing parts with the specified reliability level [15, 16].

The top-down analysis algorithm based on (2) enables to distribute the intensities and RP components over all nested levels of the schematic structures with equal success. This is the case for radioelectronic systems [10, 11]. But at the level of the mechanical system components [3], a contradiction arises: it is impossible to apply the exponential law if the development of degradation failure proceeds according to another law. The system failure will occur as a result of the sequential interaction not related to the exponential law. All the while, the development of a schematic structure for

the ES reliability has sense if it serves as the basis for designing parts and selecting standardized components with the required RP for the selected lifelength.

When analyzing ES RP with parallel component interaction (see Fig. 1, b), the following conditions are considered:

- components are constantly on,
- their failures are independent,
- each of m components has $P_j(t)$ RP,

- each of the m components is able to accept an input effect and convert it into an output parameter of the ES (see Fig. 1, b).

In this case, the ES failure will occur after the failure of the last functional component. The probability of system failure through the component failure probability:

$$F(t) = \prod_{j=1}^{m} F_j(t) . \tag{8}$$

From the property

$$P(t) + F(t) = 1 \tag{9}$$

The system survival probability through the component RP:

$$P(t) = 1 - \prod_{j=1}^{m} [1 - P_j(t)] . \tag{10}$$

For homogeneous components

$$P(t) = 1 - \left[1 - P_j(t)\right]^{m} . \tag{11}$$

If the goal is to provide the specified ES RP, and homogeneous redundant components are taken into account, then using the expression of the exponential law (2) gives a simple failure rate calculation of components or m number of components only in the ratio (11). For more complex relations (10) and combined structures (see Fig. 1, c), examples using the exponential law are not given.

Simple division into components is impossible in respect to complex structures with multidirectional component interaction with dependent failures. Performance and reliability parameters should be determined for the system as a whole, and in this case, it may be necessary to carry out a large amount of analytics and experimental works. A graphic representation of such diagrams [7, 9] is accompanied by a reference to the complexity of the functioning model and the cumbersome reliability calculations (for example, a complex closed interdependent operation of IC engine units or of jet engine).

Main Part. For the design ES implementation under any kind of interaction, it is necessary to produce parts that make up the assembly units, and then – functional modules (mechanisms, units, power boxes, control modules, etc.). The modern modular principle of building machines provides for modular operations: development, assembly and debugging, modification and modernization, repair, replacement, etc. Parts and other components are at the lower level of the hierarchical design system consisting of nested blocks. Using it as a reliability structure diagram, it is necessary to find the criterion for RP distribution over components. We should consider not $P(t)$ function, but its numerical value $P(T)$. In this case, it is possible to substitute the specified T lifelength, and to use it under the distribution of the RP numerical values over components as the replacement cost criterion for base units in the event of their failures. The replacement cost may include:

- costs of materials used for the repair, products, diagnostics and repair work;
- failure effects estimated in money equivalent (renewal of other damaged components in case of dependent failures, ES idle time losses, insurance compensation for repayment, etc.).

This study objective is to develop a top-down analysis method for reliability structure diagrams, which eliminates the above-mentioned contradictions. The ES reliability structure diagram should be a tool for the distribution of component RP for the specified ES RP in the initial stages of the project. Then the selected lifelength and the balanced component RP will be the initial data for the design with the given reliability level. For this, the structure diagram should meet a number of requirements.

1. The structure diagram should be based on the construct structure. This will simplify complex functional component relationships.

2. The structure diagram should contain a mathematical reliability model available for calculations in the early stages of the project.

3. The reliability model of according to the structure diagram should be based not on the exponential law, but only on the fundamental reliability properties of the technical objects and systems (6), (8) - (11).

4. The criterion for ranking the component RP should be the cost of the component renewal in case it fails. It can be considered as a monetary equivalent of compensation of damage from failure.

5. The top-down structural analysis should be applied equally efficiently for both sequentially interacting and redundant reliability diagrams, as well as for the combined ones.

Alternative representation of numerical value of object RP. While t time has $P(t)$ value of the reliability function argument, it is a function decreasing by any of the known laws or obtained statically. After selecting the required $t = T$ lifelength, RP receives $P(t) = P(T)$ value within $0 < P(T) < 1$ limits. Such a value can be represented in a variety of ways from which the exponential expression is selected

$$P(T) = B^X . \tag{12}$$

X determined by the ratio

$$X = lg \ (P(T)) \ / \ lg \ B. \tag{13}$$

Taking the base value of $B = 10$ degree, we obtain the expression of the numerical RP value:

$$P(T) = 10^X , \tag{14}$$

from which

$$X = lg \ P(T). \tag{15}$$

X exponent is called the ranking parameter of the ES RP. In the annex to the system components, X_i exponents are also referred to as the ranking parameters of the component RP. Further in this presentation, "the simplest and most important case" [13] of the system reliability is considered.

ES component RP under their sequential interaction. Consider the ES reliability structure diagram with the sequential component interaction (see Fig. 1, a) whose failures are independent. In this case, the system failure under the failure of any of n components at $t = T$ time is expressed through the component RP according to (6):

$$P(T) = \prod_{i=1}^{n} P_i(T) .$$

In (6), product can be obtained by a variety of $P_i(T)$ combinations and types of their presentation. Applying (14) for the numerical values of $P(T)$ system RP and its components, $P(T) = P_1(T) \times P_2(T) \times ... \times P_n(T)$ product can be represented as follows:

$$10^X = 10^{X1} \times 10^{X2} \times ... \times 10^{Xn},$$

whence the connection between the system ranking parameter and the components:

$$X = X_1 + X_2 + ... + X_n . \tag{16}$$

From the set of X_i possible combinations in (16), those ones following from C_i renewal costs of failed components are selected. At this, components with a higher renewal cost should have larger $P_i(t)$ RPs. That is, at the cost of $C_1, C_2, ..., C_n$ components restoring, the set of $1/C_1, 1/C_2, ..., 1/C_n$ inverse values should be associated with the set of $X_1, X_2, ..., X_n$ components' ranking parameters.

The indicated ratio can be written as sums

$$1 = \frac{\frac{1}{C_1}}{\sum \frac{1}{C_i}} + \frac{\frac{1}{C_2}}{\sum \frac{1}{C_i}} + ... + \frac{\frac{1}{C_n}}{\sum \frac{1}{C_i}} ,$$

in which the accepted conditions for X_i ranking parameter are obtained from the termwise equality of the summands:

$$\frac{X_i}{X} = \frac{\frac{1}{C_i}}{\sum \frac{1}{C_i}} .$$

The right-hand side of this equality is called the "weight coefficient of the renewal cost of sequentially interacting components":

$$a_i = \frac{\frac{1}{C_i}}{\sum \frac{1}{C_i}} . \tag{17}$$

X_i ranking parameter values that meet the ranking condition:

$$X_i = X a_i . \tag{18}$$

Manshin Yu. P. and the others. Reliability of parts and unrestorable components in the machine design

Маньшин Ю. П. и др. Надежность деталей и нeремонтируемых узлов при проектировании машин

The unit of measuring the renewal cost does not matter, since the cost relations are used in (17). The top-down analysis of the ES component RP with sequential interaction is considered in Example 1. The system presented below contains three components for simplicity. However, any number of components is possible for the algorithm based on (14–18).

Example 1. Calculation of the ES component RP with sequential interaction (see Fig. 1, a). Initial data:
- system RP: $P(T) = 0.9$;
- number of components: $n = 3$;
- renewal costs of components (in c.u.): $C_1 = 5000$, $C_2 = 3000$, $C_3 = 2000$.

Ranking parameter for ES RP (15): $X = lg\, P(T) = lg\, 0.9 = -0.04576$.

The results of the step-by-step calculation of the component RP are presented in Table 2.

Table 2

Calculation of ES component RP with sequential interaction

Object	C_i, c.u.	$1/C_i$	a_i (17)	X_i (18)	$P_i(T)$ (14)
ES				−0.04576	0.9
Component 1	5000	0.0002	0.193548	−0.00886	0.979814
Component 2	3000	0.000333	0.322581	−0.01476	0.966584
Component 3	2000	0.0005	0.483871	−0.02214	0.950297
Checksums and products		$\sum(1/C_i)$	$\sum a_i$	$\sum X_i$	$P(T) = \prod P_i(T)$
		0.001033	1	−0.04576	0.9

ES component RP under their parallel interaction. Consider the following case: system crash under the failure of all elements with $F(T)$ probability at $t = T$ moment of time corresponding to the selected lifelength. Then, the basic property of parallel component interaction (see Fig. 1, b), according to (8), is expressed through $F_j(T)$ component failure rate:

$$F(T) = \prod_{j=1}^{m} F_j(T).$$

Taking by the analogy with (14)

$$F(T) = 10^Y, \tag{19}$$

where Y is determined from logarithmic equation $lg\,(F(T)) = Y\, lg10$:
$$Y = lg\, F(T). \tag{20}$$

Y exponent is called the ranking parameter of the ES failure rate. When engaged the system components, Y_j exponents are called the ranking parameters of the component failure rate. The conditions (8, 19) can be represented by $10^X = 10^{Y1} \times 10^{Y2} \times ... \times 10^{Yn}$ product, whence

$$Y = Y_1 + Y_2 + ... + Y_n. \tag{21}$$

From Y_j set of possible combinations in (21), those ones following from C_j renewal costs of failed components are selected. At this, components with a higher renewal cost should have lower failure rate (which also means large RP). That is, at the cost of C_1, C_2, ..., C_m components restoring, the set of $C_1, C_2, ..., C_m$ costs should be associated with the set of $Y_1, Y_2, ..., Y_m$ exponents.

The indicated ratio can be written as sums

$$1 = \frac{Y_1}{Y} + \frac{Y_2}{Y} + ... + \frac{Y_m}{Y} \quad \text{и} \quad 1 = \frac{C_1}{\sum C_j} + \frac{C_2}{\sum C_j} + ... + \frac{C_m}{\sum C_j}.$$

Here, the selected conditions for the exponents at Y_j are obtained from the termwise equality of the summands:

$$\frac{Y_j}{Y} = \frac{C_j}{\sum C_j}.$$

The right-hand side of the equality is called the "weight coefficient of the renewal cost under parallel component interaction":

$$b_j = \frac{C_j}{\sum C_j}. \tag{22}$$

Y_j ranking parameter values fitting the above relation:

$$Y_j = Yb_j. \tag{23}$$

The top-down analysis of the failure rate and ES component RP with the parallel component interaction is considered in Example 2. The system contains three components.

Example 2. Calculation of the failure rate and ES component RP with parallel interaction (see Fig. 1, b). Initial data:

- system RP: $P(T) = 0.9$;
- component number: $m = 3$;
- component renewal costs (in c.u.): $C_1 = 5000$, $C_2 = 3000$ и $C_3 = 2000$.

We calculate the system reliability indices. System failure probability from (9):

$$F(T) = 1 - P(T) = 1 - 0.9 = 0.1.$$

Ranking parameter values for the system failure probability from (20):

$$Y = lg\, F(T) = lg\, 0.1 = -1.$$

The results of the step-by-step calculation are presented in Table 3.

Table 3

Calculation of ES component RP with parallel interaction

Object	C_j, c.u.	b_j (22)	Y_j (23)	$F_j = 10^{Y_j}$	$P_j(T) = 1 - F_j(T)$
ES			−1	0.1	0.9
Component 1	5000	0.5	−0.5	0.316228	0.683772
Component 2	3000	0.3	−0.3	0.501187	0.498813
Component 3	2000	0.2	−0.2	0.630957	0.369043
Checksums and products	$\sum C_j$	$\sum b_j$	$\sum Y_j$	$F(T) = \prod F_j(T)$	$P(T) = 1 - \prod(1 - P_j(T))$
	10000	1	−1	0.1	0.9

Example 3. Probability calculation of the nonfailure operation of the combined ES components (see Fig. 1, c). Initial data:

- number of sequentially interacting subsystems: $n = 3$;
- number of parallel interacting elements of SS 3: $m = 4$;
- system RP: $P(T) = 0.95$;
- renewal costs of subsystems (in c.u.): $C_1 = 5000$, $C_2 = 8000$, $C_3 = 12000$;
- renewal costs of parallel component interaction (in c.u.): $C_{3,1} = 3000$, $C_{3,2} = 4000$, $C_{3,3} = 5000$, $C_{3,4} = 6000$

We calculate the system reliability indices. Ranking parameter for ES RP from (15):

$$X = lg\, P(T) = lg\, 0.95 = -0.022276.$$

The results of the step-by-step calculation are presented in Table 4.

Table 4

Calculation of ES component RP with sequential interaction

Object	C_i, c.u.	$1/C_i$	a_i (17)	X_i (18)	$P_i(T)$ (14)	
ES				−0.022276	0.95	
Subsystem (SS) 1	5000	0.000200	0.489796	−0.010911	0.975190	
SS 2	8000	0.000125	0.306122	−0.006819	0.984421	
SS 3	12000	0.000083	0.204082	−0.004546	0.989587	◄*
Checksums and products		$\sum(1/C_i)$	$\sum a_i$	$\sum X_i$	$P(T) = \prod P_i(T)$	
		0.000408	1	−0.022276	0.95	
* ◄ — subsystem selection mark for further top-down analysis.						

From Table 4, RP of the SS 3 subsystem: $P_3(T) = 0.989587$. Failure rate of SS 3 (8):

$F_3(T) = 1 - P_3(T) = 1 - 0.989587 = 0.010413$. The ranking parameter for the failure rate of SS 3 (22):

$Y = lg\, F_3(T) = lg\, 0.010413 = -1.982407$.

Manshin Yu. P. and the others. Reliability of parts and unrestorable components in the machine design

Маньшин Ю. П. и др. Надежность деталей и неремонтируемых узлов при проектировании машин

The results of the step-by-step calculation are presented in Table 5.

Table 5

Calculation of SS 3 component RP with parallel interaction

Object	C_j, c.u.	b_j (22)	Y_j (23)	$F_j = 10^{Y_j}$	$P_j(T) = 1 - F_j(T)$
SS 3			−1.982407	0.010413	0.989587
Component 3.1	3000	0.166667	−0.330401	0.467303	0.532697
Component 3.2	4000	0.222222	−0.440535	0.362631	0.637369
Component 3.3	5000	0.277778	−0.550669	0.281405	0.718595
Component 3.4	6000	0.333333	−0.660802	0.218372	0.781628
Checksums and products	$\sum C_j$	$\sum b_j$	$\sum Y_j$	$F(T) = \prod F_j(T)$	$P(T) = 1 - \prod(1 - P_j(T))$
	18000	1	−1.982407	0.010413	0.989587

The required lifelength of the ES and all its elements (1) should be considered, so that the component RP calculated in Tables 2–5 will be the initial data for the calculation and selection of components with the specified reliability level.

It is necessary to determine the obtained resources by the corresponding reliability models with the calculated RPs (Tables 2, 3, 5). To do this, the dimensions and design parameters of the components (parts, standard and other nonrestorable items) obtained at the stage of preliminary design are considered. Then, measures can be taken to approximate the obtained and specified resources [15, 16].

Conclusion. The technique of top-down analysis of the machine reliability structure diagram is developed and tested on numerical examples. Its algorithm coincides with the sequence of design stages: from the machine RP – to the RP of its parts. The selection of the required lifelength and RP distribution over the parts at the initial stages of the project provide the design with the specified reliability level. The structure diagram can be based on the construct structure. This ensures a universal approach to the formation of structure reliability diagrams under various types of component interaction. The criterion for ranking the RP components is the component renewal in case of its failure. At any level of the structure diagram, it includes the monetary equivalent of the costs of materials, products, repairs, damage from failure. They are known with sufficient accuracy at the initial stage of machine development.

The need to use the exponential law under the normalization of reliability and the development of its structure diagrams is eliminated. The RP analysis relies only on the reliability fundamental properties that are common to all technical objects and systems. The analysis algorithm is maintained at all levels of the structure diagrams including part levels.

Mathematical models of the structure diagrams are simple, available for calculations in the early project stages, and equally efficient for sequentially interacting, redundant and combined reliability diagrams. They provide convenient possibilities for algorithmization, programming, and data correction.

References

1. GOST 15.001-88. Sistema razrabotki i postanovki produktsii na proizvodstvo. Produktsiya proizvodstvenno-tekhnicheskogo naznacheniya. [GOST 15.001-88. System of product development and launching into manufacture. Products of industrial and technical designation.] USSR State Standards Committee. Moscow: Izd-vo standartov, 1988, 7 p. (in Russian).

2. GOST 2.103-2013. Edinaya sistema konstruktorskoy dokumentatsii. Stadii razrabotki. [Unified system for design documentation. Stages of designing.] All-Russian Research Institute for Standardization and Certification in Mechanical Engineering; Research Center of CALS-technologies "Applied Logistics"; Federal Agency for Technical Regulation and Metrology; Interstate Council for Standardization, Metrology and Certification. Moscow: Standartinform, 2015, 6 p. (in Russian).

3. Manshin, Yu.P., Manshina, E.Yu. Planirovanie i otsenka nadezhnosti tekhnicheskoy sistemy na rannikh stadiyakh proekta. [Planning and assessing the technical system reliability in early stages of the project.] Sostoyanie i perspektivy razvitiya sel'skohozyaystvennogo mashinostroeniya: sb. statey 7-y mezhdunar. nauch.-prakt. konf. v ramkakh 17-y Mezhdunar. agroprom. vystavki «Interagromash-2014» [State and prospects of agricultural machinery development: Proc. 7th Int. Sci.-Pract. Conf. within framework of the 17th Int. Agroindustrial Exhibition "Interagromash-2014".] Rostov-on-Don: DSTU Publ. Centre, 2014, pp. 169–171 (in Russian).

Vestnik of Don State Technical University. 2018. Vol. 18, no. 4, pp. 392–400.   ISSN 1992-5980 eISSN 1992-6006

Вестник Донского государственного технического университета. 2018. Т. 18, № 4. С. 392–400.   ISSN 1992-5980 eISSN 1992-6006

4. Kovalev, A.N., Kantor, B.I., Mozhaev, A.B. Ekonomicheskoe obespechenie nadezhnosti mashin. [Economic reliability control of machines.] Moscow: Mashinostroenie, 1991, 238 p. (in Russian).

5. Dalskiy, A.M. Tekhnologicheskoe obespechenie nadezhnosti vysokotochnykh detaley mashin. [Technological support for the reliability of high-precision machine parts.] Moscow: Mashinostroenie, 1975, 225 p. (in Russian).

6. Volkov, D.P., Nikolaev, S.N. Nadezhnost' stroitel'nykh mashin i oborudovaniya. [Reliability of construction machines and equipment.] Moscow: Vysshaya shkola, 1979, 400 p. (in Russian).

7. Pronnikov, A.S. Parametricheskaya nadezhnost' mashin. [Parametric machine reliability.] Moscow: Bauman University Publ. House, 2002, 560 p. (in Russian).

8. Shubin, V.S., Ryumin, Yu.A. Nadezhnost' oborudovaniya khimicheskikh i neftepererabatyvayushchikh proizvodstv. [Reliability of chemical and oil refining equipment.] Moscow: Khimiya; KolosS, 2006, 359 p. (in Russian).

9. Androsov, A.A., Manshin, Yu.P., Manshina, E.Yu. Kursovoe proektirovanie tekhnicheskikh sistem s zadannym urovnem nadezhnosti. [Course design of engineering systems with the specified reliability level.] Rostov-on-Don: DSTU Publ. Centre, 2013, 93 p. (in Russian).

10. Polovko, A.M., Gurov, S.V. Osnovy teorii nadezhnosti. [Fundamentals of the reliability theory.] St.Petersburg: BKhV-Peterburg, 2006, 704 p. (in Russian).

11. Druzhinin, G.V. Nadezhnost' avtomatizirovannykh system. [Reliability of automated systems.] 3rd revised and enlarged ed. Moscow: Energiya, 1977, 536 p. (in Russian).

12. Manshin, Yu.P., Manshina, E.Yu. Raschety parametrov nadezhnosti elementov pri proektirovanii mashin. [Calculations of the reliability parameters of elements under machine design.] Sostoyanie i perspektivy razvitiya sel'skokhozyaystvennogo mashinostroeniya: mat-ly 7-y mezhdunar. nauch.-prakt. konf. v ramkakh 20-y mezhdunar. agroprom. vystavki «Interagromash-2017». [State and prospects of agricultural machinery development: Proc. 7th Int. Sci.-Pract. Conf. within framework of the 20th Int. Agroindustrial Exhibition "Interagromash-2017".] Rostov-on-Don: DSTU Publ. Centre, 2017, pp. 261–263 (in Russian).

13. Gnedenko, B.V., Belyaev, Yu.K., Solovyev, A.D. Matematicheskie metody v teorii nadezhnosti. [Mathematical methods in the theory of reliability.] Moscow: Nauka, 1965, 573 p. (in Russian).

14. Khozyaev, I.A. Nadezhnost' biotekhnicheskikh sistem. [Reliability of biotechnical systems.] Rostov-on-Don: DSTU Publ. Centre, 2014, 235 p. (in Russian).

15. Manshin, Yu.P., Manshina, E.Yu. Priblizhennaya otsenka resursa detali, obespechivayushchaya ee trebuemyy resurs s zadannoy veroyatnost'yu bezotkaznoy raboty. [Aproximate assession of part life, assuring its required life with specified probability of no-failure operation.] Vestnik Mashinostroeniya, 2017, no. 12, pp. 20–24 (in Russian).

16. Man'shin, Yu.P., Man'shina, E. Yu. Estimating the Life of a Machine Part. Russian Engineering Research, 2018, vol. 38, no. 3, pp. 157–162.

Authors:

Manshin, Yury P.,
associate professor of the Machine Design Principles
 Department, Don State Technical University
(1, Gagarin sq., Rostov-on-Don, 344000, RF),
Cand.Sci. (Eng.), associate professor,
ORCID: http://orcid.org/0000-0002-2246-2965
manshin@mail.ru

Manshina, Elena Yu.,
senior lecturer of the Machine Design Principles
 Department, Don State Technical University
(1, Gagarin sq., Rostov-on-Don, 344000, RF),
 ORCID:http://orcid.org/0000-0002-3027-1309
elemans@mail.ru

МАШИНОСТРОЕНИЕ И МАШИНОВЕДЕНИЕ
MACHINE BUILDING AND MACHINE SCIENCE
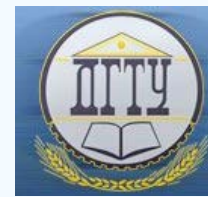
On nanoscale phenomena in the electroacoustic sputtering process[*]

W. H. Al-Tibbi[1], V. S. Minakov[2][**]

[1, 2] Don State Technical University, Rostov-on-Don, Russian Federation

К вопросу о наноразмерных явлениях в процессе электроакустического напыления[***]

В. Х. Аль-Тибби[1], В. С. Минаков[2][**]

[1, 2] Донской государственный технический университет, г. Ростов-на-Дону, Российская Федерация

Introduction. The effect of variable parameters of the electroacoustic sputtering (ELAS) process on the characteristics of the crystalline structure of hardening coatings is studied. The ELAS parameter values providing nanostructured cover coatings for machine parts and cutting tools are determined. Hardening through using such coatings allows achieving a significant (5-10 times) increase in the life of hardenable machine parts and various tools designed for mechanical processing. To obtain coatings with the desired properties of the surface layer, nanocrystalline materials should be selected. In this case, a certain content of the amorphous phase is permissible.

Materials and Methods. To carry out the X-ray structural analysis, the X-ray diffraction Russian-made device DRON-3M was used. The Scherrer-Wilson method was applied to determine the granularity of particle blocks from the value of the intrinsic broadening of the diffractogram peaks. The conclusions obtained in this paper are based on the method of separation of the affecting factor contributions into broadening the diffraction reflection peaks (the Warren-Averbach method).

Research Results. Depending on the process conditions and the technique for obtaining nanostructured materials, a non-uniquely interpretable change in the indices of the diffraction peaks broadening occurs, which is generally characteristic of nanocrystalline metals. One of the possible explanations for this phenomenon is the presence of a nanosized effect in the hardened layer. The occurrence of the nanocrystalline structure in the sputtered layer verifies the calculated values of the dimensions of the coherent scattering regions (CSR). The occurrence of affecting values of the misorientation angle of the crystal structure is verified by the CSR value for the investigated 110 and 220 reflexes, which is supported by a high percentage of the amorphous phase.

Введение. Исследовано действие варьируемых параметров процесса электроакустического напыления (ЭЛАН) на характеристики кристаллической структуры упрочняющих покрытий. Выявлены значения указанных параметров, обеспечивающие получение наноструктурных защитных покрытий деталей машин и режущего инструмента. Упрочнение при помощи подобных покрытий позволяет достичь значительного (в 5–10 раз) повышения ресурса работы упрочняемых деталей и инструментов, предназначенных для механообработки. Для получения покрытий с заданными свойствами поверхностного слоя следует выбирать нанокристаллические материалы. При этом допустимо определенное содержание аморфной фазы.

Материалы и методы. Использован рентгеноструктурный анализ, который проводился на рентгеновском дифракционном аппарате отечественного производства «ДРОН-3М». Метод Шеррера — Вилсона применен с целью определения зернистости блоков частиц по значению физического уширения пиков дифрактограммы. Выводы по результатам работы основаны на методике разделения вкладов значащих факторов в уширение пиков дифракционных отражений (метод Уоррена — Авербаха).

Результаты исследования. В зависимости от технологических режимов и метода получения наноструктурных материалов происходит неоднозначно интерпретируемое изменение показателей уширения дифракционных пиков, что, в общем, характерно для нанокристаллических металлов. Это явление можно объяснить, в частности, наличием наноразмерного эффекта в упрочненном слое. Присутствие нанокристаллической структуры в напыленном слое напрямую подтверждается вычисленными значениями размеров областей когерентного рассеивания (ОКР). Наличие значимых величин угла разориентирования структуры кристаллов подтверждается величиной ОКР для исследованных рефлексов 110 и 220, что подкрепляется высоким процентным содержанием аморфной фазы.

Discussion and Conclusions. The electroacoustic scattering method is promising for obtaining nanocrystalline structures in the surface and subsurface layers of the sprayed samples. The ELAS process variables variation leads to the parameter spread of the crystal lattice and coherent scattering areas. In this case, there is no definite trend. In the future it is expected to solve the given problem. First, experiments will be conducted to determine the optimal sputtering regimes that could stimulate the formation of nanocrystalline structures. Secondly, visual observation and evaluation of the sprayed layer structure using electron microscopy is planned.

Обсуждение и заключения. Метод электроакустического напыления перспективен для получения нанокристаллических структур в поверхностном и приповерхностном слоях напыленных образцов. Изменение технологических параметров ЭЛАН приводит к разбросу значений параметров кристаллической решетки и областей когерентного рассеивания. В этом случае не выявляется определенная тенденция. В дальнейшем предполагается решение данной проблемы. Во-первых, будут проведены эксперименты с целью определения оптимальных режимов напыления, способствующих образованию нанокристаллических структур. Во-вторых, планируется визуальное наблюдение и оценка структуры напыляемого слоя при помощи электронной микроскопии.

Introduction. To obtain nanostructured hardening coatings is an urgent and long-run engineering challenge [1, 2]. Numerous studies in the field of materials science have shown that a tangible (by several times) change in strength, hardness, and wear resistance of materials is possible with a decrease in crystal grains to a certain value.

Under this investigation, it is expected to study the crystal microstructure of hardening coatings using the method of electroacoustic sputtering (ELAS) [3, 4, 5]. Such hardening involves the use of an electric spark (highly-concentrated power flotation) and ultrasonic longitudinally-torsional vibrations. ELAS-hardening, using a specialized installation, enables to increase the operational life of parts and tools by 5-10 times.

In the paper, the ELAS operational parameters vary in order to identify their values, which contribute to obtaining nanostructural protective coatings for the parts and cutting tools. To create protective coatings with the required properties, alloys in the amorphous state are often used. However, in certain areas, nanocrystalline materials are used more often than the amorphous ones. Nanocrystals relax to a far lesser extent in use of the coating, and they are highly competitive with amorphous materials in their properties. Obviously, to obtain coatings with the desired and stable properties of the surface layer, nanocrystalline materials should be selected, though with a certain content of the amorphous phase.

Materials and Methods. Resonance methods, X-ray diffraction analysis, electron microscopy, and some other techniques [2] are widely used to identify nanocrystalline materials in the surface layer. In the present work, the most accessible method based on identifying the diffraction reflection broadening under the X-ray structural analysis of samples is used to evaluate the microstructure parameters. "DRON-3M", the X-ray diffraction Russian-made apparatus, was used for X-ray diffraction analysis. The characteristic radiation of the iron anode with the release of λK_α spectral line of the sample, as well as of the detector, was analyzed. The X-ray tube specifications were 25 kV, 5 mA. The Bragg - Brentano method of radiation focusing was used [6]. The selected detector parameters are as follows: motion speed is 1 deg/min; integration time is 5s. When determining the distances between the measurement planes, the error was ± 0.001 Å, which is similar to determining the position of diffraction maxima accurate to ± 0.02 degrees. Samples of a cylindrical shape made of 45 steel were studied. The diameter and height of the sample was 6 mm.

To identify samples, special marks were applied using ELAS on the front surface of each of them. The sample without sputtering made from 45 steel was chosen as a reference one, not the sample that is close to pure α-Fe.

Research Results. The profiles obtained during the work are presented in Fig. 1.
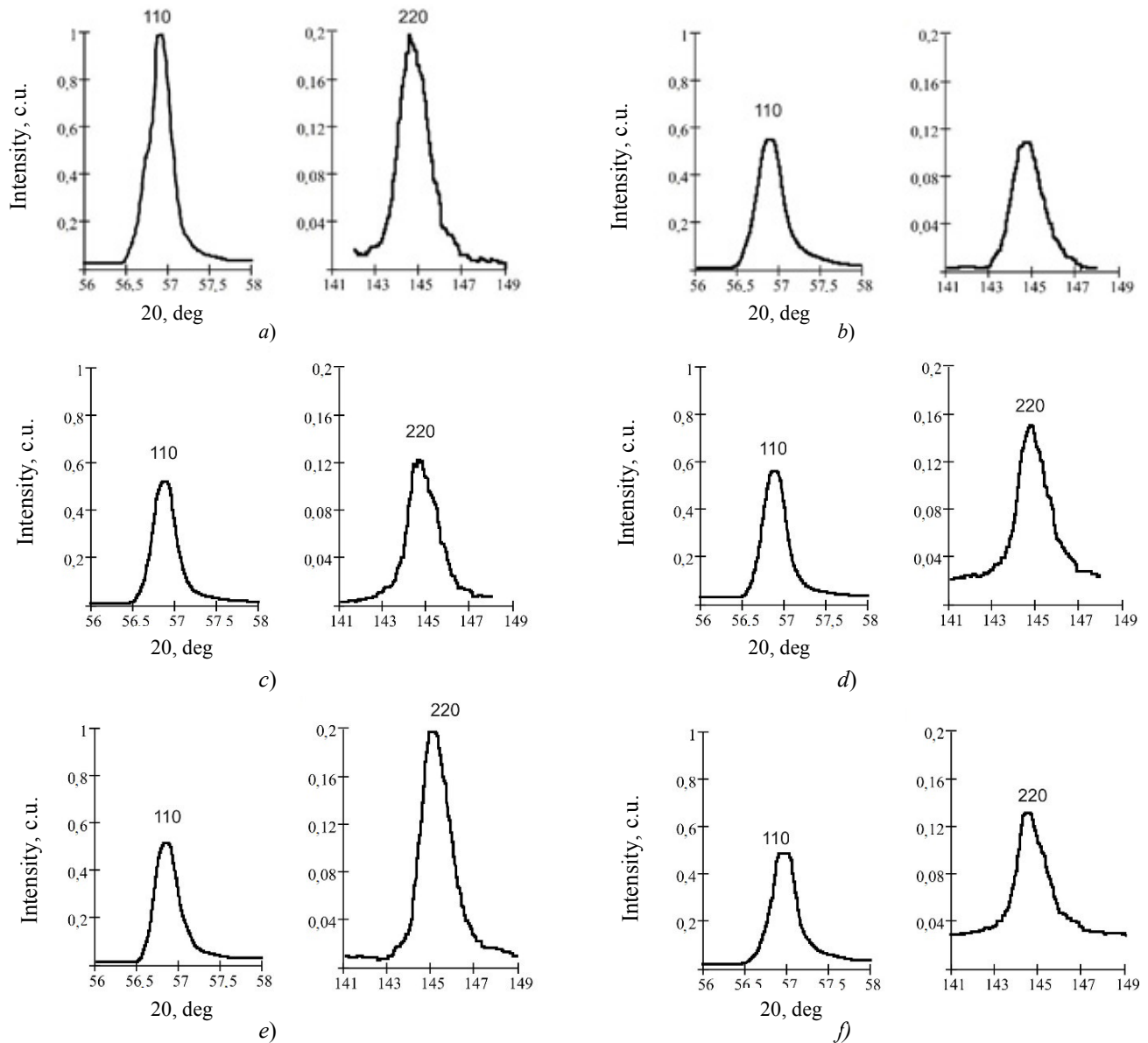
Fig. 1. Diffraction reflections with profiles: reference with coarse grain (*a*); sample for sputtering (*U* = 16.9 V, *A* = 4.9 microns) (*b*); *U* = 13.1 V, *A* = 15.2 μm (*c*); *U* = 12.9 V, *A* = 9.9 μm (*d*); *U* = 12.9 V, *A* = 5.1 μm (*e*); *U* = 9.1 V, *A* = 15.1 μm (*f*)

The shape of the diffraction profiles for the reference sample is shown in Fig. 1 (*a*), for samples with spread sputtered coating on the above modes – in Fig. 1 (*b*) - (*f*). ELAS variables are electrode-anode voltage (*U*) and amplitude value (*A*) of ultrasonic frequency oscillations.

Diffractograms of the reference and study sample show the intensity values ratio. The relationship of the crystallized and amorphous material was calculated from these data. The contribution of the texture component was not considered.

Analysis of the experimental data allows us to conclude that the main phase in most of the samples under study is α - Fe. The Scherrer-Wilson method (the best in this case) was used to determine the grain coarseness of blocks of particles according to the value of the physical broadening of the diffractogram peaks [7].

Table 1 presents the summarized data on the research results:

- β physical broadening,
- *d*-space,
- *a* dimensional parameter of the crystal lattice,
- size of coherent scattering regions.

Table 1

Design parameters of crystal structure and diffractogram data

Parameter / Sample	Reflex											
	110						220					
	1	2	3	4	5	эт.	1	2	3	4	5	ref.
$\beta \cdot 10^{-3}$, deg.	2.01	1.71	1.68	1.81	1.95	1.39	8.47	8.34	8.62	8.87	10.01	8.06
2θ, deg.	56.916	56.86	56.926	56.876	56.976	57.2	144.66	144.7	144.78	144.91	144.53	144.4
d, Å	2.026	2.028	2.025	2.027	2.024	2.019	1.013	1.0129	1.0126	1.0122	1.0132	1.0129
a, Å	2.8553	2.8581	2.8539	2.8567	2.8525	2.8465	2.8539	2.8561	2.8553	2.8793	2.8571	2.8571
D, nm	111	130	131	123	114	–	76	77	75	73	64	–
Amorphous component content, %	59	55	57.5	53.5	51	–	59	75	81	98	79	–

110 and 220 reflexes were selected as the basic ones.

Table 1 data demonstrate significant broadening of the diffraction peaks. It is logical to assume that such a width in our case is, to a greater extent, due to the highly dispersed structure of the crystallites than to the dislocation microstresses of the surface layer. To confirm this conclusion, the contributions from these factors are estimated by the Warren – Averbach method [8]. The center-of-gravity shift of the peaks on the diffractograms with a simultaneous increase in *a* lattice parameter to 1.15–1.17% serves as an indirect proof for the above formulated hypothesis. The shift itself is small, but meaningful (expressed in hundredths of a degree).

Consider the phenomena that occur when changing the values of the process conditions (electrical voltage and amplitude of oscillations), and their effect on the broadening value of the diffractogram peaks depending on the lattice dimensional parameter (Fig. 2).
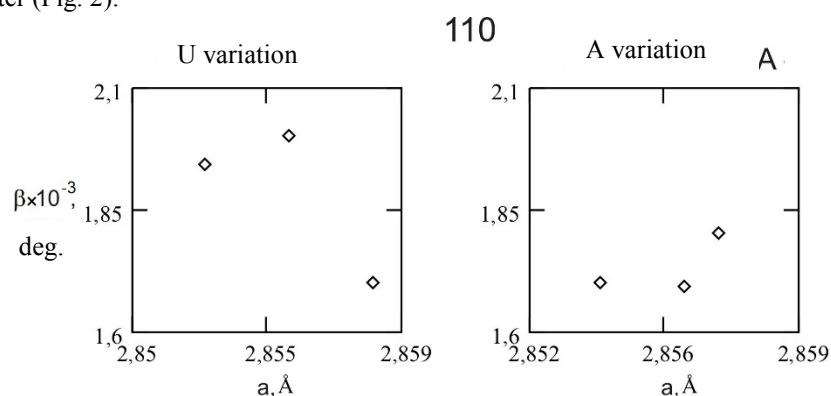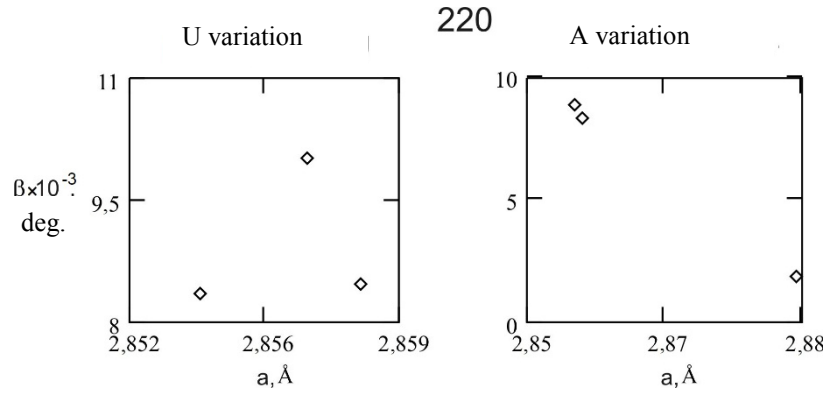
Fig. 2. Effect of ELAS regimes variation on *a* lattice parameter depending on β value of physical broadening of diffractogram peaks

As expected, a change in the deposition modes affects *a* lattice parameter without a definite traceable dependence. In this case, *a* value variations are directly proportional to the broadening value of the lines of the diffractogram lines. In [9], comparable proportional dependences can be observed for various oxides.

Such ambiguously interpolated dependences are characteristic of nanostructured materials (in particular, metals) and are determined by the physical method of their synthesis [1, 10] (Fig. 3).
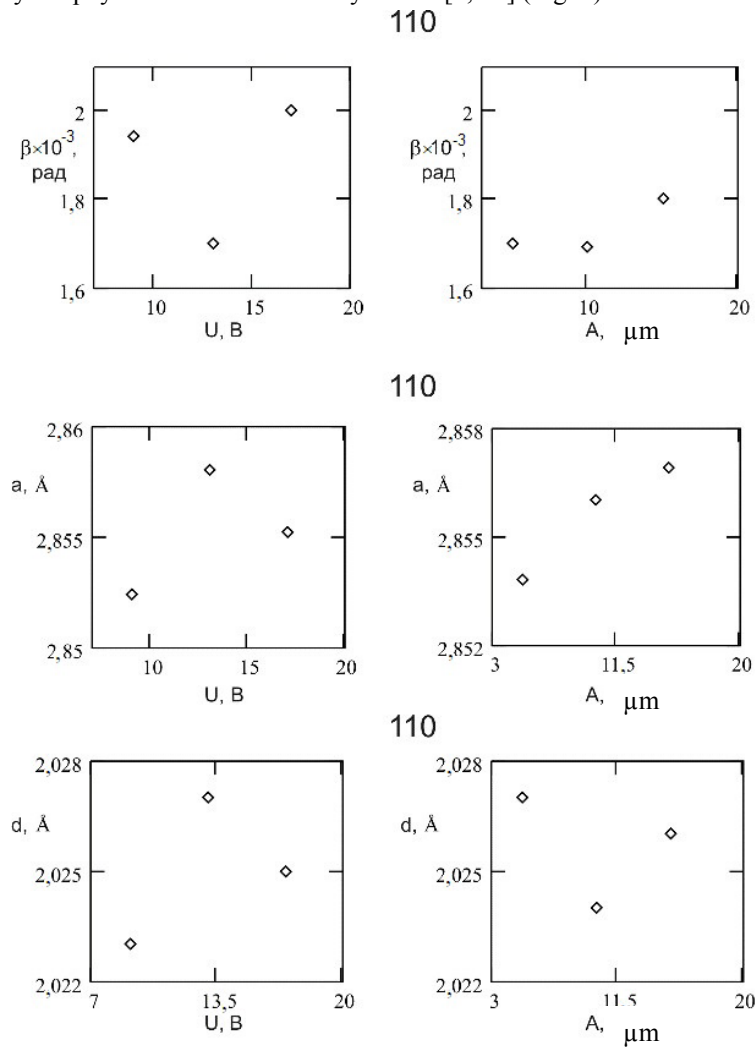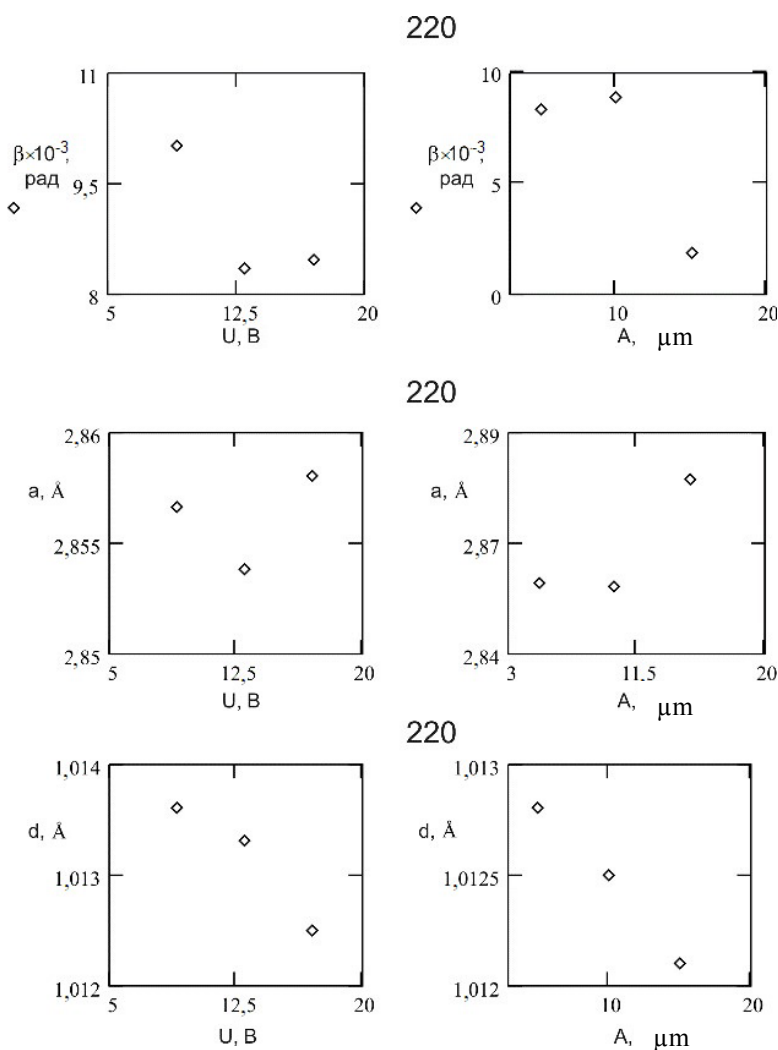
Fig. 3. Effect of ELAS variables on microstructure parameters

Perhaps, this phenomenon is explained by the occurrence of a nanoscale effect in the hardened layer. The presence of a nanocrystalline structure in the sputtered layer is directly confirmed by the calculated values of the sizes of coherent scattering regions (CSR). The significant values of the disorientation angle of the crystal structure is verified by the CSR values for 110 studied reflex, and also, noticeably, for 220 reflex, which is supported by a high percentage content of the amorphous phase. Similar phenomena can be also caused by high values of disorientation angles.

Summing up, it can be stated that all of the above phenomena (including sizes of the coherent scattering regions) directly confirm the presence of a nanoscale effect [1].

Discussion and Conclusions. Thus, the method of electroacoustic sputtering is promising for obtaining nanocrystalline structures in the surface and near-surface layers of sputtered samples. As stated in the paper, ELAS process parameter variation brings into existence the lattice parameter spread and coherent scattering regions without a definite identified tendency. In the future, this problem will be solved. This can be facilitated by the experimental determination of optimal sputtering regimes that ensure the formation of nanocrystalline structures. In addition, the structure of the sputtered layer can be observed and evaluated using electron microscopy.

References
1. Gusev, A.I., Rempel, A.A. Nanokristallicheskie materialy. [Nanocrystalline materials.] Moscow: Fizmatlit; Nauka, 2001, 222 p. (in Russian).

2. Valiev, R.Z., Aleksandrov, I.V. Ob"emnye nanostrukturnye metallicheskie materialy: poluchenie, struktura i svoystva. [Bulk nanostructured metallics: production, structure and properties.] Moscow: Akademkniga, 2007, 397 p. (in Russian).

3. Minakov, V.S. Razrabotka kompleksnykh mekhanicheskikh i elektrofizicheskikh protsessov obrabotki na osnove ispol'zovaniya energii transformiruemykh ul'trazvukovykh kolebaniy: dis. … d-ra tekh. nauk. [Development of

complex mechanical and electrical treatment processes based on the use of energy of transformable ultrasonic vibrations: Dr.Sci. (Eng.), diss.] Rostov-on-Don, 1989, 350 p. (in Russian).

4. Kochetov, A.N. Bar'yerno-dislokatsionnyy mekhanizm uprochneniya detaley mashin metodom elektroakusticheskogo napyleniya: dis. … kand. tekh. nauk. [Barrier-dislocation mechanism of hardening machine parts through electro-acoustic spraying: Cand.Sci. (Eng.), diss.] Rostov-on-Don, 1996, 185 p. (in Russian).

5. Minakov, V.S., et al. Vliyanie materialov s razlichnymi fiziko-mekhanicheskimi svoystvami na iznosostoykost' rezhushchego instrumenta, uprochnennogo metodom elektroakusticheskogo napyleniya. [The effect of materials with different physical and mechanical properties on the wear resistance of cutting tools hardened through electro-acoustic spraying.] Tekhnologii remonta, vosstanovleniya i uprochneniya detaley mashin, mekhanizmov, oborudovaniya, instrumenta i tekhnologicheskoy osnastki: mat-ly 9-y mezhdunar. prakt. konf. [Technologies of repair, restoration and hardening of machine parts, mechanisms, equipment, tools and technological equipment: Proc. 9th Int. Pract. Conf.] St.Petersburg, 2007, pp. 23–29 (in Russian).

6. Usmanskiy, Ya.S., Skakov, Yu.A. Fizika metallov. [Physics of metals.] Moscow: Atomizdat, 1978, 445 p. (in Russian).

7. Vishnyakov, Ya.D. Sovremennye metody issledovaniya struktury deformirovannykh kristallov. [Modern methods of structural study of deformed crystals.]. Moscow: Metallurgiya, 1975, 104 p. (in Russian).

8. Gorelik, S.S., Skakov, Yu.A. , Rastorguev, L.N. Rentgenograficheskiy i elektronno-opticheskiy analiz. [X-ray and electrooptic analysis.] Moscow: MISIS, 1994, 336 p. (in Russian).

9. Kofanov, N.B., Kuprina, Yu.A., Kupriyanov, M.FO razmernykh effektakh v titanate bariya. [On size effects in barium titanate.] Bulletin of the Russian Academy of Sciences: Physics, 2002, vol. 66, no. 6, pp. 839–841 (in Russian).

10. Al-Tibbi, W.H. Vliyanie dispersnosti mikrostruktury pokrytiy, poluchaemykh metodom elektroakusticheskogo napyleniya, na iznosostoykost' rezhushchego inst-rumenta : dis. … kand. tekh. nauk. [The dispersability effect of coating microstructure obtained by the method of electro-acoustic spraying on the wear resistance of the cutting tool: Cand.Sci. (Eng.), diss.]. Rostov-on-Don, 2006, 210 p. (in Russian).

Authors:

Al-Tibbi, Wisam H.,
Associate professor of the Production Automation
Department, Don State Technical University (1, Gagarin
sq., Rostov-on-Don, 344000, RF), Cand.Sci. (Eng.),
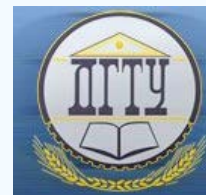associate professor,
 ORCID: http://orcid.org/0000-0002-5400-3149
nb1979@mail.ru

Minakov, Valentin S.,
professor of the Production Automation Department, Don
State Technical University (1, Gagarin sq.,
Rostov-on-Don, 344000, RF), Dr.Sci. (Eng.), professor,
ORCID: http://orcid.org/0000-0002-0882-1984
vs_minakov@mail.ru

МАШИНОСТРОЕНИЕ И МАШИНОВЕДЕНИЕ
MACHINE BUILDING AND MACHINE SCIENCE

Effect of design and kinematic parameters on energy requirement in inclined screw mixer[*]

V. F. Khlystunov[1], S.V. Braginets[2], A.S. Alferov[3], M.V. Chernutskiy[4]**

[1] Don State Technical University, Rostov-on-Don, Russian Federation
[2,3,4]Agricultural Research Centre "Donskoy", Zernograd, Rostov Region, Russian Federation

Влияние конструктивных и кинематических параметров на энергоёмкость процесса в наклонном шнековом смесителе[***]

В. Ф. Хлыстунов[1], С. В. Брагинец[2], А. С. Алфёров[3], М. В. Чернуцкий[4]**

[1] Донской государственный технический университет, г. Ростов-на-Дону, Российская Федерация
[2,3,4]Аграрный научный центр «Донской», г. Зерноград, Ростовская область, Российская Федерация

Introduction. Rational parameters and modes of an inclined batch screw mixer are validated to achieve the lowest energy-intensive feed mixing under observance of the zootechnical requirements for the feed quality on uneven mixing. The establishment of functional dependences between parameters and modes enables to design power-efficient equipment for the on-farm feed production.

Materials and Methods. Experimental studies of the feed mixing were implemented on an inclined screw batch feed mixer. The experimental design included variation of four independent factors: mixer shaft speed, filling ratio of the mixing chamber, mixing time, and mixing chamber angle. Mixing irregularity and energy intensity of the process were taken as optimization criteria characterizing the mixing efficiency.

Research Results. The optimization criteria versus the variability level factor, which are two-dimensional sections of the second-order response surfaces, are plotted. The rational values at mixing irregularity of less than 5% were as follows: mixer shaft speed was 27.5-36.5 min-1, filling ratio of the mixing chamber was 0.43–0.51, mixing time was 3.0–4.2 min, mixing chamber angle was 22°–25°. At such parameter values, the mixing irregularity will be minimal, and it will be 4.10–4.18%, and the process intensity is from 2.08 to 2.16 kW • h/t

Discussion and Conclusions. The dependences obtained as a result of the experimental studies allowed establishing the domain of rational design parameters and modes of an inclined batch screw mixer. The results obtained can be used in further studies under the development of initial requirements for the

Введение. Обоснованы рациональные параметры и режимы наклонного шнекового смесителя периодического действия для достижения наименьшей энергоемкости приготовления кормосмеси при условии соблюдения зоотехнических требований к качеству приготовляемых кормов по неравномерности смешивания. Установление функциональных зависимостей между параметрами и режимами позволяет проектировать энергоэффективное оборудование для внутрихозяйственного комбикормового производства.

Материалы и методы. Экспериментальные исследования процесса приготовления кормосмеси проводили на наклонном одновальном шнековом смесителе кормов периодического действия. План эксперимента включал варьирование четырьмя независимыми факторами: частотой вращения вала смесителя, коэффициентом заполнения камеры смесителя, продолжительностью смешивания и углом наклона смесительной камеры. В качестве критериев оптимизации, характеризующих эффективность смешивания, были приняты неравномерность смешивания и удельная энергоемкость процесса.

Результаты исследования. Построены графические зависимости критериев оптимизации от уровня варьирования факторов, представляющие собой двумерные сечения поверхностей отклика второго порядка. Рациональные значения при неравномерности смешивания менее 5% составили: частота вращения вала — 27,5-36,5 мин$^{-1}$, коэффициент заполнения камеры смесителя — 0,43–0,51, продолжительность смешивания — 3,0–4,2 мин.; угол наклона смесительной камеры — 22°–25°. При таких значениях параметров неоднородность смешивания будет минимальной и составит 4,10–4,18%, а энергоёмкость процесса составила от 2,08 до 2,16 кВт·ч/т

Обсуждение и заключения. Зависимости, полученные в результате экспериментальных исследований, позволили установить области рациональных конструктивных параметров и режимов наклонного одновального шнекового смесителя периодического действия. Полученные результаты могут быть использованы в

creation of new technical means with a gravitation effect of intensive mixing.

дальнейших исследованиях при разработке исходных требований на создание новых технических средств с гравитационным эффектом интенсивного смешивания.

Keywords: design engineering, inclined mixer, screw, gravitation shattering, mixing irregularity, mixing intensity.

Ключевые слова: проектирование, наклонный смеситель, шнек, гравитационное осыпание, неравномерность смешивания, энергоемкость смешивания.

Introduction. An urgent task in the design of new feed mixing equipment is to ensure a lower cost of feed preparation [1-3]. Thus, it is necessary to reduce the energy intensity of the processes while maintaining the required quality of the feed. High-quality feed mixing is most effectually performed by a periodic (batch) mixer [4, 5]. Among them, blade mixers and screw ones [6] are widespread. This is due to the fact that the feed composition is characterized by the presence of dry crushed grain (more than 90%), which does not change its properties in the process of mixing with additives. That is, the rheological properties of the mixture can be considered unchanged throughout the experiment [7].

One of the advanced models of the circulation mixers is a model with an inclined bunker, inside which one or two screw working bodies are installed. Herewith, the reduction of the process energy intensity is achieved due to the fact that the forced supply of the mixed material at the upper horizontal level is replaced by its gravitation shattering from the upper part of the bunker [8]. Unlike horizontal mixers, the practical absence of "pressing" feed layers in the top part of the screw improves significantly the diffusion mixing of the product [9]. When using modern crushers [10, 11], the intensive movement of the material and the equalized granulometric raw material composition enables to minimize the segregation effects that occur under shattering [12].

Materials and Methods. The experimental studies were carried out on AKM-3, an inclined single-shaft screw batch feed mixer developed in "Donskoy" Agricultural Research Centre. AKM-3 feed mixer (Fig. 1) with the capacity of 2.5 m^3 is designed to obtain a homogeneous mixture of dry powdered components (grain, farinaceous, protein-mineral raw material) under the batch (periodic) operation mode. It consists of a frame, housing with a mixing chamber in which a shaft with a spiral tape counterflow winding is placed, and of blades in the top part of the bunker. It is possible to install the housing on the strain gauges.

Fig. 1. General view of inclined single-screw batch mixer

In such a mixer, under the shaft rotation, the displacement of material particle groups from one place to another (convective mixing) is performed as follows: a screw transports the material to the upper part of the inclined bunker, and then its gravitation shattering to the lower part of the bunker takes place. Therefore, the main advantage of an inclined mixer, compared to vertical and horizontal ones, is the absence of dead zones between the working bodies and the walls of the mixing chamber [13].

Irregularity in the dispersion of the reference ingredient in the mixture and the process specific energy intensity were taken as criteria that characterize the mixing efficiency. Shredded wheat with moisture content up to 15% with dense loaded density of 750 kg / m^3 was used in the experiments as the basic ingredient (filler) of the mixture.

As a result, a two-component mixture composed of shredded wheat - 99%, ground common salt - 1% (by weight) was prepared.

Ground common salt was used as the reference ingredients to determine the mixing irregularity. Its distribution was determined by taking 20 samples weighing 50 g each from different points of the mixing chamber [14]. The selection of a specific sample was made according to GOST 13 496.0–80. The content of the dry reference component (table salt) in the samples was determined through the ionometric technique according to GOST 13 496.1–98. The variation coefficient of the actual distribution of the reference component in samples ν, % (y_1) was used as an index of mixing irregularity.

$N_{уд}$ (y_2) specific energy intensity of the mixing process was defined as the total energy intensity related to the mass of the feed mixture measured using a three-phase electric meter [15].

The mixer shaft speed was changed by DELTAVFd-075E frequency converter through the current frequency variation of the asynchronous motor.

A three-tier second-order design was implemented during the experiment. The experiments were carried out in triplicate [16,17].

The design of the experiments involved the variation of four independent factors affecting the mixing process (Table 1).

It is established that the signification of the mixing irregularity index is much higher than that of the latter factor which should be considered accessory.

Table 1

Factors and levels of variation

Factor	Coded identification	Variability range	Variability interval
Shaft speed, min^{-1}	x_1	20–40	10
Filling factor of mixing chamber	x_2	0.4–0.6	0.1
Mixing cycle (time), min	x_3	2–6	2
Tilt angle of mixing chamber, grade	x_4	15–35	10

Research Results. After processing the experimental results, the regression equations in coded form were obtained, and the corresponding correlation coefficients were determined:

$y_1 = 4.06 - 0.96x_1 + 0.29x_2 + 0.16x_3 - 0.88x_4 - 0.14x_1x_2 - 0.19x_1x_3 + 0.54x_1x_4 + 0.28x_2x_3 - 0.39x_2x_4 - 0.20x_3x_4 + 0.56x^2_1 + 0.27x^2_2 + 0.34x^2_3 + 0.64x^2_3$,

correlation coefficient $R_1 = 0.9607$;

$y_2 = 2.26 + 0.99x_1 + 0.42x_2 - 0.07x_3 - 0.28x_4 + 0.22x_1x_2 - 0.15x_1x_3 + 0.35x_1x_4 + 0.13x_2x_3 + 0.47x_2x_4 - 0.08x_3x_4 + 0.73x^2_1 + +0.37x^2_2 + 0.14x^2_3 + 0.84x^2_3$,

correlation coefficient $R_2 = 0.9781$.

The model adequacy was evaluated by the Fisher criterion. The tabular value of the Fisher criterion with the significance level $\Delta = 0.05$ equals to $F = 2.8$. The Fisher criterion value in the models is as follows: mixing irregularity - $F = 2.51$; energy intensity of the mixing process - $F = 2.65$. Comparison of the calculated values with the tabulated values has shown that their calculated values are less than the tabulated values. Consequently, regression models adequately describe the process under study. The experimental values of the Cochran test do not exceed the tabulated values. Dispersions are homogeneous.

Turning from the coded values of the factors (X_1, X_2, X_3, X_4) to natural ones (n, k, t, φ), we have obtained dependences of the mixing irregularity indicators (δ, %) and the mixing energy intensity (N, kW • h) on the basic factors in the following form:

– mixing irregularity:

$\delta = 3.76 + 11n - 0.15k - 1.02t - 2.35\varphi + 16nk - 21nt - 59n\varphi - 0.06kt + 0.98k\varphi + 2.35t\varphi + 2.15n^2 + 4.33k^2 + 3.65t^2 + 0.75l^2$;

– mixing energy intensity:

$$N = 2.19 + 23n + 4.13k + 6.25\varphi - 13nk - 3.4n\varphi - 5.23k\varphi + 0.99n^2 + 0.48k^2 + 0.39\varphi^2.$$

The experimental data processing has resulted in plotting characteristic curves of the optimization criteria versus the factor variation level. They are combined two-dimensional sections of second-order response surfaces.

Figures 3 and 4 show some two-dimensional response surfaces of the factor influence to the mixing process. In particular, the dependences of the effect of the shaft speed and the loading factor of the mixing chamber on the mixing irregularity and the process energy intensity are shown.
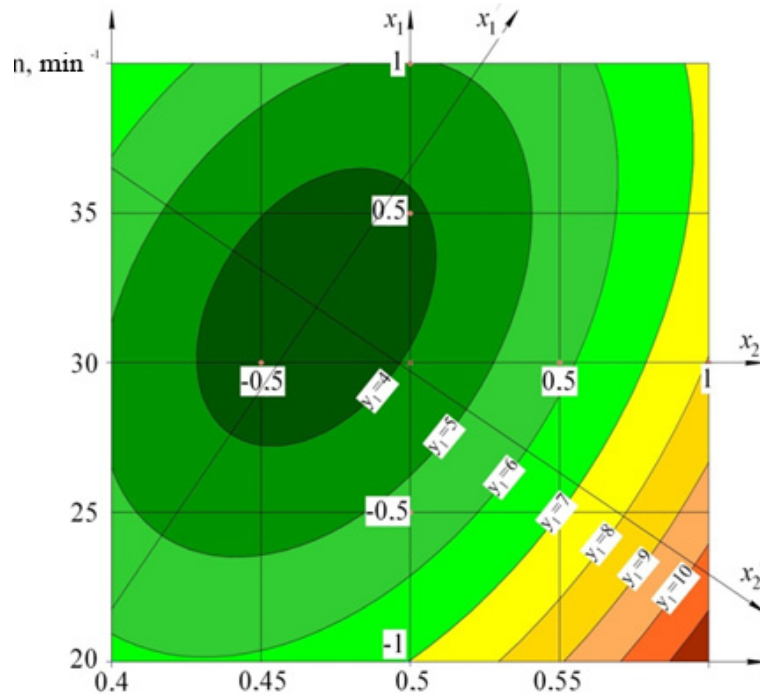
Fig. 3. Effect of shaft speed and loading ratio of the mixing chamber on mixing irregularity
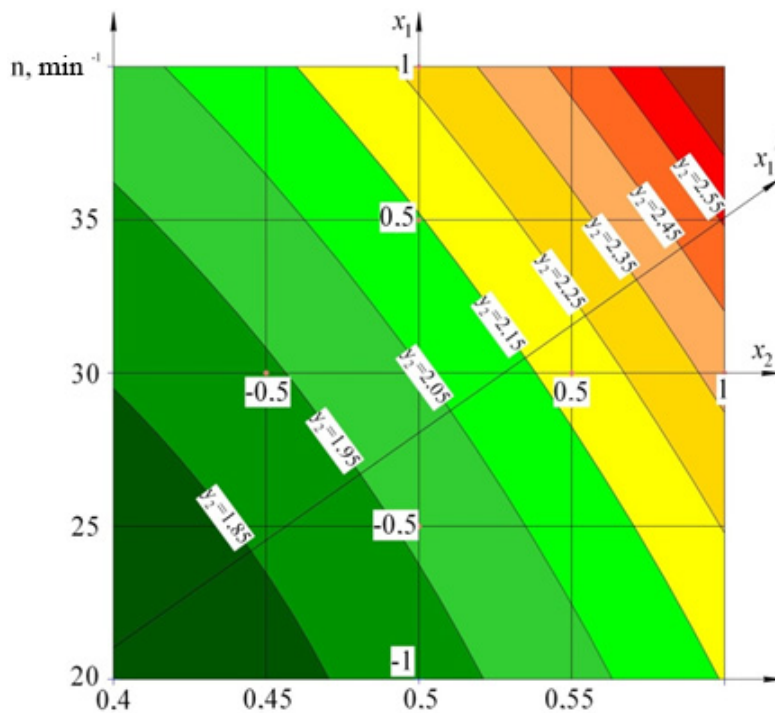
Fig. 4. Effect of shaft speed and loading factor of the mixing chamber on mixing energy

The research has resulted in determining the rational values of parameters and operation modes of the inclined single-shaft screw batch mixer with the capacity of 2.5 m[3] during the preparation of feed mixtures that meet the zootechnical requirements on mixing irregularity under the condition of minimum energy intensity of the process. The rational values to obtain mixing irregularity up to 5% are the following: shaft speed is

n = 27.5–36.5 min^{-1}; loading factor of the mixing chamber is k = 0.43–0.51; mixing time is t = 3–4.2 min; tilt angle of the mixing chamber is φ = 22–25°. In this case, the energy intensity of the process was equal to 2.08 – 2.16 kWh/t.

Besides, as a result of the experimental studies, the smallest mixing irregularity of 3.2% is set under the following mixing modes and parameters of the mixer: shaft speed is n = 35 min^{-1}; loading factor of the mixing chamber is k = 0.5; mixing time is t = 3 min; tilt angle of the mixing chamber is φ = 30°. In this case, the energy intensity of the process was 2.2 kWh / t. The smallest energy consumption of 2.1 kWh / t under mixing irregularity of 5% is obtained at the following values of parameters and operating modes of the mixer: shaft speed is n = 30 min^{-1}; loading factor of the mixing chamber is k = 0.55; mixing time is t = 3 min; tilt angle of the mixing chamber is φ = 25°.

Discussion and Conclusions. The dependences resulting from the experimental studies enable to establish domains of rational design parameters and modes of the inclined single-shaft screw batch mixer. The results can be used for the development of technical means for the production of complete feed, as well as for the modernization of existing mixed feed industry to increase their energy efficiency.

References

1. Afanasyev, V.A. Energo- i resursosberegayushchie tekhnologii kombikormov. [Energy and resource-saving technologies of all-mash.] Voronezh: VGUIT, 2017, 473 p. (in Russian).

2. Khlystunov, V.F., et al. Model' protsessa smeshivaniya kormov v portsionnom naklonnom odnoshnekovom smesitele. [Model of feed mixing process in inclined single-screw batch mixer.] Innovatsionnoe razvitie APK Rossii na baze intellektual'nykh mashinnykh tekhnologiy: sb. nauch. dokl. mezhdunar. nauch.-tekhn. konf. [Innovative development of the Russian Agro-Industrial Complex on the basis of smart machine technologies: coll.sci. papers Int. Sci.-Pract. conf.] Moscow, 2014, pp. 41–45 (in Russian).

3. Frolov, V.Yu., Sysoev, D.P., Serguntsov, A.S. K analizu tekhnologicheskikh i tekhnicheskikh sredstv protsessa prigotovleniya vysokokachestvennykh kormov. [To analysis of technological and technical means of prepargh high quality forage.] Scientific Journal of KubSAU, 2014, no. 101, pp. 2108–2120 (in Russian).

4. Pakhomov, V.I., Smolenskiy, A.V., Alferov, A.S. Oborudovanie dlya prigotovleniya polnoratsionnykh kombikormov v usloviyakh khozyaystv. [Complete feed equipment under intrafarm conditions.] Vestnik of DSTU, 2012, vol. 12, no. 7 (68), pp. 108–114 (in Russian).

5. Sabiev, U.K., Yatsunov, A.N., Chernyakov, A.V. Obosnovanie parametrov i analiz rabochikh organov smesitelya kormov. [Justification of parameters and analysis of the feed mixer working bodies.] Selskiy Mechanizator, 2016, no. 6, pp. 26–27 (in Russian).

6. Khlystunov, V.F., et al. Modelirovanie protsessa smeshivaniya kormov v shnekovom smesitele s naklonnym bunkerom. [Modeling the process of fodder mixing in a spiral mixer with inclined bin.] Vestnik of the Russian Agricultural Science, 2007, no. 4, pp. 13–15 (in Russian).

7. Barnes, H.A., Hutton, J.F. and Walters, K. An Introduction to Rheology. Rheology Series, Elsevier, 1989, vol. 3, 199 p.

8. Ottino J.M. The Kinematics of Mixing: Stretching, Chaos, and Transport, Cambridge University Press, 1989, 364 p.

9. Cullen P. J., ed. Food mixing: Principles and applications. John Wiley & Sons, 2009. doi: 10.1002/9781444312928

10. Gurinenko, L.A., et al. Diskovyy izmel'chitel' kormovogo zerna. [Disk shredder of coarse grain.] Machinery and Equipment for Rural Area, 2014, no. 10, pp. 9–11 (in Russian).

11. Pakhomov, V.I., et al. Vertikal'nye drobilki dlya proizvodstva kombikormov. [Vertical crusher for the feed production.] Selskiy Mechanizator, 2015, no. 11, pp. 27 (in Russian).

12. Rielly C. D., et al. Mixing processes for agricultural and food materials: Part 4, assessment and monitoring of mixing systems. Journal of agricultural engineering research, 1994, vol. 59, no. 1, pp. 1-18. doi: 10.1006/jaer.1994.1060

13. Paul, E.L., Atiemo-Obeng, V.A., Kresta, S.M. Handbook of Industrial Mixing. Science and Practice. John Wiley & Sons, 2004, 1440 p.

14. OST 70.19.2-83 Ispytaniya sel'skokhozyaystvennoy tekhniki. Mashiny i oborudovanie dlya prigotovleniya kormov. Programma i metody ispytaniy. [Branch Standard 70.19.2-83 Tests of agricultural machinery. Machines and equipment for feed preparation. Program and Test Methods.] Moscow: Standartinform, 1991, 94 p. (in Russian).

15. Rudolph, L., Atiemo-Obeng, V., Schaefer, M., Kraume, M. Power consumption and blend time of co-axial tank mixing systems in non-Newtonian fluids. 13$^{\text{th}}$European Conference on Mixing: London, 2009, pp. 1–8.

16. Melnikov, S.V., et al. Planirovanie eksperimenta v issledovaniyakh sel'skokhozyaystvennykh protsessov. [Planning an experiment in agricultural research.] Leningrad: Kolos, 1980, 168 p. (in Russian).

17. Grachev, Yu.P., Plaksin, Yu.M. Matematicheskie metody planirovaniya eksperimenta. [Mathematical methods for experiment planning.] Moscow: DeLiPrint, 2005, 296 p. (in Russian).

Authors:

Khlystunov, Victor F.,
professor of the Technologies and Processing Equipment for Agro-Industrial Complex Department, Don State Technical University (1, Gagarin sq., Rostov-on-Don, 344000, RF), Dr.Sci. (Eng.), professor,
ORCID: http://orcid.org/000-0002-2743-0698
vniptim@gmail.ru

Braginets, Sergey V.,
Senior Research Scholar, Agricultural Research Centre "Donskoy" (14, Lenin St., Zernograd, Rostov region, RF), Cand.Sci. (Eng.),
ORCID: http://orcid.org/0000-0001-7137-5692
sbraginets@mail.ru

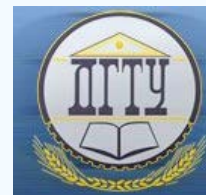**Alferov, Alexander S.,**
Research Scholar, Agricultural Research Centre "Donskoy" (14, Lenin St., Zernograd, Rostov region, RF), Cand.Sci. (Eng.),
ORCID: http://orcid.org/0000-0001-5210-781X
alfa-8303@yandex.ru

Chernutskiy, Mikhail V.,
senior engineer, Agricultural Research Centre "Donskoy" (14, Lenin St., Zernograd, Rostov region, RF),
ORCID: http://orcid.org/0000-0002-9936-1978
mux346@yandex.ru

МАШИНОСТРОЕНИЕ И МАШИНОВЕДЕНИЕ
MACHINE BUILDING AND MACHINE SCIENCE

Improvement of corrosion process control techniques at engineering facilities under high parameters of water coolants [*]

V. N. Shcherbakov[1][**]

[1]Don State Technical University, Rostov-on-Don, Russian Federation

Совершенствование методов контроля процессов коррозии на объектах машиностроения при высоких параметрах водных теплоносителей[***]

В. Н. Щербаков[1][**]

[1]Донской государственный технический университет, г. Ростов-на-Дону, Российская Федерация

Introduction. The work objective is to increase the reliability of the prediction methods for the lithium hydroxide behavior in the steam-water circuit at the thermal power plants and nuclear power plants, and for the operational monitoring of the pH index of steam solutions. A method of operational control is developed on the basis of the conductometric measurements of the hydrogen index of the corrosion inhibitor vapor solutions for construction materials of lithium hydroxide used at the TPP and NPS.

Materials and Methods. A mathematical model method is used for the practical implementation of the high-temperature operational control of the steam solution pH index.

Research Results. A method for monitoring the pH of vapor solutions of lithium hydroxide based on the determination of vapor concentration through the steam condensation in the coolable conductivity sensor located in the vapor space of the steam generator is developed. This has significantly improved the accuracy of determining the lithium hydroxide concentration. Equations describing the change in the limiting molar equivalent conductance and dissociation constants of lithium hydroxide in a wide range of state change parameters are proposed.

Discussion and Conclusions. The proposed on-line technique of testing the pH value of steam solutions, and mathematical models for calculating the limiting molar equivalent conductance and dissociation constants provide an acceptable error level calculations and the capability of measurements automation. With an increase in the vapor temperature up to 573.15 K, the necessity arises to fortify lithium hydroxide in the vapor to 10^{-2} mol / kg.

Введение. Цель работы — повышение надёжности методов прогнозирования поведения гидроксида лития в пароводяном тракте на ТЭС и АЭС и оперативного контроля водородного показателя паровых растворов. Разработан метод оперативного контроля на основе кондуктометрических измерений водородного показателя паровых растворов ингибитора коррозии конструкционных материалов гидроксида лития, применяемого на ТЭС и АЭС.

Материалы и методы. Для практической реализации высокотемпературного оперативного контроля водородного показателя паровых растворов использован метод математического моделирования.

Результаты исследования. Разработан метод контроля водородного показателя паровых растворов гидроксида лития, основанный на определении концентрации в паре путём конденсации пара в охлаждаемом кондуктометрическом датчике, размещённом в паровом пространстве парогенератора, что позволило значительно повысить точность определения концентрации гидроксида лития. Предложены уравнения, описывающие изменение предельной молярной эквивалентной электропроводности и констант диссоциации гидроксида лития в широком диапазоне изменения параметров состояния.

Обсуждение и заключения. Предложенные метод оперативного контроля водородного показателя паровых растворов и математические модели для расчёта предельной эквивалентной молярной электропроводности и констант диссоциации обеспечивают приемлемую для практических расчётов погрешность и возможность автоматизации измерений. При увеличении температуры пара до 573,15 K возникает необходимость в увеличении концентрации гидроксида лития в паре до 10^{-2} моль/кг.

Introduction. When organizing and maintaining water chemistry regimes (WCR) at TPPs and NPPs, one of the major tasks is to minimize corrosive damages to the thermal power equipment in the zone of contact with water and steam [1]. Addition of *LiOH* in sufficient quantities into feedwater provides the creation of a hard protective lithium-ferritic film on the metal surface, which slows down corrosion and stress-corrosion cracking of the heat-exchange tubes of steam generators of NPPs with VVER-1000 [2, 3], as well as a significant increase in uptime [3]. When *LiOH* is added into the feedwater of the TG – 104 drum boilers at the TPP, the formation of a protective lithium-ferritic film is also observed [4]. *LiOH* is used at the TPPs in Russia and abroad [4–6]. In advanced fourth-generation nuclear reactors – *SCWR* (*supercritical water-cooled reactor*), providing an increase in thermal efficiency compared to the existing ones (*PWR*) from 33 to 44%, at pressure *P = 25 MPa*, *T* temperature of water vapor is planned to be increased to 953 *K* [6]. We need data on Λ_o limiting equivalent conductance and K_d *LiOH* dissociation constants at high *P* and *T*, presented in an easy-to-calculate form, to create on-line monitoring of the *pH* values of aqueous and steam *LiOH* solutions at TPPs and NPPs that determine the effectiveness of anticorrosive protection. The technique for calculating the *pH* of *LiOH* solutions based on the data on χ electric conductivity proposed by the authors for the liquid phase [7] is unacceptable for the vapor phase at low ρ densities and *C* concentration due to a high error in determining χ and K_d [8].

The work objective is to increase the reliability of methods for predicting *LiOH* behavior in the steam/water circuit at TPPs and NPPs and of the operational control of the of steam solutions *pH*.

To achieve this goal, equations are developed for calculating Λ_o and K_d on the saturation line and in superheated steam at *T* up to 773.15 *K*; and a technique to control *pH* of *LiOH* vapor solutions is worked out.

Materials and Methods. Compared with the traditional control associated with sampling and cooling of samples, the operational *pH* control using conductometric sensors installed in the heat conductor of the steam generators and working at *T* and *P* close to the operating ones, is more objective and practically inertia-free [7, 8]. In *pH* calculations for the liquid phase in [7], the experimental data on K_d *LiOH* [8], K_w ionic product [9], and ε dielectric capacitance for water [10] were used. *C* concentration of *LiOH* aqueous solutions was determined in terms of *C LiOH=f* (χ *LiOH*)$_{T=Const}$, the dependences obtained on the basis of the experimental data on χ solutions.

Under measuring χ solutions in the vapor phase (especially for small ρ and *C*), when the polar properties of the solvent are weakened, the dissociation degree of *LiOH* is small, and the resistance of the interelectrode space of the measure cell of the conductometric converter can become commensurate with the resistance of the electrical insulator, which will lead to large errors in determining χ [8].

For the practical implementation of the high-temperature operative *pH* control, the necessary data on Λ_o and K_d can be obtained in the studied range of the state parameter variation through the mathematical simulation technique and be presented in the form of equations.

Research Results. Considering the analysis of existing methods, this paper proposes a method for testing *pH* of *LiOH* vapor solutions based on the determination of *C LiOH* in steam through the vapor condensation in the conductivity sensor with a cooled capillary [11] placed in the vapor space of the steam generator in the coolant flow. In this case, *C LiOH* in steam is equal to *C LiOH* in the vapor condensate and can be determined from *C LiOH=f* (χ *LiOH*)$_{T=Const}$ dependences obtained for the liquid phase [7]. Vapor condensation can significantly improve the accuracy of determining χ and *C* [8]. The *pH* calculations for *LiOH* vapor solutions were performed according to the procedure described in [12] using data from [8] on K_d.

To assess the effectiveness of using *LiOH* for corrosion protection in *SCWR* fourth-generation atomic reactors, the authors [6] calculated the *pH* of *LiOH* aqueous and steam solutions at *P = 25 MPa* in a wide variation range of ρ, *T*, *C*, on the basis of the experimental data on K_d [13–15]. Besides, an empirical equation for calculating K_a molal Kon constant [16] in ρ variation range from 50 to 1000 kg / m^3 and *T* from 373 to 873 *K* is proposed:

$$log_{10}K_a = a_1 + a_2/\tau + + (a_3 + a_4/\tau) \cdot log_{10}\delta + (a_5 + a_6/\tau) \cdot (log\delta)^2,$$

where $\delta = \rho/\rho_c$; $\tau = T/T_c$; ρ_c, T_c is the solution density and temperature at the critical point; a_1, a_2, a_3, a_4, a_5, a_6 are constants.

In superheated steam, with a decrease in ρ and T K_d $LiOH$ reduces, the difference between pH $H2O$ and pH of $LiOH$ steam solutions decreases, which reduces the effectiveness of corrosion protection of the structural elements at high P and T. The authors have calculated the pH values of $LiOH$ steam solutions at $P = 25$ MPa; $T = 673$, 723 and 773 K for $C=10^{-6}$, 10^{-5}, 10^{-4}, 10^{-3} and 10^{-2} mol/kg. The experimental data on K_d $LiOH$ [8], K_w ionic product [9], and ε dielectric capacitance of water [10] were used in the calculations. Fig. 1 shows pH dependence of aqueous and vapor $LiOH$ solutions on ρ at $P = 25$ MPa for $C=10^{-6}$–10^2 mol/kg.

In the area of ρ <330 kg/m^3, the authors [13–15] did not perform experimental studies; therefore, the figure shows only the results of calculating pH of $LiOH$ using the data on K_d $LiOH$ obtained by the authors' equation [16].
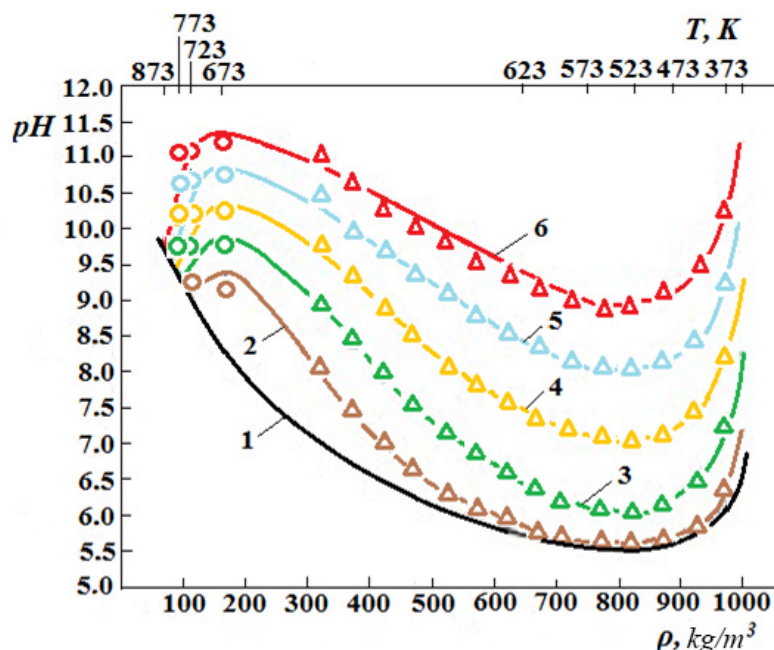
Fig.1. *pH* dependence of *LiOH* aqueous and steam solutions on ρ density at $P = 25$ *MPa*: $1 - H_2O$; 2,3,4,5,6 – C *LiOH* = 10^{-6}, 10^{-5}, 10^{-4}, 10^{-3}, 10^{-2} mol/kg; Δ, $\circ$ is calculation of *pH* from data on K_d [13-15] and [8]; 2,3,4,5,6 lines are calculation of *pH* according to K_d data obtained from equation [16].

Λ_o and K_d values [8], which are necessary for creating equations describing the change of Λ_o and K_d with changing ρ and T, are given in Tables 1 and 2 in comparison with the data from other authors. These values were previously obtained by the authors on the basis of the measurements of the electrical conductivity of high-temperature $LiOH$ solutions.

To create equations describing Λ_o behavior on the saturation line, in order to reduce the error of data approximation, ρ variation range was divided into 2 parts (from 100 to 500 and from 500 to 958 kg/m^3), for each of which an equation of the following form was proposed:

$$\Lambda_o = b_o \cdot \rho^3 + b_1 \cdot \rho^2 + b_2 \cdot \rho + b_3,$$

where b_o, b_1, b_2, b_3 are definable constants; ρ is density of the solution, kg/m^3. b_o, b_1, b_2, b_3 values for $\rho = (100$–$500)$ and $(500$–$958)$ kg/m^3 are –0.000004; 0.005878;

–2,810,820; 1942.943226 and –1.25711 10^{-5}; 0.024177411; –16.58559801; 5334,222549 respectively. For $pK_d = -log_{10}$ values, the values of d_1–d_6 coefficients are calculated in the equation similar to that presented in [16] and given above:

$$pK_d = d_1 + d_2/\tau + (d_3 + d_4/\tau) \cdot log_{10}\delta + (d_5 + d_6/\tau) \cdot (log\delta)^2,$$

where $\delta = \rho/\rho_c$; $\tau = T/T_c$; ρ_c, T_c are density and temperature of the solution at the critical point; d_1, d_2, d_3, d_4, d_5, d_6 are constants.

When calculating d_1–d_6 constants, we used previously obtained experimental data on K_d [8]. On the saturation line, we considered only our own experimental data. Calculations for the superheated steam at $T = 673.15$ and 773.15 K were made in two versions: in the first one, only the author's data on K_d [8] were considered, in the second – all the data given in Table 2.

Table 1

Dependence of Λ_o *LiOH* limiting molal conductivity on ρ density
on saturation line and in superheated steam

ρ, kg/m^3	$\Lambda_o \cdot 10$, cm·m^2 / kmol		
	Saturation line	T = 673 K	T = 773 K
100	1710[8]	1675[8]	1665[8]
130	1675[8]	1630[8]	1620[8]
160	1630[8]	1590[8]	1575[8]
200	1575[8]	1550[8]	1545[8]
300	1510[8]	1480[8]	1475[8]
400	1475[8]	1460[8]; 1392[13]	1455[8]
433		1452[15]	
500	1450[8]	1435[8]; 1539[13]	1428[8]; 1574[13]
600	1370[8]	1380[8]; 1355[13]	1388[8]; 1377[13]
621	1277[15] (P = 23.86 MPa)	-	-
700	1265[8]	1275[8]; 1270[13]	1276[13]
714	1189[15] (P = 9.52 MPa)	-	-
800	1100[8]	1088[13]	1109[13]
871	1017[15] (P = 9.91 MPa)	-	-
917	780[8]	-	-
922	754[15] (P = 9.4 MPa)	-	-
950	594[13]	-	-
958	573[8]	-	-

For the saturation line: d_1=119.50984; d_2=–115.33347; d_3=–174.20233; d_4=167.90533; d_5=–143.78368; d_6=183.09356.

For the first version of the calculation for the superheated steam: d_1=7.6323975; d_2=–3.214114; d_3=–10.9289; d_4=2.5463453; d_5=–10.34132; d_6=15.190972; for the second version of the calculation: d_1=10.113404; d_2=–6.133638; d_3=–17.85984; d_4=8.888042; d_5=–8.405401; d_6=14.648395.

The percent deviations of the experimental values of Λ_o and pK_d from those calculated by the proposed equations are presented in Table 3.

Table 2

Dependence of negative logarithm of Koff constant of *LiOH* pK_d
on ρ density on saturation line and in superheated steam

ρ, kg/m^3	pK_d, mol/kg		
	Saturation line	T = 673.15 K	T = 773.15 K
100	10.04[8]	10.07[8]; 11.06 [16]	10.16[8]; 13.34[16]
130	8.41[8]	8.56[8]	8.67[8]
160	7.24[8]	7.32[8]	7.69[8]
200	6.25[8]	6.42[8]; 6.45[16]	6.89[8]; 8.16[16]
300	4.40[8]	4.69[8]; 4.13[16]	5.20[8]; 5.64[16]
379		3.48[15]	
400	3.86[8]	3.98[8]; 2.82[16]; 3.14[13]	4.31[8]; 4.01[16]
433		3.1[15]	
500	3.28[8]	3.38[8]; 2.81[13]	3.43[8]; 3.15[13]
600	2.52[8];	2.45[8]; 2.32[13]; 1.26[16]	2.58[8]; 2.43[13]; 1.97[16]
650		2.13[13]	2.25[13]
700	2.08[8];	2.01[8]; 1.83[13]	2.07[13]
712	1.59[17]		
750		1.82[13]	1.89[13]
800		1.63[13]; 0.343[16]	1.65[13]; 0.753[16]
807	1.41[15] (P = 11.02 *MPa*)	-	-
922	1.29[15] (P = 9.4 *MPa*)	-	-

961	1.03[15] ($P = 4.88\ MPa$)	-	-

Table 3

Deviation (in%) of experimental values of limiting equivalent conductance ($\delta\Lambda_o$) and negative logarithm of molal Koff constants (δpK_d) from values calculated by equations

ρ, kg/m³	$\delta\Lambda_o$ Saturation line	δpK_d				
		Saturation line	T=673,15 K 1 calculation version	T=773,15 K 1 calculation version	T=673,15 K 2 calculation version	T=773,15 K 2 calculation version
100	0.36[8]	0.04[8]	1.20[8]	1.36[8]	3.40[8]; 5.86 [16]	10.9[8]; 15.5[16]
130	0.47[8]	0.23[8]	0.18[8]	1.22[8]	2.42[8]	11.7[8]
160	0.28[8]	0.33[8]	2.62[8]	1.86[8]	3.42 [8]	10.5[8]
200	0.34[8]	0.11[8]	0.92[8]	0.39[8]	0.52[8]; 0.98[16]	5.95[8]; 10.5[16]
300	0.09[8]		2.50[8]	0.29[8]	3.86[8]; 9.17[16]	1.99[8]; 5.96[16]
379					3.05[15]	
400	0.03[8]	0.12[8]	4.99[8]	4.07[8]	14.8[8]; 20.2[16]; 7.96[13]	6.44[8]; 0.56[16];
433					0.41[15]	
500	0.09[8]	0.16[8]	8.95[8]	2.40[8]	21.77[8]; 5.90[13]	8.78[8]; 0.67[13]
600	0.10[8]	0.17[8]	4.56[8]	6.11[8]	13.72[8]; 8.89[13]; 67.8[16]	5.24[8]; 0.60[13]; 24.1[16]
650	-	-	-	-	10.6[13]	4.02[13]
700	0.44[8]	0.05[8]	7.82[8]	-	14.38[8]; 5.95[13]	8.03[13]
750		-	-	-	14.2[13]	11.5[13]
800	0.26[8]	-	-	-	12.8[13]	11.3[13]
917	2.27[8]	-	-	-	-	-
958	1.51[8]	-	-	-	-	-

Discussion and Conclusions. As obvious from Fig. 1, *pH* values of *LiOH* obtained by the authors at $T = 673\ K$ are lower compared to those obtained through calculating [6] by a mean of 0.2; at $T = 723\ K,$ they are higher by 0.1–0.2; at $T = 773\ K,$ they are higher by 0.1–0.7 *pH* units.

Thus, the error ratio of the data on *pH* of *LiOH* in the superheated steam obtained by the authors and presented in [6] goes up with increase in *T* and *C*. Such a mismatch may be considered satisfactory if it is remembered that with decreasing ρ to 200–100 kg/m³, the experimental data [8] error on K_d *LiOH* increases to 180%, and, moreover, the authors [6] did not use the experimental data on K_d equation at ρ <330 kg/m³.

The deviation of the experimental values of Λ_o and pK_d from those calculated using the equations proposed in this paper on the saturation line does not exceed 1%, and only at ρ = 917 and ρ = 958 kg/m³, it reaches 2.27 and 1.51% for Λ_o (Table 3). In the superheated steam at $T = 673.15$ and $T = 773.15\ K$ for the first version of the calculation using only the author's experimental data on K_d [8], the greatest deviation of the experimental data of pK_d from the calculated one does not exceed 2.5% at ρ = 100–300 kg/m³ and goes up to 8.95% with an increase in ρ to 400–700 kg/m³. For the second version of the calculation, considering the data of all authors presented in Table 2, the greatest error of calculation by the equation at ρ = 100–300 kg/m³ and $T = 673.15\ K$; $T = 773.15\ K$ reaches 15.5% for these authors [16], and at ρ = 100–300 kg/m³ and $T = 673.15\ K$; $T = 773.15\ K$ – 67.8%.

Based on the analysis of the obtained results, it can be concluded that the use of *LiOH* as a corrective additive for *pH* control in order to prevent corrosion damage to structural elements of *SCVR* advanced atomic reactors of the

fourth generation creates no difficulties at $T \leq 673.15$ K and $P = 25$ MPa. With an increase in temperature already at $T = 773.15$ K, for effective corrosion protection, it is necessary to raise C $LiOH$ to 10^{-2} mol/kg, which puts forward the task to study the vapor solvability of $LiOH$ at these state parameters.

The proposed method of operative control of pH of $LiOH$ vapor solutions and mathematical models for calculating Λ_o and K_d provide the capability to determine pH using a measuring-computing complex that runs continuously in automatic mode; it has a short signal delay time, and it provides an acceptable for practical calculations error of measurement results.

The application of such devices in modern systems of chemical-engineering monitoring at TPPs and NPPs will significantly improve the reliability of pH operation control and forecasting techniques of $LiOH$ behavior of in the vapor-water circuit.

References

1. Voronov, V.N., Petrova, T.I. Vodno-khimicheskie rezhimy TES i AES. [Water chemistry regimes of thermal and nuclear power plants.] Moscow: MEI Publ. House, 2009, 238 p. (in Russian).

2. Gorbatykh, V.P., Ivanov, S.O. Perspektivy ispol'zovaniya gidroksida litiya v konturakh AES s VVER. [Substantiation of lithium hydro-oxide application in contours of NPP with VVER reactor.] MPEI Vestnik, 2007, no. 1, pp. 24–29 (in Russian).

3. Gorbatykh, V.P., Ivanov, S.O. O vozmozhnosti primeneniya gidroksida litiya na razlichnykh etapakh zhiznennogo tsikla parogeneratorov AES s VVER. [About possibility of lithium hydroxide application at various stages of the life cycle of steam generators of NPP with WWER.] MPEI Vestnik, 2011, no. 2, pp. 10–14 (in Russian).

4. Beluakov, I.I., Belokonova. A.F., Mikhaylova, A.V. Issledovanie prichin povrezhdeniya ekrannykh trub barabannykh kotlov na litievom vodnom rezhime. [Research into the causes of damage to screen tubes of drum boilers in lithium water mode.] Power Technology and Engineering, 1980, no. 6, pp. 30–34 (in Russian).

5. Gorbatenko, S.P., et al. Sovershenstvovanie vodno-khimicheskogo rezhima vtorogo kontura na Kalininskoy AES. [Improving water chemistry of the secondary circuit at the Kalinin NPP.] Thermal Engineerin, 2001, no. 1, pp. 22–28 (in Russian).

6. Carvajal-Ortiz, R.A., Plugatyr, A., Svishchev, I.M. On the pH control at supercritical water-cooled reactor operating conditions. Nuclear Engineering and Design, 2012, vol. 248, pp. 340-342.

7. Shcherbakov, V.N., Lukashov, Yu.Yu., Lukashov, Yu.M. Electrolytical properties of solution of lithium hydroxide at high temperatures and pressures. Thermal Engineering, 2013, vol. 60, no. 4, pp. 280-284.

8. Shcherbakov, V.N. Issledovanie elektrofizicheskikh svoystv vodnykh teplonositeley pri vysokikh parametrakh: dis. … kand. tekhn. nauk. [Investigation of the electrophysical properties of water coolants at high parameters: Cand.Sci. (Eng.) diss.] Moscow, 1980, 204 p. (in Russian).

9. Bandura, A.V., Lvov, S.N. The ionization constant of water over wide ranges of temperature and density. Journal of Physical and Chemical Reference Data, 2006, vol. 35, no.1, pp. 15-30.

10. Aleksandrov, A.A., Orlov, K.A., Ochkov, V.F. Teplofizicheskie svoystva rabochikh veshchestv teploenergetiki. [Thermophysical properties of working agents of heat power engineering.] Moscow: MEI Publ. House, 2009, 225 p. (in Russian).

11. Timrot, D.L., et al. Konduktometricheskiy datchik: avtorskoe svidetel'stvo 958943 SSSR: G01N 27/02. [Conductometric sensor.] USSR Authorship Certificate, no. 958943, 1982 (in Russian).

12. Damaskin, B.B., Petriy, O.A., Tsirlina, G.A. Elektrokhimiya. [Electrochemistry.] Moscow: Khimiya, 2006, 672 p. (in Russian).

13. Ho, P.C., Palmer, D.A. Determination of ion association in dilute aqueous lithium chloride and lithium hydroxide solutions to 600C and 300 MPa by electrical conductance measurements. Journal of Chemical and Engineering Data, 1998, vol. 43, no.2, pp. 162-170.

14. Ho, P.C., Bianchi, H., Palmer, D.A., Wood, R.H. Conductivity of dilute aqueous electrolyte solutions at high temperatures and pressures using a flow cell. Journal of Solution Chemistry, 2000, vol. 29, no.2, pp. 217-235.

15. Ho, P.C., Palmer, D.A., Wood, R.H. Conductivity measurements of dilute aqueous LiOH, NaOH and KOH solutions to high temperatures and pressures using a flow-through cell. Journal of Physical Chemistry B, 2000, vol. 104, no.50, pp. 12084-12089.

16. Plugatyr, A., Carvajal-Ortiz, R.A., Svishchev, I.M. Ion-pair association constant for LiOH in supercritical water. Journal of Chemical and Engineering Data, 2011, vol. 56, no.9, pp. 3637-3642.

17. Vasilenko, G.V., et al. Vzaimosvyaz' mezhdu koeffitsientami raspredeleniya primesey kotlovoy vody i konstantami dissotsiatsii. [Relationship between distribution coefficients of impurities of boiler water and dissociation

constants.] Thermal Engineering, 1995, no. 7, pp. 64–67 (in Russian).

Author:

Shcherbakov, Vladimir N.,
associate professor of the Hydraulics, Hydraulic and
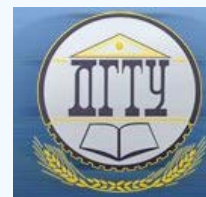Pneumatic Control Systems and Heat Processes
Department, Don State Technical University
(1, Gagarin sq., Rostov-on-Don, 344000, RF),
Cand.Sci. (Eng.), associate professor,
ORCID: http://orcid.org/10000-0001-5682-3792
vladnik48@aaanet.ru

МАШИНОСТРОЕНИЕ И МАШИНОВЕДЕНИЕ
MACHINE BUILDING AND MACHINE SCIENCE

Data measurement system for non-destructive quality testing of hard alloys [*]

I. K. Tsybriy[1], V. L. Vialikov[2], V. I. Ignatenko[3] [**]
[1, 2, 3] Don State Technical University, Rostov-On-Don, Russian Federation

Информационно-измерительный комплекс для неразрушающего контроля качества твердых сплавов [***]

И. К. Цыбрий[1], В. Л. Вяликов[2], В. И. Игнатенко[3] [**]
[1, 2, 3] Донской государственный технический университет, г. Ростов-на-Дону, Российская Федерация

Introduction. It is known that the quality of products from sintered hardmetals, if the fabrication technique is not violated, is determined by the phase composition and an average grain size of the carbide phase. However, hard alloys have a disadvantage inherent in all products of powder metallurgy - the inhomogeneity of the structure and the corresponding variation of properties. Traditional methods of monitoring the structure and phase composition according to the results of selective destructive tests prevent from receiving quality data under the production conditions and do not guarantee the identity of the properties of all batch products under study. The major method of non-destructive quality control of hard alloys is coercimetry, but domestic coercimeters are currently not produced. In this regard, the work objective is to create a domestic data measurement system for non-destructive quality testing of hard alloys and an assessment of the reliability of the results obtained with its help.

Materials and Methods. Cylindrical and spherangular rods with the diameter of 4 to 10 mm, made of alloys of VK8 and VK10HOM grades, were used in the work. The method of comparison with a certified product was used to determine the coercitive force in the data measuring system.

Research Results. The coercive force of two batches of products from hard alloys of VK10HOM and VK8 grades was measured using the developed data measuring system and KOERZIMAT 1.097 HcJ coersimeter.

Discussion and Conclusions. The experimental studies show that the values of the coercitive force of the samples obtained on different equipment have approximately the same level.

Введение. Известно, что качество изделий из спеченных твердых сплавов, при отсутствии нарушений технологии изготовления, определяется фазовым составом и средним размером зерен карбидной фазы. Однако твердые сплавы обладают недостатком, присущим в той или иной степени всем изделиям порошковой металлургии — неоднородностью структуры и соответствующей вариацией свойств. Традиционные методы контроля структуры и фазового состава, по результатам выборочных разрушающих испытаний, не позволяют оперативно в условиях производства получать информацию о качестве и не гарантируют идентичности свойств всех изделий исследуемой партии. Основным методом неразрушающего контроля качества твердых сплавов является измерение коэрцитивной силы. Однако отечественных коэрцитиметров в настоящее время не производится. В связи с этим целью настоящей работы является создание отечественного информационно-измерительного комплекса для неразрушающего контроля качества изделий из спеченных твердых сплавов и оценка достоверности полученных с его помощью результатов.

Материалы и методы. В работе использованы цилиндрические и сфероконические стержни диаметром от 4 до 10 мм, изготовленные из сплавов марок ВК8 и ВК10ХОМ. Для определения коэрцитивной силы в информационно-измерительном комплексе использован метод сравнения с аттестованным изделием.

Результаты исследования. Проведены измерения коэрцитивной силы двух партий изделий из твердых сплавов марки ВК10ХОМ и марки ВК8, выполненных с помощью разработанного информационно-измерительного комплекса и коэрцитиметра KOERZIMAT 1.097 HcJ.

Обсуждение и заключения. Проведенные экспериментальные исследования показали, что значения коэрцитивной силы образцов, полученные на разном оборудовании, имеют примерно одинаковый уровень.

The inhomogeneity of the structure characteristic of sintered hardmetals being a fabrication technique effect is confirmed. Providing that the relative error of measuring the coercitive force for each sample should be within ± 6%, the results obtained can be considered satisfactory. It is shown that the measurement algorithm proposed and implemented in the data measurement system through comparing the characteristics of the tested and certified samples with the known coercitive force, allows the manufacturer of hard alloy products to expand the sample of inspected products up to 100%, and to significantly reduce the costs for non-destructive testing of products.

Подтверждена, как следствие технологии производства, характерная для спеченных твердых сплавов неоднородность структуры. Учитывая, что относительная погрешность измерений коэрцитивной силы для каждого образца должна находиться в пределах ± 6 %, можно считать полученные результаты удовлетворительными. Показано, что предложенный и реализованный в информационно-измерительном комплексе алгоритм измерения путем сравнения характеристик испытуемых и аттестованного образца с известной коэрцитивной силой, позволяет производителю изделий из твердых сплавов расширить выборку контролируемых изделий вплоть до 100% и существенно снизить затраты на неразрушающий контроль продукции.

Introduction. Among the materials obtained through powder metallurgical techniques, hard alloys are widely used. Their basic composition is finely-divided tungsten and titanium carbides on cobalt binder. The use of products from hard alloys is due to a number of valuable properties, such as hardness, resistance to friction wear, wearability. At the same time, the breakdown in the production of powders and sintering features causes the occurrence of structural inhomogeneity within one batch of finished products, and, as a result, heterogeneity of the long-range operation factors. Consequently, sampling check of several hard-metal products from a batch using, for example, metallographic analysis or mechanical testing does not guarantee the identity of the structure and properties of the entire batch.

It is known that the quality of products from sintered hard alloys is mainly determined by the phase composition, i.e. the ratio of the amount of the ferromagnetic cobalt phase and paramagnetic carbides, and the average grain size of the carbide phase [1–3]. At the fixed content of a cobalt phase for each grade of carbide material, the finished product strength is almost completely determined by the carbide graininess [4].

An alternative to destructive testing is non-destructive quality control of hard alloys in terms of coercive force, which at a first approximation inversely depends on the carbide grain fineness. The coercive force value, along with the strength characteristics of hard alloys, is introduced into the current standards [5, 6]. However, the absence of production of domestic coercimeters forces makes manufacturers of hard alloy products use foreign analogues for non-destructive testing.

Accordingly, the work objective is to create a data measuring system for non-destructive quality control of products made of sintered hard alloys, and the validation of the control results obtained with it through comparing with the results obtained using KOERZIMAT 1.097 HcJ coercimeter from "Institut Dr. Foerster GmbH & Co. KG" [7] which is included in the Russian National Register of Measuring Equipments [8]. The results of the coercive force measurement on KOERZIMAT 1.097 HcJ coercimeter are provided by Serpukhov Tool Plant "TVINTOS".

Materials and Methods. Test items were cylindrical and spherangular rods with the diameter of 4 to 10 mm made of alloys of VK8 and VK10HOM grades.

Figure 1 shows the schematic structure of the developed data measurement system [9, 10] which consists of six functional blocks.
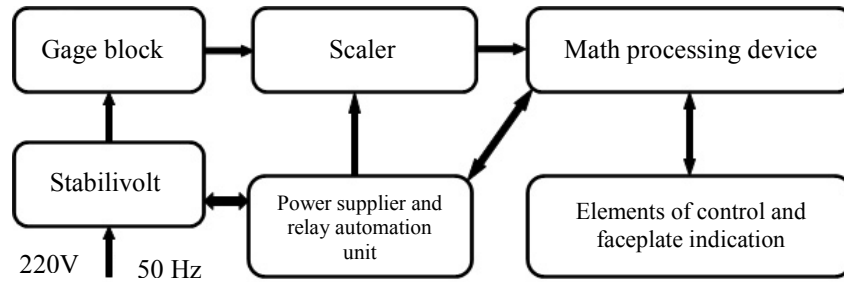
Fig. 1. Schematic structure of data measurement system

The stabilivolt is assembled on a step-up transformer and is designed to increase the supply voltage up to 300V and to feed it to the magnetization coil of the measuring unit. The transformer is turned on by a solenoid starter with a quench circuit, which ensures cushion make-break of the measuring unit. The magnetic starter is controlled by a microcontroller through a triac connection circuit.

The gage block is a solenoid with a magnetization coil and a measuring circuit fixed inside it (Fig. 2). The magnetization coil parameters enable to obtain the magnetic intensity inside the solenoid up to 350 kA/m. The magnetic strength generated in the magnetization unit solenoid enables to measure the coercitive force close to the saturation field of the material.

The scaler is designed to adjust the measuring signal level for the capabilities of the microcontroller. The power supplier and relay automation unit is designed to input various types and levels of voltages to the components of scalers, mathematical processing units, and control and indication elements.
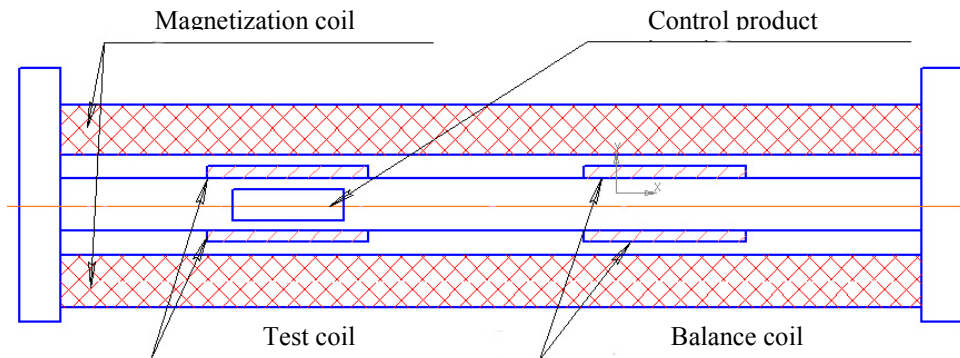
Fig. 2. Measuring unit

The mathematical processing device is designed to calculate and store the signal level corresponding to the coercitive force of the certified sample and to determine the signal level corresponding to the coercitive force of the tested product through the comparison technique.

The data measurement system algorithm is as follows:

- certified sample is placed in the measuring unit, the coercive force value is displayed on the indicator faceplate;

- U_1 voltage corresponding to the known coercitive force value is measured and stored;

- certified sample is removed from the measuring unit;

- test sample is placed in the measuring unit;

- U_2 voltage corresponding to the coercitive force value of the test sample is measured and stored;

- coercitive force value of the test sample obtained through comparing U_1 and U_2 voltages is displayed on the indicator faceplate;

- test sample is removed from the measuring unit.

If it is necessary to measure a batch of products of the same grade and of one size with the certified sample, the measurement process is repeated starting with the 4th point.

Research Results. The comparative analysis results obtained through measuring the coercitive force values of 24 product samples from hard alloys of VK10HOM grade using the developed data-measuring system (row 1) and KOERZIMAT 1.097 HcJ coercimeter (row 2) are presented in Fig. 3. Similar results for 46 product samples from hard alloys of VK8 grade are presented in Fig. 4.

Machine building and machine science
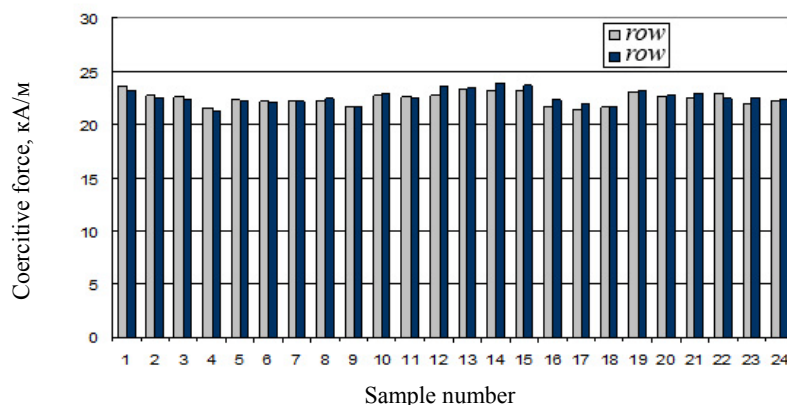
Fig. 3. Coercitive force of samples of VK10HOM grade
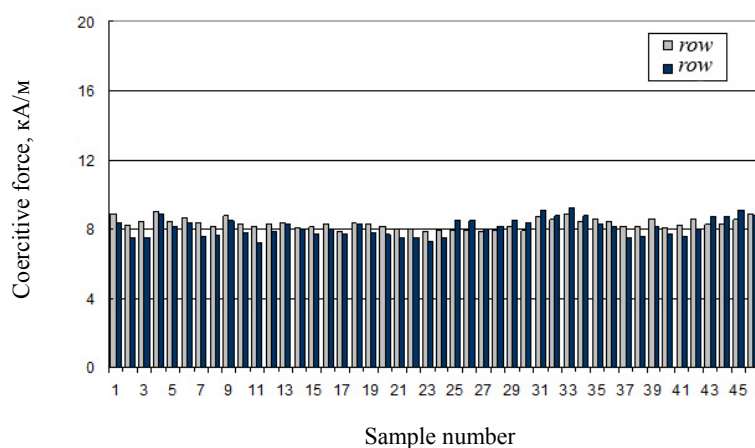
Fig. 4. Coercitive force of samples of VK8 grade

Discussion. The experimental studies have shown that the coercitive force values of the samples obtained using the KOERZIMAT 1.097 HcJ tool and the data-measuring system have approximately the same level.

Taking into account that the relative error in measuring the coercitive force for the KOERZIMAT 1.097 HcJ coercimeter is within ± 6%, the comparative tests results can be considered satisfactory.

The variation of coercitive force values of samples within one grade up to 10–12% can be caused by the following reasons:

- use of powder mixtures from different manufacturers under sintering;
- ignorance of the required process conditions;
- effect of sample configuration on the instrumental data, since lower of the coercitive force values were observed on spherangular samples as a result of a larger demagnetization factor characteristic of this type of samples.

Conclusion. Thus, comparative tests of the data-measuring system have shown the possibility of its use for quality control of products from sintered hard alloys. The proposed integrated measurement algorithm is implemented through the comparison of characteristics of the test samples and the certified sample with the known coercitive force. This allows the manufacturer of hard alloy products to expand the sample of controlled products up to 100%, to reduce time on control operations, and to significantly reduce the costs on nondestructive product inspection.

References

1. Kiffer, R., Benezovsky, F. Tverdye splavy. [Hard alloys.] Moscow: Metallurgiya, 1971, 390 p. (in Russian).

2. Chaporova, I.N., Chernyavskiy, K.S. Struktura spechennykh tverdykh splavov. [Structure of sintered hard alloys.] Moscow: Metallurgiya, 1975, 247 p. (in Russian).

3. Loshak, M.G. Prochnost' i dolgovechnost' tverdykh splavov. [Strength and durability of hard alloys.] Kiev: Nauk. dumka, 1984, 325 p. (in Russian).

4. Tsybriy, I.K. Magnitnye svoystva i metody issledovaniya struktury spechennykh tverdykh splavov: dis. na soisk. uchen. step. kand. tekhn. nauk (05.02.01). [Magnetic properties and methods for studying the structure of sintered hard alloys: Cand.Sci. (Eng.) diss. (05.02.01] Rostov-on-Don, 1984, 166 p. (in Russian).

5. GOST 20 559–75 (ISO 4884–78, ISO 4489–78). Splavy tverdye, materialy keramicheskie instrumental'nye. Pravila priemki i metody otbora prob (s Izmeneniyami № 1, 2, 3, 4). [GOST 20 559–75 (ISO 4884–78, ISO 4489–78).

Hard metals, ceramic tool materials. Regulations of acceptance and methods of sampling (with Changes nos. 1, 2, 3, 4)] Electronic Fund of Legal and Reference Documentation. Available at: http://docs.cntd.ru/document/1200009536 (accessed: 15.02.2018) (in Russian).

6. GOST 24 916–81 (ST SEV 1254–78). Splavy tverdye spechennye. Metod opredeleniya koertsitivnoy sily (s Izmeneniem № 1). [Sintered hardmetals. Method for determination of coercirity (with Change no.1).] Electronic Fund of Legal and Reference Documentation. Available at: http://docs.cntd.ru/document/1200010981 (accessed: 15.02.2018) (in Russian).

7. Förster F., Stumm W. Application of magnetic and electromagnetic nondestructive test methods for measuring physical and technological material values. Materials Evaluation, 1975, vol. 33, no. 1, pp. 515.

8. Koertsitimetr KOERZIMAT 1.097 HcJ. 67654-17: Metodika poverki MP 28-261-2017. [KOERZIMAT 1.097 HcJ. 67654-17 Coercimeter: Verification technique of MP 28-261-2017.] MetrKonsalt. Available at: http://www.all-pribors.ru/opisanie/67654-17-koerzimat-1-097-hsj-77206 (accessed: 15.02.2018) (in Russian).

9. Simonenko, N.I., Tsybriy, I.K. Ispytatel'nyy stend dlya izmereniya magnitnykh kharakteristik tverdykh splavov. [Test bench for measuring the magnetic characteristics of hard alloys.] Fundamental'nye osnovy, teoriya, metody i sredstva izmereniy, kontrolya i diagnostiki: mat-ly 19-oy mezhdunar. nauch.-prakt. konf. [Fundamental principles, theory, methods and means of measurement, control and diagnostics: Proc. 19th Int. Sci.-Pract. Conf.] Novocherkassk, 2018, pp.127–131 (in Russian).

10. Tsybriy, I.K., Simonenko, N.I., Bogdanov, I.N. Sistema tsifrovoy obrabotki signala v pribore dlya opredeleniya koertsitivnoy sily tverdykh splavov. [Digital signal processing system in the device for determining coercitive force of hard alloys.] Transformatsiya mirovogo nauchno-tekhnicheskogo znaniya : sb. nauchnykh trudov po mat-lam mezhdunar. nauch.-prakt. konf. [Transformation of world scientific and technical knowledge: Prac. Int. Sci.-Pract. Conf.] Belgorod, 2018, pp. 117–119 (in Russian).

Authors:

Tsybrii Irina K.,
head of the Instrument Making and Biomedical Engineering Department, Don State Technical University (1, Gagarin sq., Rostov-on-Don, 344000, RF), Cand. Sci. (Eng.), associate professor,
ORCID: https://orcid.org/0000-0002-6281-1832
irconst@mail.ru

Vyalikov, Ivan L.,
associate professor of the Instrument Making and Biomedical Engineering Department, Don State Technical University (1, Gagarin sq., Rostov-on-Don, 344000, RF), Cand. Sci. (Eng.),
ORCID: https://orcid.org/0000-0003-3086-745X
Vialikov@mail.ru

Ignatenko, Vitaly I.,
associate professor of the Instrument Making and Biomedical Engineering Department, Don State Technical University (1, Gagarin sq., Rostov-on-Don, 344000, RF), Cand. Sci. (Eng.),
ORCID: https://orcid.org/0000-0002-8236-3117
79043421201@yandex.ru

ИНФОРМАТИКА, ВЫЧИСЛИТЕЛЬНАЯ ТЕХНИКА И УПРАВЛЕНИЕ
INFORMATION TECHNOLOGY, COMPUTER SCIENCE, AND MANAGEMENT

Stationary model of salt ion transfer in two-dimensional electrodialysis desalting channel in galvanostatic mode[*]

A. M. Uzdenova[1], M. Kh. Urtenov[2][**]

[1] Karachay-Circassian State University, Karachaevsk, Russian Federation
[2] Kuban State University, Krasnodar, Russian Federation

Стационарная модель переноса ионов соли в двумерном электродиализном канале обессоливания в гальваностатическом режиме[***]

А. М. Узденова[1], М. Х. Уртенов[2][**]

[1] Карачаево-Черкесский государственный университет имени У. Д. Алиева, г. Карачаевск, Российская Федерация
[2] Кубанский государственный университет, г. Краснодар, Российская Федерация

Introduction. The theoretical description of the ion transport in membrane systems in the galvanostatic mode is presented. A desalting channel of the electrodialysis apparatus is considered as a membrane system. The work objectives are the development and verification of a two-dimensional mathematical model of the stationary transport of salt ions in the desalting channel of the electrodialysis apparatus for the galvanostatic mode.

Materials and Methods. A new model of ion transfer is proposed. It is based on the Nernst – Planck – Poisson equations for the electric potential and on the equation for the electric current stream function. A numerical solution to the boundary value model problem by the finite element method is obtained using the Comsol Multiphysics software package.

Research Results. The developed mathematical model enables to describe the stationary transfer of binary salt ions in the desalting channel of the electrodialysis apparatus. Herewith, the violation of the solution electroneutrality and the formation of the dilated domain of space charge at overlimiting currents in the galvanostatic mode are considered. A good agreement between the physicochemical characteristics of the transfer calculated by the models for the galvanostatic and potentiostatic modes implies adequacy of the constructed model.

Discussion and Conclusions. The developed model can interpret the experimental study results of ion transfer in membrane systems if this process takes place in the galvanostatic mode. Some electrokinetic processes are associated with the appearance of a dilated domain of space charge at overlimiting currents. When describing the formation of this domain, it is possible to find out how the processes dependent on it affect the ion transfer in the galvanostatic mode.

Введение. Статья посвящена теоретическому описанию процесса переноса ионов в мембранных системах в гальваностатическом режиме. В качестве мембранной системы рассматривается канал обессоливания электродиализного аппарата. Цели работы: создание и верификация двумерной математической модели стационарного переноса ионов соли в канале обессоливания электродиализного аппарата для гальваностатического режима.

Материалы и методы. Предложена новая модель переноса ионов. Она основана на системе уравнений Нернста — Планка — Пуассона для электрического потенциала и на уравнении для функции электрического тока. Получено численное решение краевой задачи модели методом конечных элементов с помощью программного пакета *Comsol Multiphysics*.

Результаты исследования. Разработанная математическая модель позволяет описать стационарный перенос ионов бинарной соли в канале обессоливания электродиализного аппарата. При этом учитываются нарушение электронейтральности раствора и формирование расширенной области пространственного заряда при сверхпредельных токах в гальваностатическом режиме. Об адекватности построенной модели свидетельствует хорошее совпадение физико-химических характеристик переноса, рассчитанных по моделям для гальваностатического и потенциостатического режимов.

Обсуждение и заключения. Разработанная модель позволяет интерпретировать результаты экспериментальных исследований переноса ионов в мембранных системах, если данный процесс протекает в гальваностатическом режиме. Некоторые электрокинетические процессы связаны с появлением расширенной области пространственного заряда при сверхпредельных токах. Описывая формирование указанной области, можно выяснить, каким образом зависящие от нее процессы влияют на перенос ионов в гальваностатическом режиме.

Introduction. Membrane systems form the basis for electrodialysis machines, nano- and microfluidic devices, which are used in water treatment, agricultural products (milk, wine, etc.) processing, performing chemical analysis, and in other areas of activity [1-4]. In numerous mathematical models of mass transfer processes in membrane systems for potentiostatic or potentiodynamic modes, the electrical mode is defined as a potential jump between two equipotential planes parallel to the membranes. A detailed review of the papers devoted to modeling for the potentiostatic mode is presented in [5–7].

All the while, in the practice of electrodialysis, electrochemical characterization of membranes (chronopotentiometry, impedansometry, etc.), the galvanostatic mode is often used, in which a constant average current density is maintained at the interface. A huge amount of experimental data has been compiled about this mode. They must be interpreted [8–10]. Studies in the mathematical modeling of the galvanostatic mode are conducted in several directions.

The first direction is the inverse problem method. As is clear from the name, this is about solving an inverse problem: for the specified current density at the "solution – membrane" interface, the corresponding potential jump is found, and then the problem for the potentiostatic mode is considered [11]. The low efficiency of this method is due to the fact that its implementation requires multiple solutions to the problem in potentiostatic mode for one given value of current density.

The second direction is the decomposition method. In this case, the system of Nernst – Planck – Poisson equations is replaced by a system of decomposition equations [12–16]. The assumption of a quasi-uniform charge distribution enables to obtain a model for the galvanostatic mode in the approximation of Ohm's law [17–20].

The third approach can be called the direct method. In this case, the equation replacing the Poisson equation is derived for the current density in the desalination channel [21].

The galvanostatic mode can be described differently — by numerical solution to the Nernst – Planck – Poisson equations for an electric potential with a special boundary condition that allows the current density to be set as a parameter specifying the electrical mode in the system. In [22, 23] for the one-dimensional case, the time derivative of the electric potential gradient was determined as an explicit function of the current density. This distinguishes the authors' approaches from potentiostatic models in which the difference of potentials is set.

This paper presents a stationary model of the ion transfer process in membrane systems for the galvanostatic mode. It is based on the Nernst-Planck-Poisson equation system with the boundary condition that enables to establish the current density as a parameter that sets the electric mode in the system. This solution is similar to [22, 23]. The difference is that the proposed model is two-dimensional and considers the variability of the current density along the channel.

Materials and Methods. The desalting channel of the electrodialysis apparatus (EDA) formed by the anion-exchange (AEM) and cation-exchange membranes (CEM), is taken to mean a membrane system. A binary electrolyte solution is pumped through it at V_0 average rate.

In Fig. 1, x is a coordinate normal to the membrane surface varying from 0 (border with AEM) to h (border with CEM); y is a tangential coordinate to the surface of the membrane varying from 0 (channel entrance) to l (channel exit).

Information technology, computer science, and management
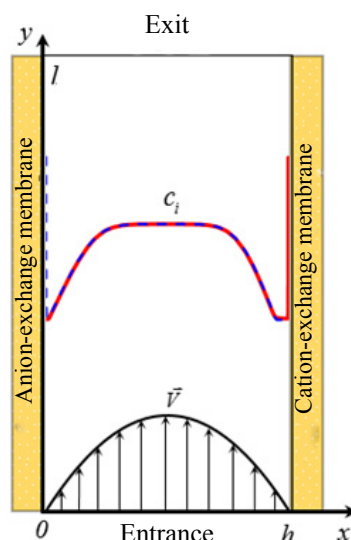
Fig. 1. Scheme of EDA desalination channel. Concentration profiles of C_1 cations (solid line) and C_2 anions (dot line), $\vec{V}$ forced flow rate are shown.

(*System of equations.* Consider a two-dimensional stationary case of the system of equations describing the transfer of a binary electrolyte with no chemical reactions [24]:

$$\vec{j}_i = -\frac{F}{RT} z_i D_i C_i \nabla\phi - D_i \nabla C_i + C_i \vec{V}, \ i = 1, 2, \tag{1}$$

$$-\operatorname{div} \vec{j}_i = 0, \quad i = 1, 2, \tag{2}$$

$$\varepsilon_0 \varepsilon_r \Delta\phi = -F(z_1 C_1 + z_2 C_2), \tag{3}$$

$$\vec{I} = F(z_1 \vec{j}_1 + z_2 \vec{j}_2). \tag{4}$$

Here, $\vec{j}_i$, D_i, z_i and C_i are, respectively, flux, diffusion coefficient, charge number, and molar concentration of the i-th ion; ϕ is electric potential; $\vec{V}$ is flow rate of the electrolyte solution; ε_0 is electric constant; ε_r is relative dielectric constant of the electrolyte solution (assumed to be constant); $\vec{I}$ is current density; F is Faraday constant; R is gas constant; T is absolute temperature; $\vec{j}_1, \vec{j}_2, \vec{I}, \phi, C_1, C_2$ are unknown functions of x and y coordinates.

The Nernst – Planck equations (1) describe the ion flux due to electromigration, diffusion, and convection; (2) is the material balance equation in the stationary case; (3) is Poisson's equation for the electric field potential; (4) is current density in the electrolyte solution. We assume that the velocity distribution in the channel corresponds to the Poiseuille flow [24]:

$$V_x = 0, \quad V_y = 6V_0 \frac{x}{h}\left(1 - \frac{x}{h}\right). \tag{5}$$

To determine the unknown functions listed above, it is necessary to set boundary conditions for the system (1) - (3). Let us consider two electrical modes: potentiostatic, when the potential jump at the system boundaries is set constant, and galvanostatic, when the density of the current flowing through the interface is constant.

Boundary conditions for modeling potentiostatic mode. We assume that the surfaces of ion-exchange membranes are equipotential. The system (1) - (4) includes the potential of the electric field only in the form of derivatives with respect to the spatial coordinate. In this case, only $\tilde{\Delta}\phi = \phi(h, y) - \phi(0, y)$ potential jump is significant, where $\tilde{\Delta}\phi$ is a known function, so we set, for example:

$$\phi(0, y) = 0. \tag{6}$$

Then

$$\tilde{\Delta}\phi = const. \tag{7}$$

The conditions (6) and (7) determine the potentiostatic mode. Other boundary conditions are given below.

At the "AEM - solution" interface ($x = 0$), the concentration of coions (cations) is determined from the condition of continuity of their flow at the "membrane – solution" boundary considering the selective AEM properties [16]:.

$$\left(\frac{\partial C_1}{\partial x} + \frac{F}{RT} z_1 C_1 \frac{\partial\phi}{\partial x}\right)(0, y) = \frac{(1 - T_2) I_x(0, y)}{z_1 F D_1}, \tag{8}$$

where T_i ($i = 1, 2$) are effective numbers of transfer of counterions in the membrane (CEM and AEM, respectively); T_i are numbers close to 1, and also for $T_i = 1$ ideally selective membrane, and the condition (8) turns into the condition of membrane impermeability for coions.

The concentration of counterions (anions) depends on the exchange capacity of the CEM, which can be specified as:

$$C_2(0, y) = C_{2m} = N_a C_0. \tag{9}$$

Here, N_a constant shows how many times this concentration differs from the concentration in the volume of the solution [25].

At the "solution - CEM" ($x = h$) interface for ion concentrations, the conditions similar to those at the "AOM - solution" ($x = 0$) border, are accepted:

$$C_1(h, y) = C_{1m} = N_c C_0, \tag{10}$$

$$\left(\frac{\partial C_2}{\partial x} + \frac{F}{RT} z_2 C_2 \frac{\partial \phi}{\partial x} \right)(h, y) = \frac{(1 - T_1) I_x(h, y)}{z_2 F D_2}. \tag{11}$$

At the channel entrance ($y = 0$) a uniform distribution of ion concentrations is assumed:

$$C_i(x, 0) = C_0, \quad i = 1, 2. \tag{12}$$

The condition for the potential of the electric field is obtained from the equations (1) and (4) considering the absence of current flow through I_x input $(x, 0, t) = 0$:

$$\frac{\partial \phi(x, 0)}{\partial y} = -\frac{RT}{F(z_1^2 D_1 + z_2^2 D_2)C_0} \left(z_1 D_1 \frac{\partial C_1(x, 0)}{\partial y} + z_2 D_2 \frac{\partial C_2(x, 0)}{\partial y} \right). \tag{13}$$

At the channel exit ($y = l$), ions are freely carried by the solution flow:

$$(\vec{n}, \vec{j}_i) = (\vec{n}, -\frac{F}{RT} z_i D_i C_i \nabla \phi - D_i \nabla C_i + C_i \vec{V}) = C_i V_y, \ i = 1, 2. \tag{14}$$

The system (14) also means that the sum of the diffusion and migration tangential components of the anions and cations flow is equal to 0:

$$\left(-\frac{\partial C_i}{\partial y} - \frac{F}{RT} z_i C_i \frac{\partial \phi}{\partial y} \right)(x, l) = 0, i = 1, 2. \tag{15}$$

A "soft" condition is accepted for the potential, meaning that there are no sharp changes in the potential at the channel exit:

$$\frac{\partial \phi}{\partial y}(x, l) = 0. \tag{16}$$

The boundary problem, which includes equations (1) - (4) and boundary conditions (6) - (16), simulates the potentiostatic mode, and its control key condition is (7).

Boundary conditions for simulating the galvanostatic mode. Under the simulation of the galvanostatic mode, the condition (6) remains, and (7) should be replaced by the condition related to the specified value of i_{av} average current density at the "solution – CEM" interface ($x = h$).

To derive such a boundary condition, we substitute the relations (1) into (4) and express the gradient of the electric field potential:

$$\nabla \phi = -\frac{RT}{F^2(z_1^2 D_1 C_1 + z_2^2 D_2 C_2)}(\vec{I} + F(z_1 D_1 \nabla C_1 + z_2 D_2 \nabla C_2) - F(z_1 C_1 + z_2 C_2)\vec{V}). \tag{17}$$

Assuming $x = h$ in (17), we obtain the relation that connects the gradient of the electric potential with the given value of the current density at the boundary, that is, the boundary condition at the "solution – CEM" interface:

$$\frac{\partial \phi}{\partial x}(h, y) = -\frac{RT}{F^2} \left(\frac{I_x + F z_1 D_1 \frac{\partial C_1}{\partial x} + F z_2 D_2 \frac{\partial C_2}{\partial x}}{z_1^2 D_1 C_1 + z_2^2 D_2 C_2} \right)(h, y). \tag{18}$$

In this case, I_x current density must satisfy the condition:

$$\frac{1}{l} \int_0^l I_x(h, y) dy = i_{av}. \tag{19}$$

Vestnik of Don State Technical University. 2018. Vol. 18, no. 4, pp. 426–437. ISSN 1992-5980 eISSN 1992-6006

Вестник Донского государственного технического университета. 2018. Т. 18, № 4. С. 426–437. ISSN 1992-5980 eISSN 1992-6006

The mathematical model of the galvanostatic mode consists of the system of equations (1) - (4). The boundary conditions (18) and (19) replace the condition (7). The other boundary conditions coincide with those for the potentiostatic mode.

The potential jump in the galvanostatic mode is a calculated value.

Transformation of the boundary conditions for simulating the galvanostatic mode. The condition (19) is inconvenient for a numerical solution, since it contains an integral. One of this condition conversion options is given below.

In the stationary case, the current density is a solenoidal vector. Indeed, if we multiply (2) by z_i and sum up, then $\mathrm{div}\vec{I} = 0$. Consequently, there is such η function that

$$\frac{\partial \eta}{\partial x} = I_y, \qquad \frac{\partial \eta}{\partial y} = -I_x . \tag{20}$$

Using η function, the conditions (18) and (19) are rewritten as follows:

$$\frac{\partial \varphi}{\partial x}(h,y) = -\frac{RT}{F^2}\left(\frac{-\dfrac{\partial \eta}{\partial y} + Fz_1 D_1 \dfrac{\partial C_1}{\partial x} + Fz_2 D_2 \dfrac{\partial C_2}{\partial x}}{z_1^2 D_1 C_1 + z_2^2 D_2 C_2}\right)(h,y), \tag{21}$$

$$\frac{1}{l}\int_0^l I_x(h,y)\,dy = -\frac{1}{l}\int_0^l \frac{\partial \eta}{\partial y}(h,y)\,dy = -\frac{1}{l}(\eta(h,l) - \eta(h,0)) = i_{av} . \tag{22}$$

The equation (22) can be rewritten as:

$$\eta(h,l) - \eta(h,0) = -i_{av} l . \tag{23}$$

To close the expression system, it is necessary to obtain an equation for η function. To this end, as in [15, 16], we inject a linear differential operator, which is a vortex function (rotor) in the two-dimensional case, for $\vec{W}$ arbitrary two-dimensional vector:

$$r(\vec{W}) = \left(\frac{\partial W_y}{\partial x} - \frac{\partial W_x}{\partial y}\right). \tag{24}$$

It is easy to check that:

1) $r(\nabla u) = 0$ for any u smooth function;

2) $r(u\vec{W}) = (\nabla u, \vec{W})_1 + u\,r(\vec{W})$ for any u smooth function and any $\vec{W}$ smooth vector.

Here, $(\nabla u, \vec{W})_1 = \dfrac{\partial u}{\partial x}W_y - \dfrac{\partial u}{\partial y}W_x$ is skew-symmetric scalar product of ∇u and $\vec{W}$ vectors, moreover, $(\vec{a},\vec{a})_1 = 0$ is for any $\vec{a}$ vector.

Applying (24) to the equation for current density (4), we obtain:

$$r(\vec{I}) = Fz_1 r(\vec{j}_1) + Fz_2 r(\vec{j}_2). \tag{25}$$

Using the formula of flows (1), we obtain the ratio:

$$r(\vec{j}_i) = -\frac{F}{RT}z_i D_i r(C_i \nabla \varphi) - D_i r(\nabla C_i) + r(C_i \vec{V}), \qquad i = 1,2 . \tag{26}$$

Hence, considering the properties of r operator:

$$r(\vec{j}_i) = -\frac{F}{RT}z_i D_i \left(\nabla C_i, \nabla \varphi\right)_1 + \left(\nabla C_i, \vec{V}\right)_1 + C_i r(\vec{V}),\ i = 1,2 . \tag{27}$$

Considering (27) and $r(\vec{I}) = \dfrac{\partial I_y}{\partial x} - \dfrac{\partial I_x}{\partial y} = \Delta \eta$, the equation (25) can be written as:

$$\begin{aligned}
\Delta \eta = &-\frac{F^2}{RT}\cdot\left(\left(z_1^2 D_1 \frac{\partial c_1}{\partial x} + z_2^2 D_2 \frac{\partial c_2}{\partial x}\right)\frac{\partial \varphi}{\partial y} - \left(z_1^2 D_1 \frac{\partial c_1}{\partial y} + z_2^2 D_2 \frac{\partial c_2}{\partial y}\right)\frac{\partial \varphi}{\partial x}\right) + \\
&+F\left(z_1 \frac{\partial c_1}{\partial x} + z_2 \frac{\partial c_2}{\partial x}\right)V_y - F\left(z_1 \frac{\partial c_1}{\partial y} + z_2 \frac{\partial c_2}{\partial y}\right)V_x + F\left(z_1 c_1 + z_2 c_2\right)\left(\frac{\partial V_y}{\partial x} - \frac{\partial V_x}{\partial y}\right).
\end{aligned} \tag{28}$$

It follows from (28) and (20) that η function is determined up to a constant, therefore we can assume:

$$\eta(h,0) = 0 . \tag{29}$$

Then we obtain from (23)

Vestnik of Don State Technical University. 2018. Vol. 18, no. 4, pp. 426–437.   ISSN 1992-5980 eISSN 1992-6006

Вестник Донского государственного технического университета. 2018. Т. 18, № 4. С. 426–437.   ISSN 1992-5980 eISSN 1992-6006

$$\eta(h,l) = -i_{av}l \, .\tag{30}$$

The conditions (29) and (30) are boundary for η function.

Mathematical model for the galvanostatic mode in a dimensionless form. For a numerical study of boundary value problems, it is convenient to go to a dimensionless form. So we can simplify the equations and find out the actual number and set of parameters that determine the system behavior. Dimensionless variables describe a class of similar processes characterized by the same value of dimensionless numbers.

Characteristic values describing the problem. When simulating mass transfer processes in the EDA desalination chamber, a number of characteristic values are taken:

- for spatial coordinates – h intermembrane distance;

- for ion concentrations – C_0 volume concentration of the electrolyte;

- for speed – V_0 average speed of the forced flow;

- for diffusion coefficients – $D = D_1 D_2 (z_1 - z_2)/(D_1 z_1 - D_2 z_2)$ diffusion coefficient of the electrolyte;

- for electric potential – $\varphi_0 = RT/F$ thermal potential;

- for current density – $i_0 = FDC_0/h$ value (analogue of the limiting density of diffusion current);

- for ion flow – $j_0 = DC_0/h$ diffusion flow.

Transition formulas. We translate the equations into a dimensionless form through the following relations ((u) index denotes the dimensionless variants of quantities):

$$x^{(u)} = \frac{x}{h}, \quad y^{(u)} = \frac{y}{h}, \quad l^{(u)} = \frac{l}{h}, \quad \vec{V}^{(u)} = \frac{\vec{V}}{V_0}, \quad C_i^{(u)} = \frac{C_i}{C_0}, i = 1, 2,$$

$$\phi^{(u)} = \frac{\phi}{\phi_0}, \quad \vec{I}^{(u)} = \frac{1}{i_0}\vec{I}, \eta^{(u)} = \frac{\eta}{FDC_0}, \quad \vec{j}_i^{(u)} = \frac{1}{j_0}\vec{j}_i, i = 1, 2, \quad D_i^{(u)} = \frac{D_i}{D}.\tag{31}$$

The system of equations in a dimensionless form has the form ((u) index is omitted for simplicity):

$$\vec{j}_i = -z_i D_i C_i \nabla\phi - D_i \nabla C_i + PeC_i\vec{V}, \ i = 1, 2 \, ,\tag{32}$$

$$-\mathrm{div}\,\vec{j}_i = 0, \quad i = 1, 2 \, ,\tag{33}$$

$$\varepsilon\Delta\phi = -(z_1 C_1 + z_2 C_2) \, ,\tag{34}$$

$$\Delta\eta = -\left(\left(z_1^2 D_1 \frac{\partial c_1}{\partial x} + z_2^2 D_2 \frac{\partial c_2}{\partial x}\right)\frac{\partial\phi}{\partial y} - \left(z_1^2 D_1 \frac{\partial c_1}{\partial y} + z_2^2 D_2 \frac{\partial c_2}{\partial y}\right)\frac{\partial\phi}{\partial x}\right) +$$

$$+ Pe\left(z_1 \frac{\partial c_1}{\partial x} + z_2 \frac{\partial c_2}{\partial x}\right)V_y - Pe\left(z_1 \frac{\partial c_1}{\partial y} + z_2 \frac{\partial c_2}{\partial y}\right)V_x + Pe(z_1 c_1 + z_2 c_2)\left(\frac{\partial V_y}{\partial x} - \frac{\partial V_x}{\partial y}\right),\tag{35}$$

$$\vec{I} = z_1\vec{j}_1 + z_2\vec{j}_2 \, .\tag{36}$$

The system of equations (29) - (35) contains two dimensionless numbers: the Peclet number $Pe = V_0 h/D$ and $\varepsilon = \varepsilon_r \varepsilon_0 RT/(C_0 h^2 F^2)$. The physical meaning of ε parameter is that it is double square of dimensionless Debye length - l_D: $\varepsilon = 2(l_D/h)^2$ [5].

Estimation of the parameter values shows that under natural conditions for electrodialysis, the Peclet number has $10^2 - 10^6$ order, ε number has $10^{-13} - 10^{-7}$ order, that is, it can be considered a small parameter.

For computational convenience, we transform the system of equations through plugging the flux density (32) in the equations (33) and (36):

$$div\left(-z_i D_i C_i \nabla\varphi - D_i \nabla C_i + PeC_i\vec{V}\right) = 0, \quad i = 1, 2 \, ,\tag{37}$$

$$\vec{I} = \sum_{i=1}^{2} z_i \left(-z_i D_i C_i \nabla\phi - D_i \nabla C_i + PeC_i\vec{V}\right).\tag{38}$$

Thus, the system of equations contains the following unknown x, y functions: C_1, C_2, ϕ, I_x, I_y. The fields of C_1, C_2 concentrations and φ potential are determined by solution to the equations (37), (34), respectively. I_x, I_y current density components are calculated using (38). Speed distribution (5) in dimensionless form:

$$V_x = 0, \quad V_y = 6x(1-x) \, .\tag{39}$$

Information technology, computer science, and management

431

Vestnik of Don State Technical University. 2018. Vol. 18, no. 4, pp. 426–437.   ISSN 1992-5980 eISSN 1992-6006

Вестник Донского государственного технического университета. 2018. Т. 18, № 4. С. 426–437.   ISSN 1992-5980 eISSN 1992-6006

The presence of ε small parameter in the Poisson equation (34) means that the boundary problem is singularly perturbed. This significantly complicates its numerical solution, since such problems are stiff [26]. φ potential of the electric field and C_1, C_2 ion concentrations change very quickly in a narrow boundary layer whose thickness is equal to l_D Debye length [5].

To solve this problem, it is advisable to compact the computational grid in the boundary layer and use special methods for solving stiff problems [26].

Boundary conditions in dimensionless form. At the "AEM – solution" interface ($x = 0$):

$$\left(\frac{\partial C_1}{\partial x} + z_1 C_1 \frac{\partial \phi}{\partial x}\right)(0, y) = \frac{(1 - T_2) I_x(0, y)}{z_1 D_1}, \tag{40}$$

$$C_2(0, y) = N_a, \tag{41}$$

$$\phi(0, y) = 0, \tag{42}$$

$$\frac{\partial \eta}{\partial x}(0, y) = 0. \tag{43}$$

At the "solution – CEM" interface ($x = 1$):

$$C_1(1, y) = N_c, \tag{44}$$

$$\left(\frac{\partial C_2}{\partial x} + z_2 C_2 \frac{\partial \phi}{\partial x}\right)(1, y) = \frac{(1 - T_1) I_x(1, y)}{z_2 D_2}, \tag{45}$$

$$\frac{\partial \phi}{\partial x}(1, y) = -\left(\frac{-\dfrac{\partial \eta}{\partial y} + z_1 D_1 \dfrac{\partial C_1}{\partial x} + z_2 D_2 \dfrac{\partial C_2}{\partial x}}{z_1^2 D_1 C_1 + z_2^2 D_2 C_2}\right)(1, y), \tag{46}$$

$$\frac{\partial \eta}{\partial x}(1, y) = 0. \tag{47}$$

At the channel entrance ($y = 0$):

$$C_i(x, 0) = 1, \quad i = 1, 2, \tag{48}$$

$$\frac{\partial \phi(x, 0)}{\partial y} = -\frac{1}{z_1^2 D_1 + z_2^2 D_2}\left(z_1 D_1 \frac{\partial C_1}{\partial y} + z_2 D_2 \frac{\partial C_2}{\partial y}\right)(x, 0), \tag{49}$$

$$\eta(x, 0) = 0. \tag{50}$$

At the channel exit ($y = l$):

$$\left(-\frac{\partial C_i}{\partial y} - z_i C_i \frac{\partial \phi}{\partial y}\right)(x, l) = 0, i = 1, 2, \tag{51}$$

$$\frac{\partial \phi}{\partial y}(x, l) = 0, \tag{52}$$

$$\eta(x, l) = -i_{av} l, \ i_{av} = const. \tag{53}$$

After numerical calculation of the system (34), (35), (37) - (53), $\tilde{\Delta}\varphi$ potential jump in the desalination channel is determined by the formula:

$$\tilde{\Delta}\varphi = \frac{1}{l}\int_0^l \varphi(1, y)\, dy. \tag{54}$$

The numerical solution is found by the finite element method using the Comsol Multiphysics package on an uneven computational grid (the density of grid elements is increased at the "solution – membrane" boundaries) [27].

Research Results. The calculations are performed for $\varepsilon = 1{,}9 \cdot 10^{-9}$, $Pe = 2355$, which corresponds to the following values of the system parameters:

- input concentration of the electrolyte solution of NaCl: $C_0 = 0.1$ mol/m^3;
- temperature: $T = 298$ K;
- diffusion coefficients of cations and anions, respectively: $D_1 = 1.33 \cdot 10^{-9}$ m^2/s, $D_2 = 2.05 \cdot 10^{-9}$ m^2/s;
- numbers of counterions transfer in the membranes: $T_1 = 0.972$, $T_2 = 1$;
- ion charge numbers: $z_1 = 1$, $z_2 = -1$;
- ratio of the counterions concentration at the boundary with the membranes to its value at the channel entrance: $N_c = N_a = 1$;

Vestnik of Don State Technical University. 2018. Vol. 18, no. 4, pp. 426–437.   ISSN 1992-5980 eISSN 1992-6006

Вестник Донского государственного технического университета. 2018. Т. 18, № 4. С. 426–437.   ISSN 1992-5980 eISSN 1992-6006

- channel width: $h = 10^{-3}$ m;
- channel length: $l = 2 \cdot 10^{-3}$ m;
- rate of the solution pumping: $V_0 = 3,8 \cdot 10^{-3}$ m/s.

Fig. 2 shows the fields of C_1 и C_2 concentrations, φ potential and η functions calculated at $i_{av} = 1,5 i_{lim}$ current density, where i_{lim} is the limiting current density determined by the Leveque formula (in dimensionless form) [28]:

$$i_{\lim} = \frac{1}{T_1 - t_1}\left(1,47\left(\frac{h^2 V_0}{lD}\right)^{1/3} - 0,2\right). \tag{55}$$

Here, $t_1 = 0.395$ is kation transport number in the solution [9].
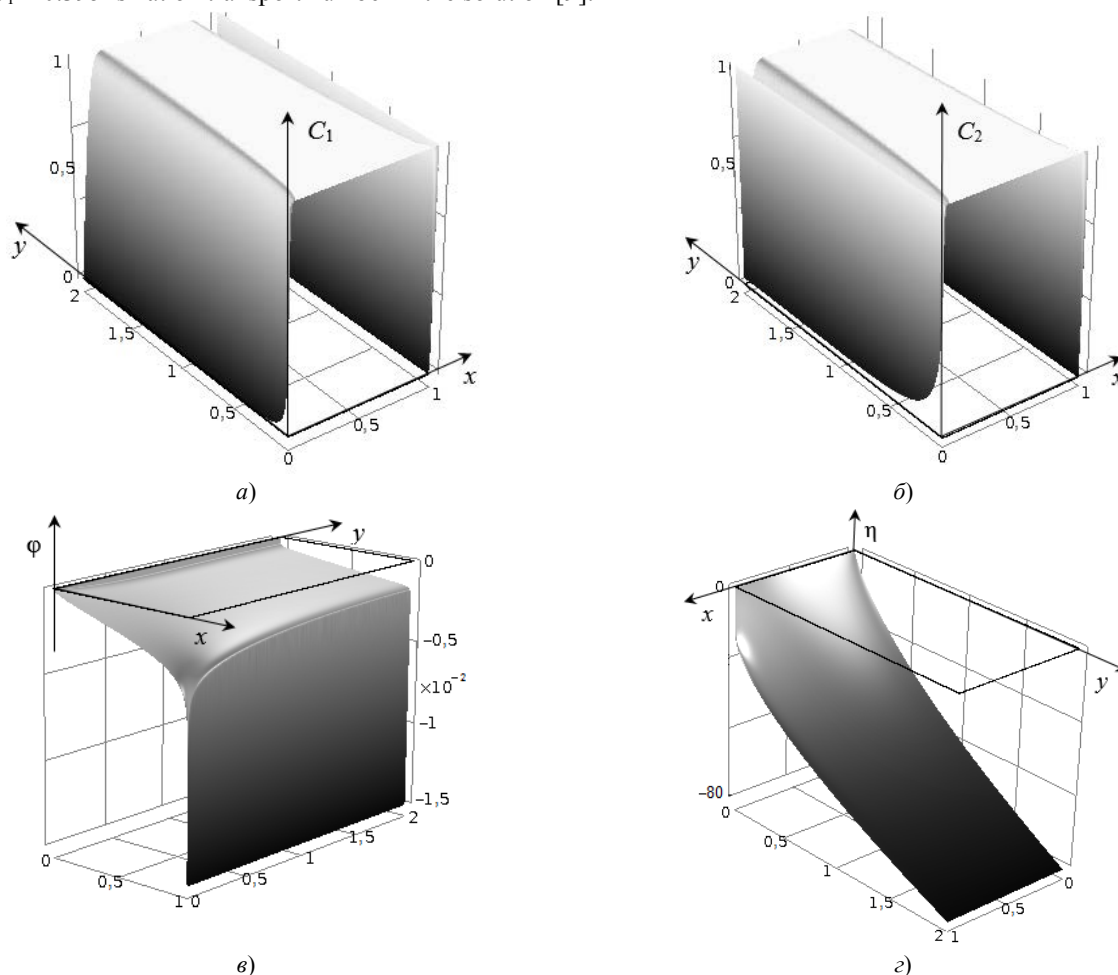
Fig. 2. Concentration fields of cations C_1 (*a*) and anions C_2 (*b*), φ potential (*c*) and η function (*d*). Model calculation for galvanostatic mode at $i_{av} = 1.5\, i_{lim}$ current density.

The forced flow acts in the channel, therefore in the areas near the membranes, the depletion of the ion concentration increases with distance from the channel entrance (along the direction tangential to the membrane surfaces). Accordingly, the thickness of the expanded space-charge region increases along the channel (Fig. 3).

Information technology, computer science, and management

433
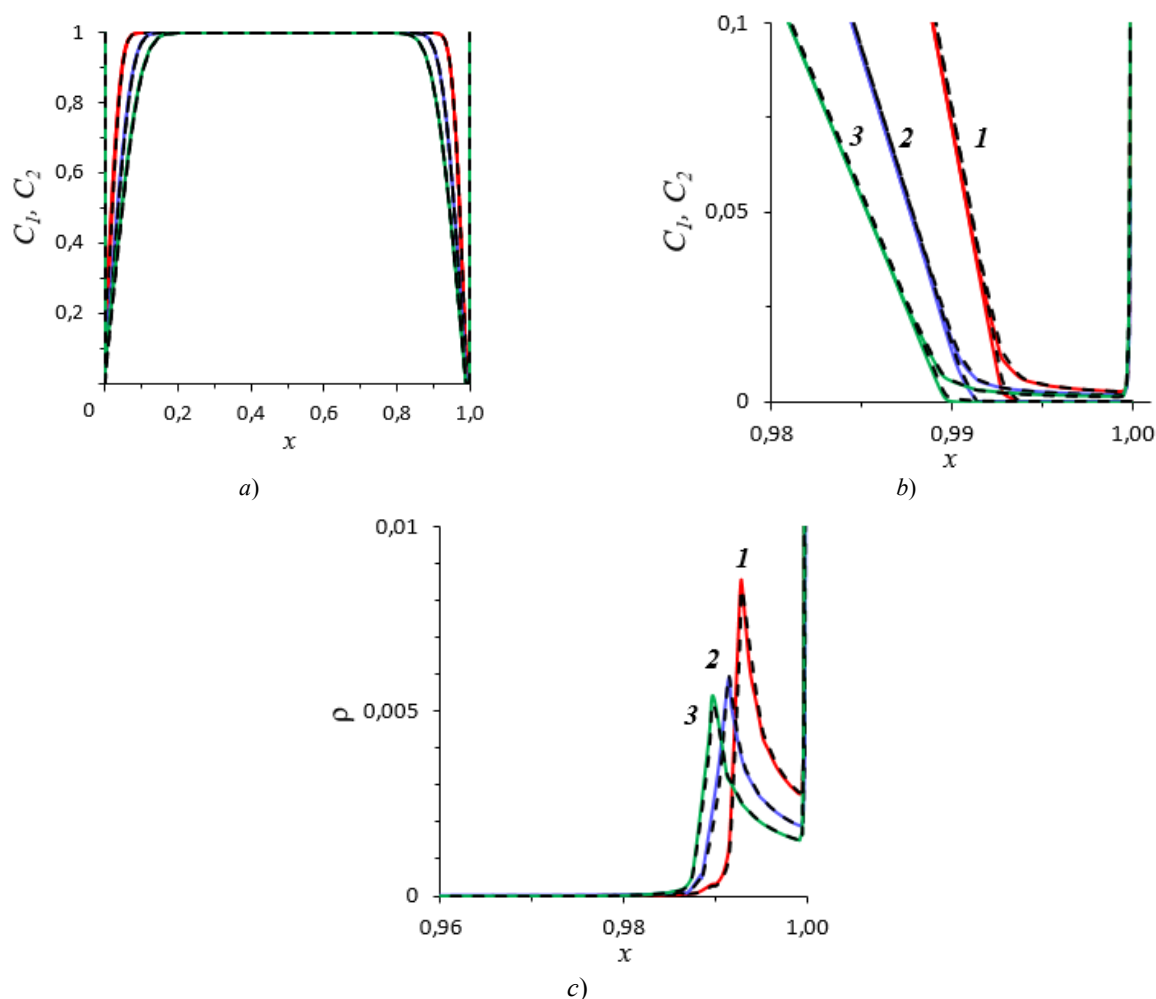
Fig. 3. Results of numerical calculation based on the model for galvanostatic (solid lines) and potentiostatic (dot lines) modes at $i_{av} = 1,5i_{lim}$ current density in cross sections $y = 0,1l$ (1), $y = 0,4l$ (2), $y = 0,9l$ (3): C_1 and C_2 concentration profiles (*a*); enlarged fragment of fig. 3, a (*b*); $\rho = z_1C_1 + z_2C_2$ space charge density (*c*)

The volt-ampere characteristic (VAC, curve 1 in Fig. 4) is calculated on the basis of the galvanostatic model. In this case, the specified current density changed: $i_{av} = 0; 0,005i_{lim}; \ldots; 1,5i_{lim}$.

Fig. 4. VACs calculated on the models for galvanostatic (1) and potentiostatic (2) modes; i_{lim} limiting current density (3) determined by formula (55)

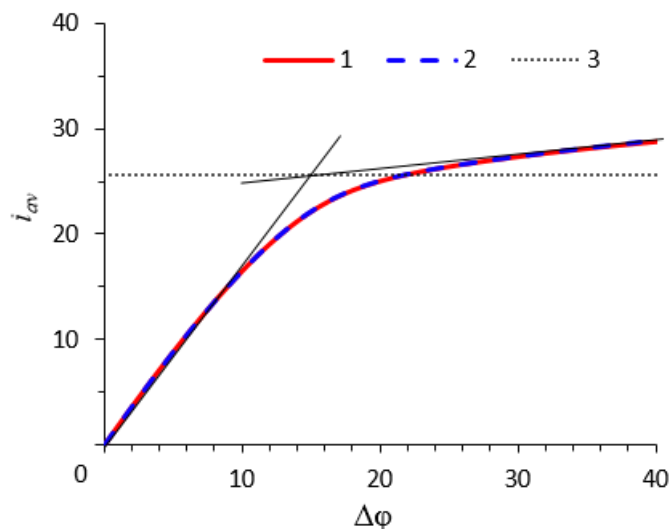The limiting current density is determined by the point of intersection of the tangents to the VAC in the initial part and on the inclined plateau [5]. Here it coincides with i_{lim} value estimated using the approximate Leveque formula

(55). Besides, the VAC was calculated on the basis of the potentiostatic model under a change in the potential jump $\Delta\varphi$ = 0; 0.4; ...; 40 (curve 2 in Fig. 4). As Fig. 4 shows, VAC 1 and 2 are congruent. Thus, there is a unique correspondence to each potential jump of a certain current density, and vice versa.

Fig. 3 and 4 demonstrate a fairly good agreement of various physicochemical transport characteristics calculated on the models for galvanostatic and potentiostatic modes. This proves the adequacy of the model of the transport in galvanostatic mode built by the authors.

The computational costs of the proposed model were estimated as follows. The time spent on solving boundary value problems for the galvanostatic and potentiostatic modes was recorded. Herewith, the specified accuracy values of the calculations and the system parameters were the same, and $i_{av} = 1,5\, i_{lim}$. Then time indicators were compared. Thus, it has been found that the calculation on the galvanostatic model requires 1.6 times more time. This is due to the fact that:

- galvanostatic model contains an additional equation for determining the current density distribution;
- for the potential at $x = 1$ boundary, the condition of the second kind (46) is established.

Complex potential of the electro-membrane system for the galvanostatic mode. In [25], a generalization of the impedance of an electrochemical system using η function introduced under the electroneutrality conditions was proposed. A similar generalization is acceptable in this case. Note that when using electrochemical impedance, an object is considered only as a "black box", and its intrinsic properties are determined indirectly. The results obtained above enable to introduce the concept of a complex potential of the electro-membrane system: $P = \phi + i \cdot \eta$. Complex potential is a coordinate function of any point inside the object, therefore, unlike the electrochemical impedance, it allows us to explore the intrinsic properties of the object.

Discussion and Conclusions. A new technique of mathematical simulation of the stationary process of mass transfer in the galvanostatic mode for membrane systems is described. In this case, the two-dimensional case is considered with the use of a special boundary condition that enables to specify current density in the system. The equations for the current electric function are presented. The numerical solution results for potentiostatic and galvanostatic models are in good agreement. This shows the adequacy of the proposed transport model in the galvanostatic mode.

The developed model makes it possible to interpret the experimental studies results of the ion transfer in membrane systems if this process proceeds in the galvanostatic mode. Some electrokinetic processes are associated with the appearance of a dilated space-charge region under over-limiting currents. The description of the formation of this region allows us to find out how the processes dependent on it affect the ion transfer in the galvanostatic mode.

References

1. Shannon, M.A., Bohn, P.W., Elimelech, M., Georgiadis, J.G., Mariñas, B.J., Mayes A.M. Science and technology for water purification in the coming decades. Nature, 2008, vol. 452 (7185), pp. 301–10. DOI: 10.1038/nature06599.

2. Kim, S.J., Ko, S.-H., Kang, K.H., Han, J. Direct seawater desalination by ion concentration polarization. Nature Nanotechnology, 2010, vol. 5, pp. 297–301. DOI: 10.1038/nnano.2010.34.

3. Kim, S.J., Song, Y.-A., Han, J. Nanofluidic concentration devices for biomolecules utilizing ion concentration polarization: theory, fabrication, and applications. Chem. Soc. Rev., 2010, vol. 39(3), pp. 912–922. DOI: 10.1039/b822556g.

4. Elimelech, M., Phillip, W.A. The Future of Seawater Desalination: Energy, Technology, and the Environment. Science, 2011, vol. 333, pp. 712–717. DOI: 10.1126/science.1200488.

5. Nikonenko, V.V., Pismenskaya, N.D., Belova, E.I., Sistat, P., Huguet, P., Pourcelly, G., Larchet, C. Intensive current transfer in membrane systems: Modelling mechanisms and application in electrodialysis. Adv. Colloid Interface Sci., 2010, vol. 160, pp. 101–123. DOI: 10.1016/j.cis.2010.08.001.

6. Nikonenko, V.V., Kovalenko, A.V., Urtenov, M.K., Pismenskaya, N.D., Han, J., Sistat, Ph., Pourcelly G. Desalination at overlimiting currents: State-of-the-art and perspectives. Desalination, 2014, vol. 342. pp. 85–106. DOI: 10.1016/j.desal.2014.01.008.

7. Nikonenko, V.V., Mareev, S.A., Pismenskaya, N.D., Uzdenova, A.M., Urtenov, M.Kh., Pourcelly, G. Effect of electroconvection and its use in intensifying the mass transfer in electrodialysis (Review). Russian Journal of Electrochemistry, 2017, vol. 53(10), pp. 1122–1144. DOI: 10.1134/S1023193517090099.

8. Belova, E.I., Lopatkova, G.Yu., Pismenskaya, N.D., Nikonenko, V.V., Larchet, C., Pourcelly G. Effect of Anion-exchange Membrane Surface Properties on Mechanisms of Overlimiting Mass Transfer. J. Phys. Chem. B, 2006, vol. 110, pp. 13458–13469. DOI: 10.1021/jp062433f.

Information technology, computer science, and management

9. Gil, V.V, Andreeva, M.A., Pismenskaya, N.D., Nikonenko, V.V., Larchet, C., Dammak L. Effect of counterion hydration numbers on the development of Electroconvection at the surface of heterogeneous cation-exchange membrane modified with an MF-4SK film. Petroleum Chemistry, 2016, vol. 56(5), pp. 440–449. DOI: 10.1134/S0965544116050066.

10. Korzhova, E., Pismenskaya, N., Lopatin, D., Baranov, O., Dammak, L., Nikonenko V. Effect of surface hydrophobization on chronopotentiometric behavior of an AMX anion-exchange membrane at overlimiting currents. J. Membr. Sci., 2016, vol. 500, pp. 161–170. DOI: 10.1016/j.memsci.2015.11.018.

11. Lavrent'ev, A.V., Pismenskiy, A.V., Urtenov, M.K. Matematicheskoe modelirovanie perenosa v ehlektromembrannyh sistemah s uchetom konvektivnyh techenij. [Mathematical modeling of transport in electromembrane systems taking into account convective currents.] Krasnodar: KubSTU, 2006, 147 p. (in Russian).

12. Pismensky, A.V., Urtenov, M.K., Nikonenko, V.V., Sistat, Ph., Pismenskaya, N.D., Kovalenko, A.V. Model and Experimental Studies of Gravitational Convection in an Electromembrane Cell. Russian Journal of Electrochemistry, 2012, vol. 48 (7), pp. 830–841. DOI: 10.1134/S1023193512070075.

13. Kovalenko, A.V., Kazakovtseva, E.V., Urtenov, M.Kh. 3D modelirovanie perenosa binarnogo ehlektrolita v gal'vanostaticheskom rezhime v usloviyah ehlektronejtral'nosti. [3D modeling of transport binary electrolyte in the galvanostatic mode in the condition of electroneutrality.] Scientific journal of KubSAU, 2015, vol. 110(06), pp. 1–12 (in Russian).

14. Mareev, S.A., Nichka, V.S., Butylskii, D.Yu., Urtenov, M.Kh., Pismenskaya, N.D., Apel, P.Yu., Nikonenko V.V. Chronopotentiometric Response of Electrically Heterogeneous Permselective Surface: 3D Modelling of Transition Time and Experiment. J. Phys. Chem. C, 2016, vol. 120, pp. 13113–13119. DOI: 10.1021/acs.jpcc.6b03629.

15. Mareev, S.A., Butylskiy, D.J., Uskov, A.V., Pismenskaya, N.D., Nikonenko, V.V. Odnomernoe modelirovanie rezul'tatov hronopotenciometrii v sverhpredel'nyh tokovyh rezhimah. [1D simulation of chronopotentiometric data obtained in overlimiting current modes.] Condensed matter and interphases, 2015, vol. 17, №2, pp. 171–180 (in Russian).

16. Mareev, S.A., Butylskii, D.Yu., Pismenskaya, N.D., Nikonenko V.V. Chronopotentiometry of ion-exchange membranes in the overlimiting current range. Transition time for a finite-length diffusion layer: modeling and experiment. J. Membr. Sci., 2016, vol. 500, pp. 171–179. URL: https://doi.org/10.1016/j.memsci.2015.11.026.

17. Kovalenko, A.V., Urtenov, M.Kh., Chubyr, N.O., Khromikh, A.A., Uzdenova A.M., Barsukova V.J. Analiz kraevoj zadachi modeli perenosa binarnogo ehlektrolita v priblizhenii zakona Oma. [The model to transport binary electrolyte in approximation of Ohm's law the analysis of boundary problem.] Scientific journal of KubSAU, 2012, vol. 77(03), pp. 1–14. URL: http://ej.kubagro.ru/2012/03/pdf/57.pdf.

18. Kovalenko, A.V., Urtenov, M.Kh., Chubyr, N.O., Khromikh, A.A., Uzdenova A.M., Barsukova V.J. CHislennoe reshenie kraevoj zadachi modeli perenosa binarnogo ehlektrolita v priblizhenii zakona Oma. [Numerical solution transport model binary electrolyte in approximation of Ohm's law.] Scientific journal of KubSAU, 2012, vol. 77(03), pp. 1–16. URL: http://ej.kubagro.ru/2012/03/pdf/58.pdf.

19. Khromyh, A.A., Kovalenko, A.V., Urtenov, M.Kh. Asimptoticheskoe reshenie kraevoj zadachi modeli ZOM ternarnogo ehlektrolita. [Asymptotic solution of a boundary problem of the model of Ohm's law ternary electrolyte.] Fundamental'nye issledovaniya, 2014, vol. 8 (3), pp. 600–606. URL: https://www.fundamental-research.ru/ru/article/view?id=34601.

20. Kovalenko, A.V. Khtomykh, A.A., Urtenov M.K. Decomposition of the two-dimensional Nernst-Planck-Poisson equations for a ternary electrolyte. Doklady Mathematics, 2014, vol. 90 (2), pp. 635–636. DOI: 10.1134/S1064562414060271.

21. Kovalenko, A.V., Uzdenova, A.M., Urtenov, M.Kh. 2D modelirovanie perenosa ionov soli dlya binarnogo ehlektrolita v gal'vanodinamicheskom rezhime. [2D modeling of the transport of salt ions in the binary electrolyte in galvanic dynamic mode.] Ecological Bulletin of Research Centers of the Black Sea Economic Cooperation (BSEC), 2013, vol. 3, pp. 67–76. URL: http://vestnik.kubsu.ru/article/view/511/789.

22. Manzanares, J.A., Murphy W.D., Mafe S., Reiss H. Numerical Simulation of the Nonequilibrium Diffuse Double Layer in Ion-Exchange Membranes. J. Phys. Chem., 1993, vol. 97, pp. 8524–8530. DOI: 10.1021/j100134a023.

23. Moya, A.A. Electrochemical impedance of ion-exchange systems with weakly charged membranes. Ionics, 2013, vol. 19, pp. 1271—1283. DOI: 10.1007/s11581–013–0850–0.

24. Newman, J.S. Electrochemical systems. N.J.: Prentice Hall, 1973, 464 p.

25. Rubinstein, I., Shtilman L. Voltage against current curves of cation exchange membranes. J. Chem. Soc. Faraday Trans., 1979, vol. 75, pp. 231–246. DOI: 10.1039/F29797500231.

26. Doolan, E.P., Miller, J.J.H., Schilders, W.H.A. Uniform numerical methods for problems with initial and boundary layers. Dublin: Boole Press, 1980, 324 p.

27. Kovalenko, A.V., Uzdenova, A.M., Urtenov, M.H., Nikonenko V.V. Matematicheskoe modelirovanie fiziko-himicheskih processov v srede Comsol Multiphysics 5.2. [Mathematical modeling of physical and chemical processes in Comsol Multiphysics 5.2.] St. Petersburg: Lan, 2017, 228 p. (in Russian).

28. Yaroslavtsev, A.B., ed. Membrany i membrannye tekhnologii. [Membranes and membrane technologies] Moscow: Nauchnyj mir, 2013, 612 p.

29. Kovalenko, AV, Yaroshchuk, A.E., Zholkovskiy, E.K., Urtenov, M. Kh. 2D-modelirovanie perenosa binarnogo elektrolita v elektromembrannykh sistemakh. [2D modeling of the binary electrolyte transfer in electromembrane systems.] Izvestiya Kubanskogo gosudarstvennogo universiteta. Estestvennye nauki, 2013, vol. 2, pp. 52–57 (in Russian).

Autors:

Uzdenova, Aminat M.,
associate professor of the Informatics and Computational
Mathematics Department, Karachay-Circassian State
(29, Lenin St., Karachaevsk, 369202, RF), Cand.Sci.
(Phys.-Math.), associate professor,
ORCID: https://orcid.org/0000-0001-5951-9876
uzd_am@mail.ru

Urtenov, Makhamet A. Kh.,
Head of the Applied Mathematics Department, Kuban
State University (149, Stavropolskaya St., Krasnodar,
350040, RF), Dr.Sci. (Phys.-Math.), professor,
ORCID: https://orcid.org/0000-0002-0252-6247
urtenovmax@mail.ru

Information technology, computer science, and management

ИНФОРМАТИКА, ВЫЧИСЛИТЕЛЬНАЯ ТЕХНИКА И УПРАВЛЕНИЕ
INFORMATION TECHNOLOGY, COMPUTER SCIENCE, AND MANAGEMENT

Estimation of proximity of controls synthesized on basis of maximum principle and ADAR method [*]

V. P. Lapshin[1], I. A. Turkin[2], V. V. Khristoforova[3][**]

[1, 2, 3] Don State Technical University, Rostov-on-Don, Russian Federation

Пример оценки близости управлений, синтезированных на основе принципа максимума и метода АКАР[***]

В. П. Лапшин[1], И. А. Туркин[2], В. В. Христофорова[3][**]

[1, 2, 3] Донской государственный технический университет, г. Ростов-на-Дону, Российская Федерация

Introduction. A special case of synthesizing the same electromechanical control system by the Pontryagin maximum principle and by the synergetic synthesis method is considered. The task was to solve the synthesis problem of the time optimal electromechanical position control system; herewith the travel resistance modulus linearly depended on the output coordinate of the system. This approach to the selection of the synthesis problem was because the synthesis of time optimal systems is one of the most widespread problems, and it is solved by increasing the efficiency of the existing control systems.

Materials and Methods. Synthesis of the time optimal linear control system based on the maximum principle is a widely accepted problem in the modern control theory. However, the procedure of synergistic synthesis does not have such formalization. This being the case, the paper suggests an approach that brings together these two methods, which, in our opinion, will increase the efficiency of the synergistic synthesis method through adding some features of the synthesis methodology for optimal systems.

Research Results. The paper formulates two key concepts. The first one is as follows: the application of the maximum principle for an object of the DC motor class when synthesizing the positioning algorithm under the conditions of linear loading functionally dependent on the engine rotation angle allows the time optimal system to be optimized. The second concept states that synthesis of a control system based on the synergistic approach enables to obtain a system close to optimal (quasioptimal), but after modifying the synergetic synthesis method itself. A hypothesis is formulated on the possible connection between the introduced (when implementing the procedure of state space extension in the

Введение. Рассмотрен частный случай синтеза одной и той же электромеханической системы управления методом максимума Понтрягина и методом синергетического синтеза. В качестве задачи была определена задача синтеза оптимальной по быстродействию электромеханической системы позиционирования, при этом момент сопротивления движению линейно зависел от выходной координаты системы. Этот подход к выбору задачи синтеза был обусловлен тем, что синтез оптимальных по быстродействию систем является одной из самых широко распространенных задач, которая решается при повышении эффективности действующих систем управления.

Материалы и методы. Синтез оптимальной по быстродействию линейной системы управления на основе принципа максимума — широко распространенная задача в современной теории управления. Однако процедура синергетического синтеза такой формализации не имеет. Исходя из этого, в статье предложен подход, сближающий эти два метода, который, по мнению авторов, позволит повысить эффективность метода синергетического синтеза, добавив в него некоторые особенности методологии синтеза оптимальных систем.

Результаты исследования. В работе сформулированы два основных научных положения. Первое - применение принципа максимума для объекта класса двигатель постоянного тока при синтезе алгоритма позиционирования в условиях линейной нагрузки, функционально зависящей от угла поворота двигателя, позволяет оптимизировать систему по быстродействию. Второе - синтез системы управления на основе синергетического подхода позволяет получить систему, близкую к оптимальной (квазиоптимальную), но уже после модификации самого метода синергетического синтеза. Сформулирована гипотеза о возможной связи между вводимыми, при реализации процедуры расширения пространства состояния в методе синергетического синтеза, постоянными времени с

synergetic synthesis method) time constants with the optimal switching time of control defined in the maximum method.

Discussion and Conclusions. The synthesis through the maximum control technique and the ADAR method is performed. In virtue of the comparison of efficiency of these methods, a hypothesis is put forward on the possible compatibility of the studied methods.

определяемым в методе максимума оптимальным временем переключения управления.

Обсуждение и заключения. Выполнен синтез управления методом максимума и методом Аналитического Конструирования Агрегированных Регуляторов АКАР. На основании сравнения эффективности применения методов выдвигается гипотеза о возможной совместимости исследуемых методов.

Introduction. In the 20th century, the engineering requirements, in particular, in space engineering, put forward a range of problems for which a new theory was developed – the theory of optimal control [1]. One of the main techniques for the synthesis of optimal control systems is the maximum principle developed by Soviet mathematician L. S. Pontryagin and his disciples in the fifties-sixties of the 20th century [2]. The application of this principle is based on the formalization of the synthesis problem with the transition to the form of the Mayer problem and the subsequent solution to systems of linear or, in some special cases, nonlinear differential equations [1]. It is worth noting that the need to solve systems of differential equations, and in the nonlinear case this is not always possible, is in many ways a limitation of both the maximum principle itself and the whole concept of synthesis of optimal control systems.

In recent decades, a new approach to the synthesis of control systems has been widely adopted. It relies on the synergetic concept of the analysis and synthesis of systems. The technique used, the author of which is A. A. Kolesnikov, is called the method of analytical design of aggregated regulators (ADAR) [4–5]. The proposed approach is based on the concept of synthesis of nonlinear feedbacks. They provide the asymptotic stability of the control system with respect to the required motion of the attractor in the state space [4]. This method differs from the methods of synthesis of optimal control systems in the absence of both the optimization criterion of the control system and the statement of the synthesized control optimality. From the point of view of the implementation of the synthesis procedure, the ADAR method has an undeniable advantage over the synthesis methods of optimal systems, which is expressed in the absence of restrictions on the nonlinearity of the system of differential equations [4-5].

From a practical standpoint, synthesis of the process or object management should be able to answer the question if there is another control that has the property of superiority over all others. Thus, the modern mass production constantly requires efficiency improvement to ensure market competition. One of the most popular ways to increase this efficiency is to optimize management processes. This approach is applicable both to the systems of automated assembly of equipment [6–7] and to the metal-cutting systems, in particular, to drilling control systems in metal-cutting machines [8–15]. The idea of combining these approaches to synthesis of the control systems has, from the authors' the point of view, an undoubted practical effect. In science terms, it is important to combine the ADAR method advantages, which are expressed in the possibility of considering synthesis of the complex nonlinear process dynamics in mechanical engineering [16–19], with a neat and definite formalization of the synthesis problem formulation and assessment of its achievement in the maximum principle [1–2] .

1. Synthesis of basic mathematical model and formulation of research problem

In the modern economy, the direction of the time optimal system synthesis, which enables to obtain a significant increase in the global system efficiency [7–8], has become a frequent practice. Thus, under solving the problems of automating the assembly processes of various equipment, the task of attaching different types of parts to each other [6–7] often arises. Here, the economic efficiency of the entire production process depends on the speed of this operation. The same situation is observed in metal cutting systems on metal-cutting machines [9–19], in which the faster the machining process is, the lower the costs of the entire production process. Based on the reasoning, under the

Information technology, computer science, and management

assumption that it is necessary to synthesize a time optimal control system, which, considering the similarity of the processes of automated fastening of parts and drilling deep holes, can be illustrated by the following diagram (Fig. 1).
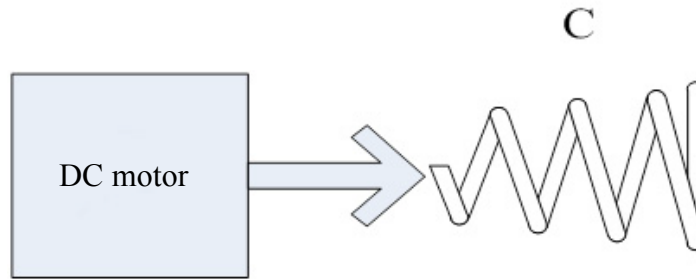

Fig. 1. Illustration diagram

Fig. 1 shows a DC motor performing either an equipment fastening operation or a feed in a drilling unit. In the first case, C is the combined load-deflection characteristic of the material that is compressed under twisting. In the second case, C characterizes a linear increase in the feed resistance under the accumulation of chips in the chip removal channels of the drill.

The electric drive, which ensures the conversion of electrical energy to mechanical energy of motion of the system actuators, is the basis for the support subsystem of the control system in both cases considered. Let us assume that in the present case, such a transformation is carried out by a DC motor with collector control, which is described through the following system of equations [20]:

$$U - c_e\omega = L\frac{di}{dt} + Ri$$
$$c_m i = J\frac{d\omega}{dt} + M_c$$

where U is voltage applied to the engine manifold; i is current consumed by the motor; R, L are parameters of the electrical part of the engine; J is parameter characterizing the inertial properties of the engine rotor, the reduced inertial moment of all rotating masses; ω is engine rotor speed; M_c is external moment of resistance; c_m, c_e are mechanical and electric engine constants. In this case, the moment is presented as a function of the angle of rotation of the engine rotor, that is $M_c = C\alpha$. With this in mind (1), we rewrite as:

$$U - c_e\omega = L\frac{di}{dt} + Ri$$
$$c_m i = J\frac{d\omega}{dt} + C\alpha$$
$$\frac{d\alpha}{dt} = \omega$$

(2)

We express the current value in the second equation, apply the obtained value in the first equation, and get:

$$U\frac{1}{c_e} - \omega = \frac{LJ}{c_e c_m}\frac{d^2\omega}{dt^2} + \frac{RJ}{c_e c_m}\frac{d\omega}{dt} + \frac{LC}{c_e c_m}\omega + \frac{RC}{c_e c_m}\alpha$$
$$\frac{d\alpha}{dt} = \omega$$

(3)

We solve the first equation with respect to the highest derivative and rewrite it with the second one, and then we receive:

$$\frac{d\alpha}{dt} = \omega$$
$$\frac{d^2\omega}{dt^2} = -\frac{R}{L}\frac{d\omega}{dt} - (\frac{c_m c_e}{LJ} + \frac{C}{J})\omega - \frac{RC}{LJ}\alpha + \frac{c_m}{LJ}U$$

(4)

Let us put $\alpha = x_1, \omega = x_2, \frac{d\omega}{dt} = x_3$; as constants, we introduce $\frac{R}{L} = a_{33}, (\frac{c_m c_e}{LJ} + \frac{C}{J}) = a_{32}, \frac{RC}{LJ} = a_{31}, \frac{c_m}{LJ} = b$.

Then the system (4) takes the form:

Vestnik of Don State Technical University. 2018. Vol. 18, no. 4, pp. 438–448.   ISSN 1992-5980 eISSN 1992-6006

Вестник Донского государственного технического университета. 2018. Т. 18, № 4. С. 438–448.   ISSN 1992-5980 eISSN 1992-6006

$$\frac{dx_1}{dt} = x_2$$
$$\frac{dx_2}{dt} = x_3 \qquad . \tag{5}$$
$$\frac{dx_3}{dt} = -a_{31}x_1 - a_{32}x_2 - a_{33}x_3 + bU$$

or in matrix-vector form:

$$\dot{x} = Ax + Bu , \tag{6}$$

where $A = \begin{pmatrix} 0 & 1 & 0 \\ 0 & 0 & 1 \\ -a_{31} & -a_{32} & -a_{33} \end{pmatrix}$, $B = \begin{pmatrix} 0 \\ 0 \\ b \end{pmatrix}$, $x = \begin{pmatrix} x_1 \\ x_2 \\ x_3 \end{pmatrix}$, $u = \begin{pmatrix} 0 \\ 0 \\ U \end{pmatrix}$.

We take the DC motor whose parameters provide the following constant values: a_{31}=4.65, a_{32}=4.6, a_{33}=2, as a drive ensuring the system motion.

A matrix, with this in mind, will take the form: $A = \begin{pmatrix} 0 & 1 & 0 \\ 0 & 0 & 1 \\ -4,65 & -4,6 & -2 \end{pmatrix}$. From knowing A matrix, we find λ

eigenvalues of A matrix: $\lambda_1 = -1.2666 + 0.0000i$, $\lambda_2 = -0.3667 + 1.8806i$, $\lambda_3 = -0.3667 - 1.8806i$.

As is clear from the obtained eigenvalues of the matrix, the control system is asymptotically stable according to Lyapunov [21]. Moreover, we can argue about the oscillatory nature of the processes proceeding in the system, since the eigenvalues contain not only negative real parts, but nonzero imaginary parts.

2. Synthesis of control by Pontryagin's maximum principle

First, we formulate the problem of the optimal control synthesis in the following form:

- using the maximum principle for the object described by the System (5), determine the optimal equation algorithm that ensures the transfer of the object from the initial state $x_1(0)$=50, $x_2(0)$=0, $x_3(0)$=0 to the final state $x_1(T)$=0, $x_2(T)$=0, $x_3(T)$=0 for T minimum time. Herewith, it is necessary to determine transition count, switching torque, and to construct curves of $u(t)$ control and $x_1(t)$, $x_2(t)$, $x_3(t)$ coordinates.

$|u| \le U_{max}$ restriction is imposed on the control action. The system parameters are as follows: $a_{31} = 1, a_{32} = 12, a_{33} = 20, b = 1$, U_{max}=440 V.

Solution: We write the Hamiltonian:

$$H = \sum_{i=1}^{2} \psi_i f_i , \tag{7}$$

where ψ_i and f_i are coordinates of $\vec{\psi}$ and $\vec{f}$ vectors. In addition to the system (5), we construct a system of equations for ψ_i auxiliary variables, where $i = 1,2$, using the following relation:

$$\frac{d\psi_i}{dt} = -\sum_{j=1}^{2} \psi_i \frac{\partial f_i}{\partial x_i}, \quad i = 1,2.$$

Or open :

$$\frac{d\psi_1}{dt} = -\left[\frac{\partial f_1}{\partial x_1} \psi_1 + \frac{\partial f_2}{\partial x_1} \psi_2 + \frac{\partial f_3}{\partial x_1} \psi_3 \right]$$

$$\frac{d\psi_2}{dt} = -\left[\frac{\partial f_1}{\partial x_2} \psi_1 + \frac{\partial f_2}{\partial x_2} \psi_2 + \frac{\partial f_3}{\partial x_2} \psi_3 \right] \tag{8}$$

$$\frac{d\psi_3}{dt} = -\left[\frac{\partial f_1}{\partial x_3} \psi_1 + \frac{\partial f_2}{\partial x_3} \psi_2 + \frac{\partial f_3}{\partial x_3} \psi_3 \right]$$

Considering (5), the equation system (8) takes the form:

$$\begin{cases} \dfrac{d\Psi_1}{dt} = 4,65\Psi_3 \\ \dfrac{d\Psi_2}{dt} = -\Psi_1 + 4,6\Psi_3 \\ \dfrac{d\Psi_3}{dt} = -\Psi_2 + 2\Psi_3 \end{cases} \tag{9}$$

$$\begin{cases} \dfrac{d\Psi_1}{dt} = 4,65\Psi_3 \\[2mm] \dfrac{d\Psi_2}{dt} = -\Psi_1 + 4,6\Psi_3 \\[2mm] \dfrac{d\Psi_3}{dt} = -\Psi_2 + 2\Psi_3 \end{cases} \qquad (9)$$

Eigenvalue matrix for (9) case:

$$A^{\Psi-D} = \begin{pmatrix} 1.2666 & 0 & 0 \\ 0 & 0.3667+1.8806i & 0 \\ 0 & 0 & 0.3667+1.8806i \end{pmatrix}$$

The solution to the system (9) for the diagonalized case of $A^{\psi-D}$ matrix takes the form:

$$\begin{cases} \Psi_1 = C_1 e^{1.2666t} \\ \Psi_2 = C_2 e^{(0.3667+1.8806i)t} \\ \Psi_3 = C_3 e^{(0.3667-1.8806i)t} \end{cases} . \qquad (10)$$

Considering V^ψ matrix, the solution in the initial basis will be:

$$\begin{cases} \Psi_1 = -0.9474C_1 e^{1.666t} + (0.5812-0.3347i)C_2 e^{(0.3667+1.8806i)t} + (0.5812+0.3347i)C_3 e^{(0.3667-1.8806i)t} \\ \Psi_2 = -1.1893C_1 e^{1.2666t} + 0.6883C_2 e^{(0.3667+1.8806i)t} - 0.6883C_3 e^{(0.3667-1.8806i)t} \\ \Psi_3 = -0.2581C_1 e^{1.2666t} + (0.1812+0.2086i)C_2 e^{(0.3667+1.8806i)t} + (0.1812-0.2086i)C_3 e^{(0.3667-1.8806i)t} \end{cases},$$

where C_1, C_2, C_3 are integration constants.

The general expression describing the Hamilton function:

$$H = \Psi_1 f_1 + \Psi_2 f_2 + \Psi_3 f_3 \qquad (11)$$

In the expression (11), an important – from the point of view of the method of synthesis – role is played by the member, which includes the control:

$$H^* = \Psi_3 U = (-C_1 0.2581 e^{1.2666t} + C_2(0.1812+0.2086i) + C_3(0.1812-0.2086i)e^{(0.3667-1.8806i)t})bU .$$

In order for H Hamiltonian calculated by the formula (11) to take the maximum positive value, H^* term must be always positive and the greatest. For this, the optimal control algorithm should be $u(t)=\sigma U_{max}$, where:

$$\sigma = sign(-0.2581C_1 e^{1.2666t} + (0.1812+0.2086i)e^{(0.3667+1.8806i)t} + (0.1812-0.2086i)e^{(0.3667-1.8806i)t}) .$$

$u(t)$ optimal control is a piecewise constant function, taking $\pm U_{max}$ values, and it has no more than two intervals of constancy, since the nonlinear function

$$-0.2581C_1 e^{1.2666t} + (0.1812+0.2086i)e^{(0.3667+1.8806i)t} + (0.1812-0.2086i)e^{(0.3667-1.8806i)t}$$

changes the sign no more than once. In this case, the possible sign change occurs from plus to minus, that is, to fulfill the maximum principle, it is required to first apply U= +U$_{max}$, to the engine, and then U= –U$_{max}$. Let us verify these arguments through constructing Ψ_3 obtained functional dependence in the *Matlab* package (Fig. 2).
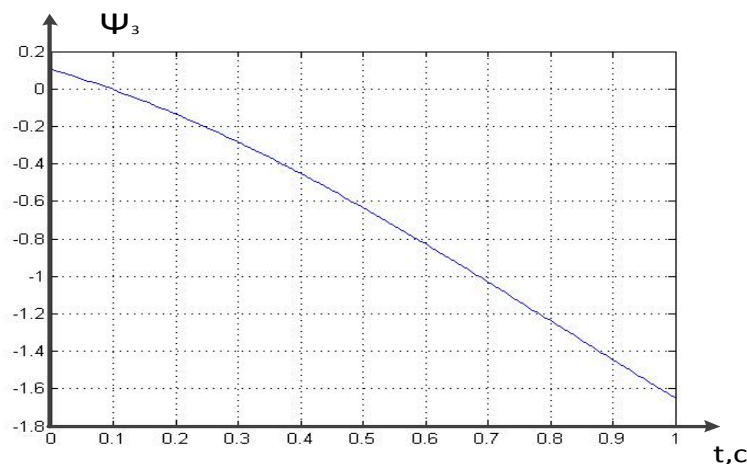

Fig. 2. Graph of Ψ_3 variance

As can be seen from Fig. 2, Ψ_3 does change the sign from (+) to (–) only once. With this in mind, we define an optimal equation algorithm that ensures the transfer of an object from $x_1(0)=0$, $x_2(0)=0$, $x_3(0)=0$ initial state to $x_1(T)=50$, $x_2(T)=0$, $x_3(T)=0$ final state for T minimum time. Here we note that under modern conditions, there is no need to obtain an analytical solution to the original system of equations. Using the available capabilities of modern software packages like *Matlab*, we straightforward and clearly can obtain a numerical solution to the case under consideration.

The numerical simulation results for the calculated time optimal control algorithm are presented in Fig. 3. The model parameters are selected in such a way that it fulfills the boundary condition required by the right-hand border.
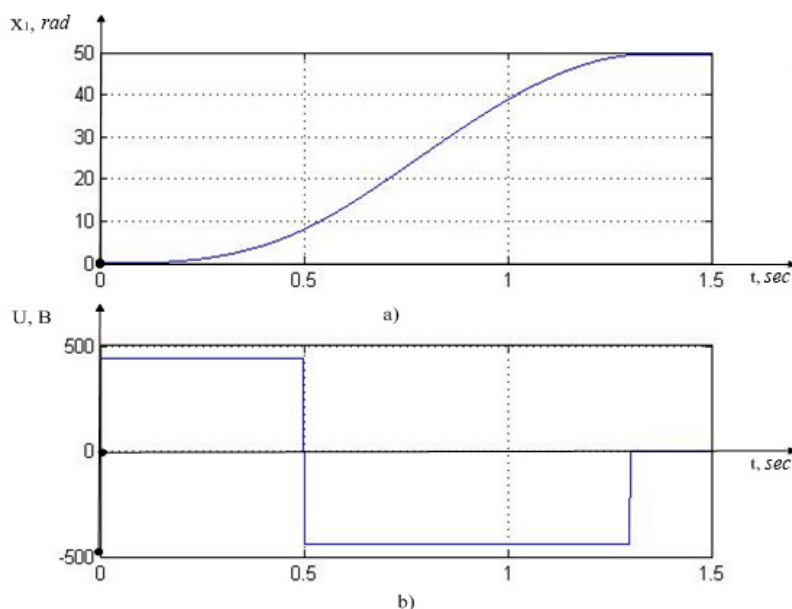

Fig. 3. Graphs of output coordinate (a) and control switching
at $t_1 = 0.5$ (b)

Fig. 3 shows that the control switching time from (+U$_{max}$) to (–U$_{max}$) is selected as $t_1 = 0,5$ seconds, and the total control time is $T = 1.3$ seconds. In this case, the control system comes to the required output level, that is, the right-hand boundary of the boundary conditions is reached.

3.   Synthesis of control system through ADAR method

To synthesize a control system using the ADAR method, it is possible not to make a transition to the abstract case of the state space (see (5)), but it is easy to use the original system (2). However, it needs to be translated to the following form:

$$\frac{dx_1}{dt} = x_2$$
$$\frac{dx_2}{dt} = -a_{21}x_1 + a_{23}x_3 \qquad , \qquad (12)$$
$$\frac{dx_3}{dt} = -a_{32}x_2 - a_{33}x_3 + bU$$

where $\alpha = x_1, \omega = x_2, i = x_3$ are variables; $\frac{c_m}{J} = a_{23}, \frac{C}{J} = a_{21}, \frac{c_e}{L} = a_{32}, \frac{R}{L} = a_{33}, \frac{1}{L} = b$ are introduced as constants. Considering the previously defined values, we receive: $a_{23} = 1.515, a_{21} = 2.325, a_{32} = 1.5, a_{33} = 2, b = 1$ and the system (12) takes the form:

$$\frac{dx_1}{dt} = x_2$$
$$\frac{dx_2}{dt} = -2.325x_1 + 1.515x_3 , \qquad (13)$$
$$\frac{dx_3}{dt} = -1.5x_2 - 2x_3 + U$$

With this in mind, *A* matrix takes the form:

$$A = \begin{pmatrix} 0 & 1 & 0 \\ -2.325 & 0 & 1.515 \\ 0 & -1.5 & -2 \end{pmatrix}.$$

From knowing A matrix, we find λ eigenvalues of A matrix: $\lambda 1 = -1.2674 + 0.0000i$; $\lambda 2 = -0.3663 + 1.8801i$; $\lambda 3 = -0.3663 - 1.8801i$. As is clear from these results, it is referred to the control system case considered in the synthesis through the maximum principle.

The coordinate characterizing the angle of rotor rotation (x_1) is the output coordinate of the system. Therefore, in order to form requirements for the desired system behavior in the state space, we introduce a macrovariable of $\Psi_1 = x_1 - x_{01} \Rightarrow 0$ order, where x_{01} is the specified target value of x_1 coordinate. The velocity value of the angle change must ensure that the angle of rotor rotation tends to the value specified above. To this end, we introduce another macrovariable – $\Psi_2 = x_2 - \phi_2(x_1) \Rightarrow 0$, where $\phi_2(x_1)$ is a certain function describing $x_2 \Rightarrow \phi_2(x_1)$ tendency in the stationary state. Further, we introduce a macrovariable of order in $\Psi_3 = x_3 - \phi_3(x_1, x_2) \Rightarrow 0$ coordinate, where $\phi_3(x_1, x_2)$ is a certain function that describes the relationship between the coordinates in the stationary state of the system and, therefore $x_3 \Rightarrow \phi_3(x_1, x_2)$.

For newly introduced Ψ_1, Ψ_2, Ψ_3 macrovariables, we require the asymptotically stable law of change, that is, execution of the following system of differential equations:

$$\begin{cases} T_1 \dfrac{d\Psi_1}{dt} + \Psi_1 = 0 \\ T_2 \dfrac{d\Psi_2}{dt} + \Psi_2 = 0 \\ T_3 \dfrac{d\Psi_3}{dt} + \Psi_3 = 0 \end{cases}, \tag{14}$$

where T_1, T_2, T_3 are time constants that determine the vanishing rate of the introduced macrovariables, or, in other words, the shrinking rate of an arbitrary path of the system in the state space to the desired attractor.

The system of equations introduced in the expression (14) has expanded the system state space from the 3rd to the 6th, which is one of the main provisions of the ADAR method. Further synthesis of the control system is reduced to a stage-by-stage process of decomposition (compression) of this space to the initial level [1–2]. We start the decomposition process with the substitution of the system (14) to the first equation instead of Ψ_1 macrovariable of its value in the coordinates of the controlled process. As a result, we obtain:

$$T_1 \frac{dx_1}{dt} + (x_1 - x_{01}) = 0, \tag{15}$$

Considering (13), the equation (15) is written as:

$$T_1 x_2 + (x_1 - x_{01}) = 0. \tag{16}$$

Considering the next step of the synthesis algorithm, because of which it was assumed that $x \Rightarrow \phi_2(x_1)$, we find $\phi_2(x_1)$ value as:

$$\phi_2(x_1) = -\frac{(x_1 - x_{01})}{T_1} \tag{17}$$

With this context, Ψ_2 macrovariable is as follows:

$$\Psi_2 = x_2 - \phi_2(x_1) = x_2 + \frac{(x_1 - x_{01})}{T_1} \tag{18}$$

Validity of the expression (17), in terms of the control objectives, is confirmed by the fact that the value in the steady state is as follows: $x_2 \Rightarrow \phi_2(x_1) \Rightarrow 0$. Then, considering (18), the second equation of the system (14) will take the following form:

$$T_2 \frac{dx_2}{dt} - T_2 \frac{d\phi_2(x_1)}{dt} + x_2 - \phi_2(x_1) = 0. \tag{19}$$

Or, considering $\phi_2(x_1)$:

$$T_2 \frac{dx_2}{dt} + \frac{T_2}{T_1} \frac{dx_1}{dt} + x_2 + \frac{(x_1 - x_{01})}{T_1} = 0. \tag{20}$$

Vestnik of Don State Technical University. 2018. Vol. 18, no. 4, pp. 438–448. ISSN 1992-5980 eISSN 1992-6006

Вестник Донского государственного технического университета. 2018. Т. 18, № 4. С. 438–448. ISSN 1992-5980 eISSN 1992-6006

At the next step of the synthesis algorithm, using the same reasoning as before, and the fact that we determine $x_3 \Rightarrow \phi_3(x_1, x_2)$ from (20), considering (13), $\phi_3(x_1, x_2)$ value in coordinates of the controlled process:

$$\phi_3(x_1, x_2) = 1,535x_1 - 0,66\frac{(T_2 + T_1)}{T_1}x_2 - 0,66\frac{(x_1 - x_{01})}{T_2 T_1}0 \,. \tag{21}$$

Having obtained $\phi_3(x_1, x_2)$ value in the coordinates of the controlled process, we can determine the value of Ψ_3 macrovariable in the coordinates of the system state and solve the third equation of the system (14).

$$T_3[\frac{dx_3}{dt} - \frac{d\phi_3(x_1, x_2)}{dt}] + x_3 - \phi_3(x_1, x_2) = 0 \,. \tag{22}$$

After substituting the previously obtained $\phi_3(x_1, x_2)$ values from (21) into (22) and using the system (13) at this step of decomposing the state space of the control system, we define the control value in the coordinates of the controlled process:

$$\begin{aligned} U &= 1,5x_2 + 2x_3 + 1,535x_2 + 1,5x_1 \frac{(T_1 T_3 + T_2 T_3 + T_1 T_2)}{T_1 T_2 T_3} - x_3 \frac{(T_1 T_3 + T_2 T_3 + T_1 T_2)}{T_1 T_2 T_3} - \Leftrightarrow \\ &\Leftrightarrow 0,66x_2 \frac{(T_1 + T_2 + T_3)}{T_1 T_2 T_3} - 0,66\frac{(x_1 - x_{01})}{T_1 T_2 T_3} \end{aligned} \tag{23}$$

The expression (23) determines the asymptotically stable control action on the control system described by the equations (13).

The simulation results of the system of differential equations (13) with the required value of the engine rotor angle: x_{10}=50 rad, and the values of $T_1 = 0.1$, $T_2 = 0.2$, $T_3 = 0.3$ time constants entered are shown in Fig. 4.
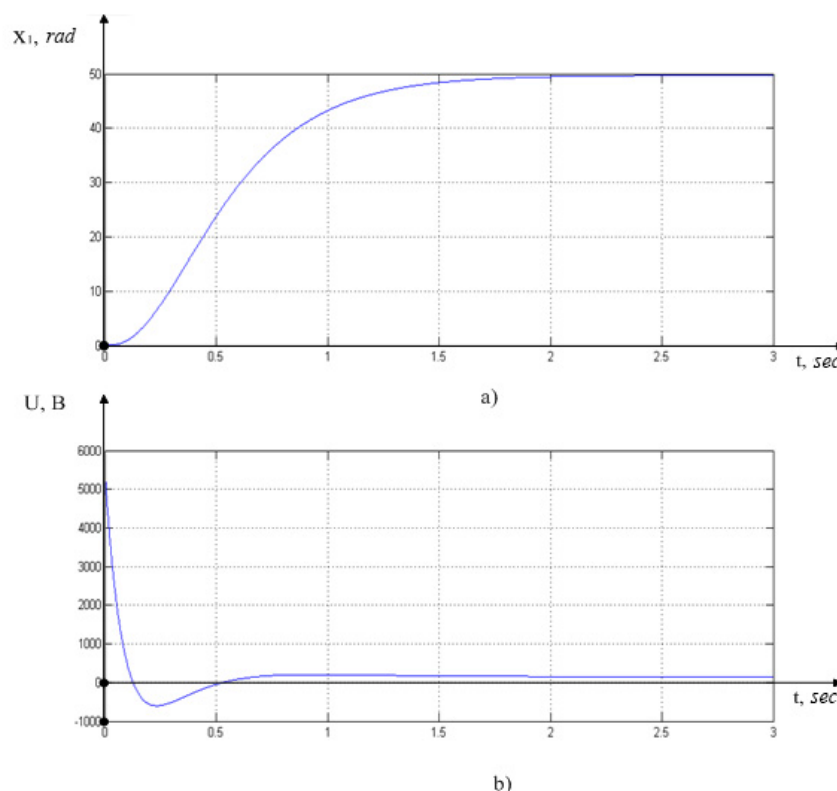

Fig. 4. Simulation results with control at $T_1 = 0.1$, $T_2 = 0.2$, $T_3 = 0.3$: transition process on output coordinate (a); control change schedule (b)

Fig. 4 shows that, in comparison with Fig. 3, the control structure is the same in both cases, that is, the point is that at the beginning, a positive control is applied, and then its sign changes to the opposite one. The settling time increases dramatically to the value close to 2.5 seconds, but with this, the maximum control reaches values greater than 5,000 V. This is unacceptable according to the maximum method. To limit the maximum control value, we introduce a nonlinear link of the "saturation" type with the same threshold as in the case of the maximum into the control loop. The results of the system simulation, with this threshold and with selected values of T_1, T_2, T_3 constants, are presented in Fig. 5.

Information technology, computer science, and management

445

Fig. 5. Simulation results with control at $T_1 = 0.15$, $T_2 = 0.16$, $T_3 = 0.17$:

output coordinate transition (a); control change schedule (b)

Fig. 5 shows that the introduction of a nonlinear constraint on the control of the "saturation" type enables to obtain the desired result from the point of view of the control admissibility. In this case, the control structure determined by the maximum method is really observed, but the control is not time optimal. It should be noted here that such a modification of the ADAR method could also lead to the loss in system stability (Fig. 6).
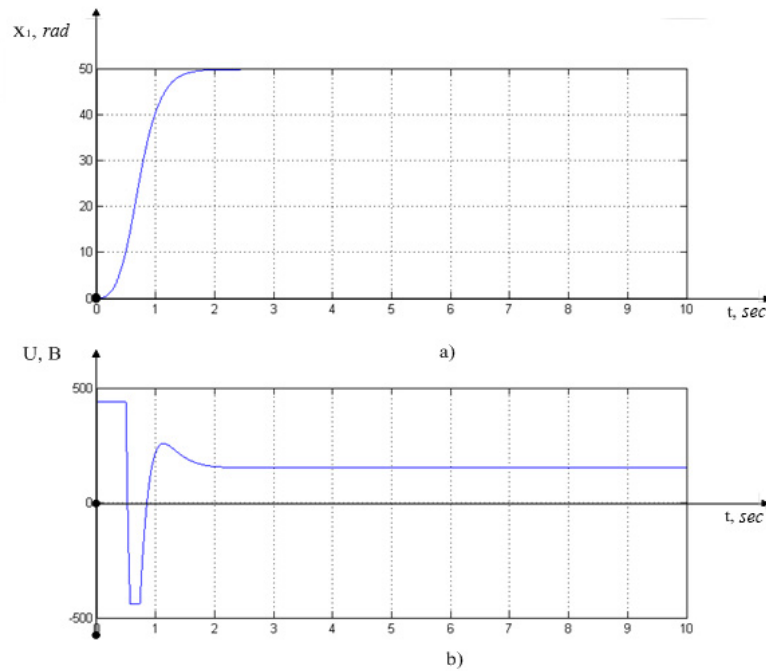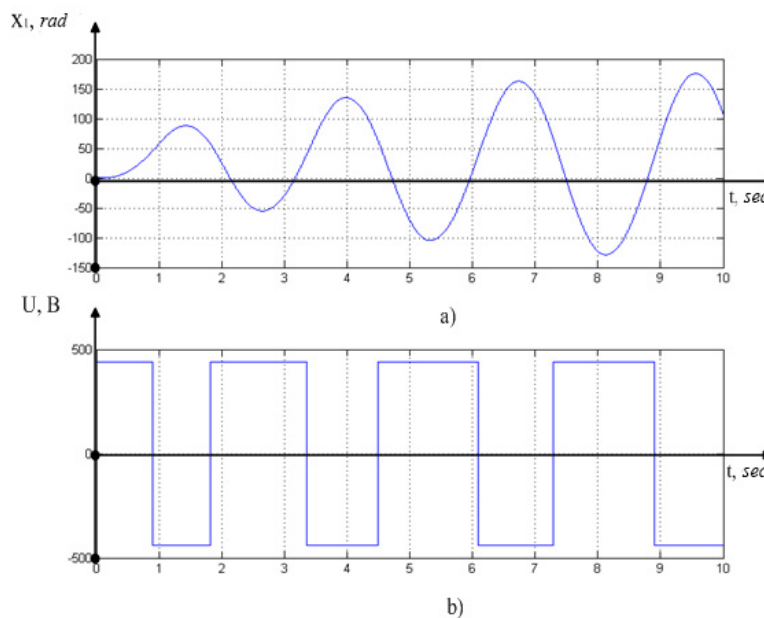

Fig. 6. Simulation results with control at $T_1 = 0.015$, $T_2 = 0.016$, $T_3 = 0.017$:

output coordinate transition (a); control change schedule (b)

However, despite the result presented in Fig. 6, the addition of amplitude constraint of the control signals to the control system obtained by the ADAR method essentially brings it closer to the solutions obtained through implementing the synthesis procedure by the maximum method.

Discussion and Conclusions. Thus, for the basic model of the control system (2), the time optimal control was synthesized by the maximum method. For the same case, in the third part of the paper, with the same system parameters and boundary conditions, the control of the ADAR method was synthesized. Both of these controls look different.

In case of the maximum method, this is a software piecewise-constant control where the optimal time instant of the sign change of the control signal is important. In ADAR case, it is a continuous smooth functional control dependence on the coordinates of the system state. However, their implementation shows the structural similarity expressed in changing the control sign. After the ADAR method modification, the structural similarity has become even more visible. Note that the parametric similarity of the implemented controls can be achieved through selecting the time constants introduced by the ADAR method during the synthesis. This allows the authors to formulate the following hypothesis.

- Selection of the values of T_1, T_2, T_3 time constants introduced by the ADAR method in the synthesis procedure, in case of modification of the obtained control by the method proposed in the article, makes it possible to get time optimality of the synergetic control. The authors failed to obtain a general proof from this intuitive hypothesis. However, this task was not set within the framework of this paper. The numerical experiments with T_1, T_2, T_3 variation helped us to achieve quasioptimality of the control obtained by the ADAR method.

References

1. Pontryagin, L.S., Boltyanskiy, V.G. Matematicheskaya teoriya optimal'nykh protsessov. [Mathematical theory of optimal processes.] Moscow: Nauka, 1976, 392 p. (in Russian).

2. Dykgta, V.A., Derenko, N.V. Chislennye metody resheniya zadach optimal'nogo impul'snogo upravleniya, osnovannye na variatsionnom printsipe maksimuma. [Numerical methods for solving problems of optimal impulse control, based on variational maximum principle.] Izvestia Vuzov. Russian Mathematics, 2001, no. 12, pp. 32–40 (in Russian).

3. Kolesnikov, A.A. Prikladnaya sinergetika: osnovy sistemnogo sinteza. [Applied synergetics: basics of system synthesis.] Taganrog: TTI SFU, 2007, 384 p. (in Russian).

4. Kolesnikov, A.A. Sinergetika i problemy teorii upravleniya. [Synergetics and problems of control theory.] Moscow: Fizmatlit, 2004, 504 p. (in Russian).

5. Zakovorotny, V.L., et al. Sinergeticheskiy sistemnyy sintez upravlyaemoy dinamiki metallorezhushchikh stankov s uchetom evolyutsii svyazey. [Synergetic system synthesis of controlled dynamics of machine tools with coupling evolution.] Rostov-on-Don: DSTU Publ. Centre, 2008, 324 p. (in Russian).

6. Zhitnikov, Yu.Z., Zhitnikova, I.V. Analiz pogreshnostey momentov zatyazhki odnoshpindel'nymi gaykovertami na osnove muft predel'nogo momenta. [Analysis of the possibility of increasing the tightening torque accuracy using single-spindle screwdrivers on the basis of torque-limiting clutches.] Assembling in Mechanical Engineering and Instrument-Making, 2011, no. 8, pp. 12–15 (in Russian).

7. Uzunov, O.V. The screwdriver technology of the model building for simulating of the processes in the mechatronic objects. Solid State Phenomena, 2009, vol. 1. no.1, pp. 468–473.

8. Zakovorotny, V.L., Lapshin, V.P., Gubanova, A.A. Opredelenie optimal'nykh koordinat pereklyucheniya tsiklov obrabotki v evolyutsionnoy dinamicheskoy sisteme rezaniya. [Determination of optimal coordinate switching cycles in the evolutionary dynamic cutting system.] University News. North-Caucasian region. Technical Sciences Series, 2014, no. 4 (179), pp. 59–63 (in Russian).

9. Zakovorotny, V.L., Lapshin, V.P., Turkin, I.A. Upravlenie protsessom sverleniya glubokikh otverstiy spiral'nymi sverlami na osnove sinergeticheskogo podkhoda. [Process control drilling deep holes twist drills based on the synergetic approach.] University News. North-Caucasian region. Technical Sciences Series, 2014, no. 3 (178), pp. 33–41 (in Russian).

10. Lapshin, V.P., Turkin, I.A. Modelirovanie dinamiki formoobrazuyushchikh dvizheniy pri sverlenii glubokikh otverstiy malogo diametra. [Modelling of the dynamics of form-building movements in drilling deep openings of small diameter.] Bulletin of Adyghea State University, 2012, no. 4 (110), pp. 226–233 (in Russian).

11. Lapshin, V.P., Turkin, I.A. Dynamic influence of the spindle servo drive on the drilling of deep narrow holes. Russian Engineering Research, 2015, vol. 35, no. 10, pp. 795–797.

12. Lapshin, V.P., Turkin, I.A. Modeling tractive effort torque of wheel in deformation movements of pneumatic tire wheel. Procedia Engineering, 2017, vol. 206, pp. 594–599.

13. Zakovorotny, V.L., Lapshin, V.P., Babenko, T.S. Assessing the Regenerative Effect Impact on the Dynamics of Deformation Movements of the Tool during Turning. Procedia Engineering, 2017, vol. 206, pp.68–73.

14. Zakovorotny, V.L., Lapshin, V.P., Turkin, I.A. Зависимость перестройки динамической системы сверления глубоких отверстий спиральными сверлами от параметров серводвигателей / В. Л. Заковоротный,

В. П. Лапшин, И. А. Туркин // Известия ВУЗов. Сев.-Кавк. регион. Серия: Технические науки. — 2014. — № 1. — С. 36–42 (in Russian).

15. Zakovorotny, V.L., Lapshin, V.P., Turkin, I.A. Upravlenie protsessom sverleniya glubokikh otverstiy spiral'nymi sverlami na osnove sinergeticheskogo podkhoda. [Process control drilling deep holes twist drills based on the synergetic approach.] University News. North-Caucasian region. Technical Sciences Series, 2014, no. 3 (178), pp. 33–41 (in Russian).

16. Zakovorotny, V.L., Lukyanov A.D., Gubanova, A.A., Khristoforova, V.V. Bifurcation of stationary manifolds formed in the neighborhood of the equilibrium in a dynamic system of cutting. Journal of Sound and Vibration, 2016, vol. 368, pp. 174–190.

17. Zakovorotny, V.L., Vinokurova, I.A. Mathematical modeling of the dynamic cutting system taking into account the irreversible transformation in the area of cutting. Modern informatization problems in the technological and telecommunication systems analysis and synthesis Proceedings of the XXII–th International Open Science Conference. Editor in Chief O.Ja. Kravets. 2017, pp. 351–356.

18. Zakovorotny, V.L., Lukyanov, A.D. System synthesis of machine tool manufacturing process control based on synergetic conception. Procedia Engineering 2. Ser. 2nd International Conference on Industrial Engineering, ICIE 2016, pp. 370–375.

19. Zakovorotny, V.L., Bykador, V.S. Cutting-system dynamics. Russian Engineering Research, 2016, vol. 36, no. 7, pp. 591–598.

20. Lapshin, V.P., Turkin, I.A. Elektrodvigatel' postoyannogo toka — privod elektromobilya. [DC-drive for electro mobile.] Avtomotive Industry, 2017, no. 1, pp. 16–18 (in Russian).

21. Mladov, A.G. Sistemy differentsial'nykh uravneniy i ustoychivost' dvizheniya po Lyapunovu. [Systems of differential equations and stability of motion according to Lyapunov.] Moscow: Vysshaya shkola, 1966, 223 p. (in Russian).

Authors:

Lapshim, Victor P.,
associate professor of the Production Automation Department, Don State Technical University (1, Gagarin sq., Rostov-on-Don, 344000, RF), Cand.Sci. (Eng.), associate professor,
ORCID: https://orcid.org/0000-0002-5114-0316
 i090206.lapshin@yandex.ru

Turkin, Ilya A.,
senior lecturer of the Production Automation Department, Don State Technical University (1, Gagarin sq., Rostov-on-Don, 344000, RF), Cand.Sci. (Eng.),
ORCID: https://orcid.org/0000-0003-4792-4959
Tur805@mail.ru

Khristoforova, Veronika V.,
associate professor of the Production Automation Department, Don State Technical University (1, Gagarin sq., Rostov-on-Don, 344000, RF), Cand.Sci. (Eng.),
ORCID:https://orcid.org/0000-0002-0583-6654
nikaapp@rambler

ИНФОРМАТИКА, ВЫЧИСЛИТЕЛЬНАЯ ТЕХНИКА И УПРАВЛЕНИЕ
INFORMATION TECHNOLOGY, COMPUTER SCIENCE, AND MANAGEMENT

Parallel construction of binary tree based on sorting[*]

Ya. E. Romm[1], D. A. Chabanyuk[2]**

[1,2] Taganrog Chekhov Institute, Rostov State University of Economics (RINH) branch, Rostov-on-Don, Russian Federation

Параллельное построение двоичного дерева на основе сортировки[***]

Я. Е. Ромм[1], Д. А. Чабанюк[2]**

[1,2] Таганрогский институт имени А. П. Чехова (филиал) Ростовского государственного экономического университета (РИНХ)", г. Таганрог, Российская Федерация

Introduction. Algorithms for the parallel binary tree construction are developed. The algorithms are based on sorting and described in a constructive form. For the N element set, the time complexity has $T(R) = O(1)$ and $T(R) = O(\log_2 N)$ estimates, where $R = (N^2 - N)/2$ is the number of processors. The tree is built with the uniqueness property. The algorithms are invariant with respect to the input sequence type. The work objective is to develop and study ways of accelerating the process of organizing and transforming the tree-like data structures on the basis of the stable maximum parallel sorting algorithms for their application to the basic operations of information retrieval on databases.

Materials and Methods. A one-to-one relation between the input element set and the binary tree built for it is established using a stable address sorting. The sorting provides maximum concurrency, and, in an operator form, establishes a one-to-one mapping of input and output indices. On this basis, methods for the mutual transformation of the binary data structures are being developed.

Research Results. An efficient parallel algorithm for constructing a binary tree based on the address sorting with time complexity of $T(N^2) = O(\log_2 N)$ is obtained. From the well-known analogues, the algorithm differs in structure and logarithmic estimation of time complexity, which makes it possible to achieve the acceleration of $O(N^\alpha)$, $\alpha \geq 1$ order analogues. As an advanced version, an algorithm modification, which provides the maximum parallel construction of the binary tree based on a stable address sorting and a priori calculation of the stored subtree root indices is suggested. The algorithm differs in structure and estimation of $T(1) = O(1)$ time complexity. A similar estimate is achieved in a sequential version of the mod-

Введение. Разработаны алгоритмы параллельного построения двоичного дерева. Алгоритмы выполнены на основе сортировки и описаны в конструктивной форме. Для множества из N элементов временная сложность имеет оценки $T(R) = O(1)$ и $T(R) = O(\log_2 N)$, где число процессоров $R = (N^2 - N)/2$. Дерево строится со свойством единственности. Алгоритмы инвариантны относительно вида входной последовательности. Целью работы являлась разработка и исследование способов ускорения процесса организации и преобразований древовидных структур данных на основе алгоритмов устойчивой максимально параллельной сортировки для их применения к базовым операциям информационного поиска в базах данных.

Материалы и методы. Взаимно однозначное соответствие множества входных элементов и построенного для него двоичного дерева устанавливается при помощи устойчивой адресной сортировки. Сортировка обладает максимальным параллелизмом, в операторной форме устанавливает взаимно однозначное соответствие входных и выходных индексов. На этой основе разрабатываются методы взаимного преобразования двоичных структур данных.

Результаты исследования. Получен эффективный параллельный алгоритм построения двоичного дерева на основе адресной сортировки с временной сложностью $T(N^2) = O(\log_2 N)$. От известных аналогов алгоритм отличается структурой и логарифмической оценкой временной сложности, позволяющей достигать ускорения аналогов порядка $O(N^\alpha)$, $\alpha \geq 1$. В качестве усовершенствованного варианта предложена модификация алгоритма, обеспечивающая максимально параллельное построение двоичного дерева на основе устойчивой адресной сортировки и априорного вычисления хранимых индексов корней поддеревьев. Алгоритм отличается структурой и оценкой временной сложности $T(1) = O(1)$. Аналогичная оценка достигается в последовательном варианте модифициро-

ified algorithm, which allows obtaining the acceleration of known analogs of $O(N^{\alpha})$ $\alpha > 1$ order.

Discussion and Conclusions. The results obtained are focused on the creation of effective methods for the dynamic database processing. The proposed methods and algorithms can form an algorithmic basis for an advanced deterministic search on the relational databases and information systems.

ванного алгоритма, что позволяет достигать ускорения известных аналогов порядка $O(N^{\alpha})$, $\alpha > 1$.

Обсуждения и заключение. Полученные результаты направлены на организацию эффективных способов динамической обработки баз данных. Предложенные способы и алгоритмы могут составить алгоритмическую основу для ускоренного детерминированного поиска в реляционных базах данных и информационных системах.

Introduction. There is a tendency to the convergence of parallel information processing technologies and various processor architectures in the field of modern high-performance computing. Despite the variety of processor architectures and ways of presenting information, the idea of parallel processing is one of the most important tasks of computer science to increase the data-rate. To accelerate processing speed, the authors propose to use a stable address sorting algorithm with maximum parallelism.

Method of parallel construction of a binary tree. For $A = \left(a_0, a_1, \ldots, a_{n-1} \right)$ array, the comparison matrix is developed according to [1, 2]. a_{ij} element of this matrix is defined as

$$a_{ij} = \mathrm{sign}\left(a_j - a_i \right) = \begin{cases} +, & a_j > a_i \\ 0, & a_j = a_i \\ -, & a_j < a_i \end{cases},$$

where $i, j = 1, 2, \ldots, n$.

a_j element in $C = \left(c_0, c_1, \ldots, c_{n-1} \right)$ sorted array gets the number $k = \sum_{i=1}^{n} a_{ij}$, where $a_{ij} \geq 0$ at $i \leq j$, $a_{ij} > 0$ at $i > j$. All comparisons are mutually independent; the sorting is stable and as parallel as possible with the estimate of $T\left(\dfrac{N^2 - N}{2} \right) = O(1)$ time complexity. On this basis, you can perform a parallel construction of a binary tree [3, 4].

Suppose we are given a set of N elements, all elements of which are represented as a single-dimension array. On the set, $\leq$ ordering relation is assumed. It is required to convert the array into a binary tree. For this, the described array sorting is performed. C medial array cell has $j_{ср} = \left\lceil \dfrac{N}{2} \right\rceil$ index and is taken as the root of the tree [3]. All C array components to the left of $C_{j_{ср}}$ form a left subtree (left subarray). The components to the right of $C_{j_{ср}}$ form a right subtree (right subarray). The left subarray is interpreted as a new array. It similarly contains $j_{ср.\,лев.\,1/2} = \left\lceil \dfrac{1}{2}\left(\left\lceil \dfrac{N}{2} \right\rceil - 1 \right) \right\rceil = \left\lceil \dfrac{j_{ср} - 1}{2} \right\rceil$ root index. Here, $C_{j_{ср.\,лев.\,1/2}}$ is the left-nearest descendant of the root of $C_{j_{ср}}$ tree. All components of the subarray to the left of $C_{j_{ср.\,лев.}}$ do not exceed $C_{j_{ср.\,лев.\,1/2}}$; all components of the subarray on the right are not less than $C_{j_{ср.\,лев.\,1/2}}$. Simultaneously, the root index of $j_{ср.\,прав.\,1/2} = \left\lceil \dfrac{N}{2} \right\rceil + \left\lceil \dfrac{1}{2}\left(\left\lceil \dfrac{N}{2} \right\rceil - 1 \right) \right\rceil = j_{ср} + \left\lceil \dfrac{j_{ср} - 1}{2} \right\rceil$ right subarray is determined. At this, $C_{j_{ср.\,прав.\,1/2}}$ is the nearest descendant of the root of $C_{j_{ср}}$ tree. The process recursively resumes in each pair of the adjacent subarrays:

http://vestnik.donstu.ru

$$j_{\text{ср. лев. } 1/2^i,\, 1} = \left\lceil \frac{j_{\text{ср. лев. } 1/2^{i-1}} - 1}{2} \right\rceil,$$

$$j_{\text{ср. лев. } 1/2^i,\, 2} = j_{\text{ср. лев. } 1/2^{i-1}} + \left\lceil \frac{j_{\text{ср. лев. } 1/2^{i-1}} - 1}{2} \right\rceil,$$

$$j_{\text{ср. прав. } 1/2^i,\, 1} = j_{\text{ср. прав. } 1/2^{i-1}} - \left\lceil \frac{j_{\text{ср. прав. } 1/2^{i-1}} - j_{\text{ср. прав. } 1/2^{i-2}} - 1}{2} \right\rceil,$$

$$j_{\text{ср. прав. } 1/2^i,\, 2} = j_{\text{ср. прав. } 1/2^{i-1}} + \left\lceil \frac{j_{\text{ср. прав. } 1/2^{i-1}} - j_{\text{ср. прав. } 1/2^{i-2}} - 1}{2} \right\rceil, \quad i = 1,\, 2,\, \ldots,\, \log_2 N.$$

As a result, all components of the lower level of the binary tree are formed in $O(1)$ time. The process can continue until $\log_2 N$ exhaustion of the levels of the binary tree.

The number of algorithm steps for constructing the binary tree in a parallel form is the sum of the sorting step and the step sequence when calculating the indices of the roots of subtrees. From here, $T(R) = \log_2 N \tilde{\tau} + \tau = O(\log_2 N)$, where R is the number of processor elements, τ is the time of binary comparison, and $\tilde{\tau}$ is the time for calculating one root index. R number of processors is determined by the maximum N parallel sorting of input elements, and then – through the calculation of indices with doubling by the number of tree levels. When calculating the indices, this number will not exceed $2^{\log_2 N - 1} = N/2$, therefore the number of processors involved in sorting is sufficient. As a result, R will be less than $\frac{N^2 - N}{2}$ [3]. Finally, the time complexity of the parallel algorithm for constructing the binary tree will be

$$T\left(\frac{N^2 - N}{2} \right) = O(\log_2 N).$$

Example [3]. The binary tree for an array of 15 elements $X = (14,\ 9,\ 24,\ 7,\ 11,\ 20,\ 28,\ 3,\ 8,\ 10,\ 13,\ 17,\ 21,\ 25,\ 30)$ is constructed as follows.

The result of the sort is the array

$$C = (3,\ 7,\ 8,\ 9,\ 10,\ 11,\ 13,\ 14,\ 17,\ 20,\ 21,\ 24,\ 25,\ 28,\ 30).$$

The root of the binary tree is the medial element of C array: $j_{\text{ср}} = \left\lceil \frac{15}{2} \right\rceil = 8$, $C_8 = 14$. The left subarray has $j_{\text{ср. лев. } 1/2} = \left\lceil \frac{8-1}{2} \right\rceil = 4$ root, $C_4 = 9$ element is the root of the left subtree, which is the left-nearest descendant of $C_{j_{\text{ср}}}$ medial component. The right subarray has $j_{\text{ср. прав. } 1/2} = 8 + \left\lceil \frac{8-1}{2} \right\rceil = 12$ root, $C_{12} = 24$ element is the root of the right subtree and the right-nearest descendant of $C_{j_{\text{ср}}}$ root. Further, $j_{\text{ср. лев. } 1/4, 1} = \left\lceil \frac{4-1}{2} \right\rceil = 2$, $C_2 = 7$ element is the root of the subtree on the left and the left-nearest descendant of the root of $C_{j_{\text{ср. лев. } 1/2}}$ subtree. In the right subtree, the root has $j_{\text{ср. лев. } 1/4, 2} = 4 + \left\lceil \frac{4-1}{2} \right\rceil = 6$ number, $C_6 = 11$ element is the root of the right subtree and right-nearest child of $C_{j_{\text{ср. лев. } 1/2}}$. Similarly, to the left of $C_{j_{\text{ср. прав. } 1/2}}$, $j_{\text{ср. прав. } 1/4, 1} = 12 - \left\lceil \frac{12-8-1}{2} \right\rceil = 10$ root is determined, $C_{10} = 20$ element is the root of

the left subtree from it and the left-nearest descendant of $C_{j_{\text{ср. прав. 1/2}}}$ subtree root. For the subarray, adjacent to the right one

discussed above, the root has $j_{\text{ср. прав. 1/4,2}} = 12 + \left\lceil \dfrac{12-8-1}{2} \right\rceil = 14$ number, $C_{14} = 28$ element is $C_{j_{\text{ср. прав. 1/2}}}$ right-nearest

descendant and the right subtree root. The lower level of the tree will be formed by the descendants remaining to the left
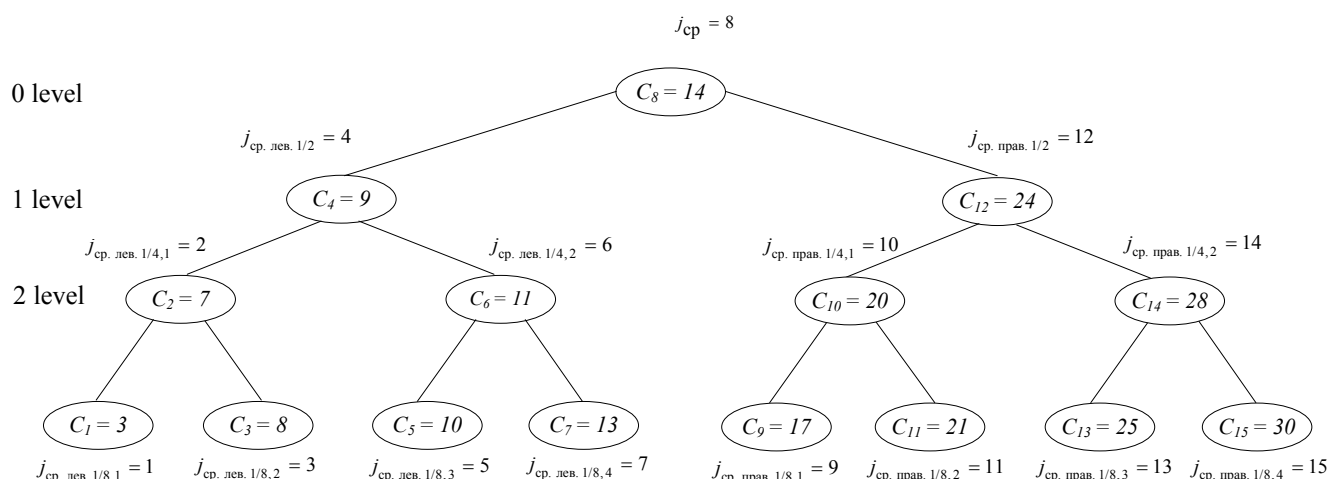and to the right of each of four identified roots (Fig. 1):

Fig. 1. Example of constructing binary tree based on sorting

There is **Theorem 1** [3]. For a single-dimensional array of N components, a binary tree can be built in parallel

using sorting with $T\left(\dfrac{N^2}{2}\right) = O(\log_2 N)$ time complexity.

The used sorting is stable; the binary tree is implied to be constructed with uniqueness. The indices of all me-
dial components (all roots of subtrees) can be identified [3]. Considering this modification, all the indices from the
above example for N subtree values can be calculated synchronously and mutually independently. This leads to a sin-
gle estimate of the build time of the binary tree. For each specific N, all the values of the tree node indices can be cal-
culated a priori and stored in the computer memory. With their help, the sorted components can be synchronously and
mutually independently addressed to all the tree nodes. Formulas for calculating the node indices depend only on the
total number of N input elements and are in no way dependent on their mutual arrangement after the stable sorting. To
simplify memory addressing, the computed indices can be ordered at each level and arranged in ascending levels. Then,
the entire population of the ordered node indices is read from N key. It only remains to arrange the sorted tree elements
by the read-in addresses. Based on the above, there is

Theorem 2. For a single-dimensional array of N components, a binary tree can be built in parallel using sorting and

prior calculation of indices with $T\left(\dfrac{N^2}{2}\right) = O(1)$ time complexity.

The following unified table contains the formal estimates of time complexity of sequential and parallel algo-
rithms for constructing a binary tree versus the proposed algorithms.

Table 1

Comparative estimates of time complexity of sequential and parallel algorithms for constructing binary tree versus proposed algorithms

Binary tree algorithm	Algorithm time complexity	Acceleration when using unit time-complexity algorithm	Acceleration when using logarithmic time-complexity algorithm
Algorithm of A. Lagana and V. Kumar (2004) [5]	$\tilde{T} = O\left(N^{\frac{k+1}{k}}\right)$ [5]	$\dfrac{\tilde{T}}{T^*} = O\left(\dfrac{N^{\frac{k+1}{k}}}{1}\right)$	$\dfrac{\tilde{T}}{T} = O\left(\dfrac{N^{\frac{k+1}{k}}}{\log_2 N}\right) = O(N \ln 2)$
Algorithm of P. Chalermsook (2015) [6]	$\tilde{T} = O(N^2)$ [6]	$\dfrac{\tilde{T}}{T^*} = O(N^2)$	$\dfrac{\tilde{T}}{T} = O\left(\dfrac{N^2}{\log_2 N}\right) = O(N^2 \ln 2)$
Polynomial algorithm (2016) [7]	$\tilde{T} = O(N^3)$ [7]	$\dfrac{\tilde{T}}{T^*} = O(N^3)$	$\dfrac{\tilde{T}}{T} = O\left(\dfrac{N^3}{\log_2 N}\right) = O(N^3 \ln 2)$
"Left child – right sibling" algorithm (2014) [8]	$\tilde{T} = O(N^2)$ [8]	$\dfrac{\tilde{T}}{T^*} = O(N^2)$	$\dfrac{\tilde{T}}{T} = O\left(\dfrac{N^2}{\log_2 N}\right) = O(N^2 \ln 2)$
Pattern-based algorithm (1991) [9]	$\tilde{T} = O(|D|\log_2 D)$ [9]	$\dfrac{\tilde{T}}{T^*} = O\left(\dfrac{|D|\log_2 D}{1}\right)$	$\dfrac{\tilde{T}}{T} = O\left(\dfrac{|D|\log_2 D}{\log_2 N}\right)$
The presented algorithm with logarithmic estimate of time complexity (2015) [3]	$T = O(\log_2 N)$ [3]	–	–
The presented algorithm with single estimate of time complexity (2015) [3]	$T^* = O(1)$	–	–

In Table 1: D is capacity of the template dictionary, N is the number of input elements of the binary tree, k is the dimension of the space in which sorting is performed.

The table shows that the proposed algorithm with a logarithmic estimate of time complexity abstractly improves estimates of the known algorithms. Minimum acceleration is achieved with respect to the algorithm from [5]: $\dfrac{\tilde{T}}{T} = O(N^2 \ln 2)$, or $\dfrac{\tilde{T}}{T} = O(N)$; and maximum acceleration is achieved relative to the polynomial algorithm from [7]: $\dfrac{\tilde{T}}{T} = O\left(\dfrac{N^3}{\log_2 N}\right)$ or $\dfrac{\tilde{T}}{T} = O(N^3)$. Regarding the proposed algorithm with a single estimate of time-complexity, the evaluation of the known algorithms also improves. In this case, minimum acceleration is achieved relative to the algorithm from [5]: $\dfrac{\tilde{T}}{T^*} = O(N)$, and maximum acceleration is achieved with respect to the polynomial algorithm from [7]: $\dfrac{\tilde{T}}{T^*} = O(N^3)$.

Conclusion. The developed algorithms differ from the known techniques [5–7, 10, 11] of constructing a binary tree in that they use maximum parallel sorting to calculate the indices of the nodes. In this case, either a logarithmic number of steps is consumed by building a tree, or additional time is not spent at all, if the values of the indices are a priori calculated for all N values in some real boundaries and stored in the computer memory. The proposed parallel algorithm for constructing a binary tree can be used to organize efficient methods for dynamic processing of databases.

Information technology, computer science, and management

References

1. Romm, Ya.E., Chabanyuk, D.A. Sravnenie slov s edinichnoy vremennoy slozhnost'yu. [Comparison of words with the complexity of identity] Izvestiya SFedU. Engineering Sciences. 2014, no. 7 (156), pp. 230–238 (in Russian).

2. Romm, Ya.E. Parallel'naya sortirovka sliyaniem po matritsam sravneniy. II [Parallel sorting by merging on comparison matrices. II] Cybernetics and Systems Analysis, 1995, no. 4, pp. 13–37 (in Russian).

3. Romm, Y.E., Chabanyuk, D.A. Postroenie dvoichnogo dereva na osnove parallel'noy sortirovki. [Constructing binary tree based on parallel sorting algorithm.] Fundamental Research, 2015, vol. 8., no. 3, pp. 509–513 (in Russian).

4. Romm, Ya.E., Chabanyuk, D.A. Parallel'noe postroenie dvoichnogo dereva na osnove sortirovki. [Parallel construction of binary tree based on sorting algorithm.] Aspekty razvitiya nauki, obrazovaniya i modernizatsii promyshlennosti: mater. Vseross. nauchno-prakt. konf. [Aspects of development of science, education and industrial modernization: Proc. All-Russian Sci.-Pract. Conf.] Taganrog, 2017, vol. 1, pp. 77–84 (in Russian).

5. Laganà A., Kumar, A., Tan, V.C. Computational Science and Its Applications: Lecture Notes in Computer Science. Assisi: Springer Science & Business Media, 2004, 1044 p. – DOI: 10.1007/b98048

6. Chalermsook, P., Goswami, M., eds. 2015 IEEE 56th Annual Symposium on Foundations of Computer Science (FOCS 2015). Piscataway, NJ: IEEE, 2015, pp. 410-423 – DOI: 10.1109/FOCS.2015.98

7. Gavrikov, A.V. T-neprivodimye rasshireniya dlya orientirovannykh binarnykh derev'ev. [T-irreducible extensions of directed binary trees.] Computer Sciences and Information Technologies, 2016, no. 6, pp. 123–125 – DOI 10.17223/20710410/34/6 (in Russian).

8. Gritsenko, N.S., Belov, Yu.S. Postroenie dvoichnogo dereva na osnove modifitsirovannoy skhemy khraneniya derev'yev obshchego vida «left child»-«right sibling» (LCRS). [Creation of a binary tree based on the modified storage diagram of general appearance trees "left child - right sibling" (LCRS).] Engineering Journal: Science and Innovation ,2014, no. 3, pp. 75–84 — DOI: 10.18698/2308-6033-2014-3-1281 (in Russian).

9. Amir, A., Farach, M., Adaptive dictionary matching. Foundations of Computer Science, 1991. Proceedings., 32nd Annual Symposium on. IEEE, 1991, pp. 760-766 – DOI: 10.1109/SFCS.1991.185445

10. Fischer, J., Heun, V. Theoretical and Practical Improvements on the RMQ-Problem, with Applications to LCA and LCE. Combinatorial Pattern Matching. Berlin, Heidelberg: Springer Berlin Heidelberg, 2006, vol. 4009, pp. 36-48.

11. Institute of Electrical and Electronics Engineers. Pattern-Avoiding Access in Binary Search Trees. Computer Society. 2015 IEEE 56th Annual Symposium on Foundations of Computer Science (FOCS 2015), 2015, no. 56, pp. 410-423 - DOI: 10.1109/FOCS.2015.32

Authors:

Romm, Yakov Ye.,

Head of the Information Technology Department,

Taganrog Chekhov Institute, Rostov State University of

Economics (RINH) branch (48, Initsiativnaya St.,

Taganrog, RF), Dr.Sci. (Eng.), professor,

ORCID: http://orcid.org/0000-0002-7251-2844

romm@list.ru

Chabanyuk, Denis A.,

associate professor of the Theoretical, General Physics and

Technologies Department, Taganrog Chekhov Institute,

Rostov State University of Economics (RINH) branch

(48, Initsiativnaya St., Taganrog, RF),

ORCID http://orcid.org/0000-0003-2972-0944

denchabanyuk@gmail.com